Mechanics Of Particle Motion In A Spouted Bed.

INFORMATION TO USERS

This reproduction was made from a copy of a document sent to us for microfilming. While the most advanced technology has been used to photograph and reproduce this document, the quality of the reproduction is heavily dependent upon the quality of the material submitted.

The following explanation of techniques is provided to help clarify markings or notations which may appear on this reproduction.

1. The sign or "target" for pages apparently lacking from the document photographed is "Missing Page(s)". If it was possible to obtain the missing page(s) or section, they are spliced into the film along with adjacent pages. This may have necessitated cutting through an image and duplicating adjacent pages to assure complete continuity.

2. When an image on the film is obliterated with a round black mark, it is an indication of either blurred copy because of movement during exposure, duplicate copy, or copyrighted materials that should not have been filmed. For blurred pages, a good image of the page can be found in the adjacent frame. If copyrighted materials were deleted, a target note will appear listing the pages in the adjacent frame.

3. When a map, drawing or chart, etc., is part of the material being photographed, a definite method of "sectioning" the material has been followed. It is customary to begin filming at the upper left hand corner of a large sheet and to continue from left to right in equal sections with small overlaps. If necessary, sectioning is continued again—beginning below the first row and continuing on until complete.

4. For illustrations that cannot be satisfactorily reproduced by xerographic means, photographic prints can be purchased at additional cost and inserted into your xerographic copy. These prints are available upon request from the Dissertations Customer Services Department.

5. Some pages in any document may have indistinct print. In all cases the best available copy has been filmed.

University Microfilms International
300 N. Zeeb Road
Ann Arbor, MI 48106

Amirshahidi, Mohammad Sayed

MECHANICS OF PARTICLE MOTION IN A SPOUTED BED

Lehigh University

PH.D. 1984

MECHANICS OF PARTICLE MOTION IN A SPOUTED BED

By

Mohammad S. Amirshahidi

A Dissertation
Presented to the Graduate Committee
of Lehigh University
in Candidacy for the Degree of
Doctor of Philosophy

in
Chemical Engineering

Lehigh University
1984

CERTIFICATION OF APPROVAL

Approved and recommended for acceptance as a dissertation in partial fulfillment of the requirements for the degree of Doctor of Philosophy

March 30, 1984

Professor in Charge

Accepted March 30, 1984

Special Committee directing the doctoral work of Mr. Mohammad S. Amirshahidi

Dr. T.S. Caram

Dr. W.E. Schiesser

Dr. C.A. Silebi

Dr. D.P. Updike

To my wife, Fataneh, for her patience, encouragement and support.

Acknowledgments

I wish to express my special thanks and gratitude to my advisor Dr. Hugo S. Caram for his guidence, encouragement, critical suggestions and comments and to Dr. Dean P. Updike for long discussions about the plasticity and yield surfaces.

To Dr. Leonard A. Wenzel, the chairman of the department at the time, for extending the support to complete this work.

Last but not definitely least, to my wife for her understading and patience and to my son, Amin, who made my life more enjoyable.

TABLE OF CONTENTS

		Page
Title Page		i
Certification of approval		ii
Dedication		iii
Acknowledgements		iv
Table of Contents		v
Nomenclature		viii
List of Tables		x
List of Figures		xi
Abstract		1
CHAPTER ONE		
1.0	INTRODUCTION	3
1.1	The Spouting Phenomena	6
1.2	The Effect of Gas Flow on the Bed Condition	9
1.3	Literature Survey	12
CHAPTER TWO		
2.0	BASIC RULES IN SOIL MECHANICS, PLASTICITY AND FLOW OF BULK SOLID	25
2.1	Definitions and Concepts	25
2.1.1	Principal stresses	25
2.1.2	Mohr circle	26
2.1.3	Effective stress	28
2.1.4	Strains and principal strains	30
2.1.5	Plane strain	31
2.2	Stress-Strain Behavior of a Soil Mass	32
2.3	Shear Strenght and Mohr-Coulomb Failure Law	34
2.4	Flow of Bulk Solids, Soil Mechanics, and plasticity	42
2.4.1	Yield locus, effective yield locus, plastic potential and normality	46

--yield locus, yield surfaces 47
--effective yield locus 52
--plastic potential function and the normality condition in steady flow 55
--case of plane strain, incompressible, cohesionless materials 58
--isotropy in steady flow 60

CHAPTER THREE

3.0 BASIC EQUATIONS 62
3.1 Effect of the Gas 63
3.1.1 Spout pressure distribution 63
3.1.2 Annulus pressure distribution 64
3.2 The Effective Density 69
3.3 The Equations of Motion for the Solid 70
3.3.1 Stress field 70
3.3.2 Velocity field 74
3.3.3 Boundary conditions 75
--top boundary 75
--bed wall 77
--boundary of dead zone 78
--spout annulus interface 80

CHAPTER FOUR

4.0 EXPERIMENTAL OBSERVATIONS AND BOUNDARY OF DEAD ZONE 86
4.1 Experimental Observations 86
4.1.1 Apparatus 86
4.1.2 Observations 87
4.2 Determination of the Boundary of Dead Zone Using the Method of the Slices 94
4.2.1 The equations of equilibrium 95
4.2.2 Calculation procedure and results 101

CHAPTER FIVE

5.0	ANALYSIS OF STRESS AND VELOCITY FIELDS		110
5.1	The Method of Differential Slices (MOS)		113
5.2	Stress Field by Method of Integrals (MOI)		130
	5.2.1	The governing equations	132
	5.2.2	The vertical part	137
	5.2.3	The conical part	138
	5.2.4	Stress discontinuity and the boundary conditions	142
	5.2.5	Results and discussion	145
5.3	Stress Field by the Method of Characteristics (MOC)		156
	5.3.1	The characteristics equations	157
	5.3.2	characteristics equations of the stress field	161
	5.3.3	Improvement of accuracy of the computations	164
	5.3.4	Treatment of discontinuities	166
	5.3.5	Corner points and computations near the walls	170
	5.3.6	Results and discussion	176
	5.3.7	Slip lines	191
5.4	Velocity Field		194
	5.4.1	Characteristics equations of the velocity field	197
	5.4.2	Results and discussion	199
	5.4.3	Shear lines	214

CHAPTER SIX

6.0	CONCLUSION	217
Bibliography		224
Appendix 1		231
Appendix 2		236
Appendix 3		242
Appendix 4		246
Vita		247

NOMENCLATURE

Roman Symbols

$a(y)$	:	function used to express stress distribution in the method of integral
B	:	an indicator of gas flow in annulus, distribution factor, ratio of pressure drop per unit depth to that at the maximum spoutable depth condition
$b(y)$	:	functional form of the dead zone boundary
b_o	:	width of the annulus, from the spout wall to the bed wall
D	:	distribution factor
d_{ave}	:	average particle diameter
E	:	Young's Modulus
G	:	Shear Modulus
g	:	gravitational acceleration
H	:	depth of the material in the bed, moisture content
H_D	:	height of dead zone from the base of the bed
H_m	:	maximum spoutable bed depth
h	:	ratio of bed depth to maximum spoutable bed depth
K_i	:	Darcy's constant in the i direction
l_i	:	elongation in the i direction
P_f	:	fluid pressure
r	:	Mohr circle radius
r_1, r_2	:	roots of the characteristic equation in MOI
T	:	temperature
t	:	time
u	:	velocity component in x direction
v	:	velocity component in y direction
W	:	total solid circulation
w	:	velocity component in z direction

Greek Symbols

α	:	angle between forces on a side of a slice
β	:	angle of effective yield surface
γ	:	specific weight of the solids, shear strain
$\dot{\gamma}$	:	shear strain rate
Δ	:	difference
δ	:	effective angle of internal friction
$\dot{\epsilon}$	:	strain rate vector
ϵ_o	:	annulus porosity

ε_i : normal compressive strain in the i direction
$\dot{\varepsilon}_i$: normal compressive strain rate in the i direction
η : angle of shock surface
θ_{cr} : angle between failure plane and major principal plane
ψ : half angle between slip lines
ν : Poisson ratio
π : 3.1415962
ρ : angle of internal friction
ρ_b : bulk density
ρ_e : effective density
ρ_f : fluid density
ρ_p : particle density
σ : mean horizontal and vertical stresses
σ_r : radial stress
σ_x, σ_y : normal horizontal , vertical stress
σ_θ : circumferential stress
σ_y : average vertical stress
$\sigma_{1,2,3}$: major, minor, intermediate principal stress
τ : shear stress
ϕ : angle of major principal stress direction wih the vertical axis
ϕ_v : anglof strainratect
χ : characteristic direction
ψ : roughness ratio
ω : angle of inclination of free stress boundary with horizontal axis

Subscripts

b : boundary of dead zone
c : conical part
D : dead zone
f : fluid
s : spout wall
t : top boundary
w : bed wall
x,y,z : coordinates direction

List of Tables

Table 1: Solid Particles Used for Experiments

LIST OF FIGURES

Figure 1 Schematic diagram of a flat based spouted bed
a) spout
b) annulus
c) dead zone

Figure 2 Spouted wheat bed in a 6" sectional column

Figure 3 Effect of gas flow on pressure drop in a bed of solids (Based on Mathur and Gishler, 1955)

Figure 4 Mohr circle of stress representation
a) equations for state of stress at a point
b) Mohr diagram for state of stress at a point

Figure 5 Determination of pole of a Mohr circle
a) Mohr stress circle
b) physical planes

Figure 6 Results of a triaxial compression test upon a well graded calcareous sand from Libya (Lambe & Whitman, 1973)

Figure 7 Critical Mohr circles and the Mohr envelop

Figure 8 Stresses at failure

Figure 9 Relations between ϕ and principal stresses at failure

Figure 10
Yield loci of Tresca and Mises
Yield surfaces in stress space
Mises type of extension of Coulomb criterion
Tresca's type of extension of Coulomb criterion

Figure 11 Evolution of the yield surface pyramid

Figure 12 Yield loci and the direction of ε

Figure 13 The effective yield pyramid

Figure 14 One half of the two dimensional spouted bed and the boundaries of annulus

Figure 15 Ratio of wall pressure to spout pressure

as a function of the dimensionless depth of the material

Figure 16 Relations between principal stress and sliplines
a) Mohr stress circle
b) physical plane

Figure 17a Mohr circle of stress construction for material at the bed wall (active state)

Figure 17b Mohr circle of stress construction for material at the spout wall (active state)

Figure 18 The annulus region of spouted bed with the boundary conditions for the stress and velocity fields along its boundaries

Figure 19 Observed spout shape for a two-dimensional bed

Figure 20 Spout shape
a) cylindrical spouted bed
b) Two-dimensional spouted bed

Figure 21 Method of slices
a) semi-spouted bed with position of slices
b) forces acting on a slice

Figure 22 Side forces and angle α

Figure 23 Functions α employed in the method of slices

Figure 24 Boundary of dead zone (Function 23-a)

Figure 25 Boundary of dead zone (Function 23-b)

Figure 26 Percent of wall occupied by the dead zone for different ϕ and ϕ_w

Figure 27 Comparison of the boundary of dead zone with the model

Figure 28 Differential element and force balance

Figure 29 Relation between the vertical and shear stresses at the wall (active case) as a function of the internal (δ) and wall friction angles (δ_w)

Figure 30 Relation between the vertical and shear stresses at the wall of the spout (active case) with $\delta/\delta_s=10$

Figure 31 Distribution coefficients (D_w) relating the vertical normal stress at the wall $(\sigma_y)_w$ to the average normal stress σ_y across the width of annulus vs. the angles of internal (δ) and wall (δ_w) friction

Figure 32 Distribution coefficients (D_s) relating the vertical normal stress at the spout wall $(\sigma_y)_w$ to the average normal stress σ_y across the width of annulus vs. the angles of internal (δ) and spout wall (δ_s) friction

Figure 33a Stress distributions obtained using the method differential slices (MOS) in the active case ($\delta=40^o$, $\delta_w=20^o$, $\delta_s=4^o$ and H=3)

Figure 33b Distribution of the average normal stress (σ_y) obtained for three different bed depth using the method of slices considering the gas flow (B=1) ($\delta=40^o$, $\delta_w=20^o$ and $\delta_s=4^o$)

Figure 34 Distribution of the average normal stress for various δ_w ($\delta=30^o$, $\delta_s=3^o$, H=3)

Figure 35 Half spouted bed and position of x-y and $x-y_c$ coordinates

Figure 36 Dimensionless stresses at the spout wall obtained for the vertical part of the annulus using the method of integral relations ($\delta=40^o$, $\delta_w=20^o$, $\delta_s=4^o$)

Figure 37 Dimensionless stresses at the bed wall obtained for the vertical part of the annulus using the method of integral relations ($\delta=40^o$, $\delta_w=20^o$, $\delta_s=4^o$)

Figure 38 Dimensionless stresses at the spout wall obtained using the method of integral relations (MOI)

(δ=40°, δ_w=20°, δ_s=4°)

Figure 39 Dimensionless stresses at the spout wall obtained using the method of integral relations (MOI) (δ=40°, δ_w=20°, δ_s=4°)

Figure 40 Initial arc Γ and the associated characteristics mesh

Figure 41 Characteristic curves approximated by straight lines

Figure 42 Characteristics of the Active Rankine Zone and computations at the corner points and near the walls

Figure 43 Stress characteristics for the case of spouted bed (gas flow, B=1) and variable wall friction angles (δ=40°, $\delta_{w_{Max}}$=20°, $\delta_{s_{Max}}$=4°)

Figure 44 Distribution of the vertical normal stress at the spout and bed walls obtained using the method of characteristics for the case of no gas flow in the annulus (B=0) (δ=40°, $\delta_{w_{Max}}$=20°, $\delta_{s_{Max}}$=4°)

Figure 45 Distribution of the horizontal normal stress at the spout and bed walls obtained using the method of characteristics for the case of no gas flow in the annulus (B=0) (δ=40°, $\delta_{w_{Max}}$=20°, $\delta_{s_{Max}}$=4°)

Figure 46 Distribution of the shear stress at the spout and bed walls obtained using the method of characteristics for the case of no gas flow in the annulus (B=0) (δ=40°, $\delta_{w_{Max}}$=20°, $\delta_{s_{Max}}$=4°)

Figure 47 Dimensionless stresses at the spout wall obtained for the vertical part of the annulus using the method of characteristics for the spouted bed (gas flow, B=1) (δ=40°, $\delta_{w_{Max}}$=20°, $\delta_{s_{Max}}$=4°)

Figure 48 Dimensionless stresses at the bed wall obtained for the vertical part of the annulus using the method of characteristics for the spouted bed (gas flow, B=1)

(ϕ=40°, $\delta_{w_{Max}}$=20°, $\delta_{s_{Max}}$=4°)

Figure 49 Horizontal variation of the vertical stress component by the method of characteristics, method of integrals and method of slices at different depth of the vertical part of the spouted bed annulus (ϕ=40°, $\delta_{w_{Max}}$=20°, $\delta_{s_{Max}}$=4°)

Figure 50 Horizontal variation of the horizontal stress component by the method of characteristics, method of integrals and method of slices at different depth of the vertical part of the spouted bed annulus (ϕ=40°, $\delta_{w_{Max}}$=20°, $\delta_{s_{Max}}$=4°)

Figure 51 Horizontal variation of the shear stress component by the method of characteristics, method of integrals and method of slices at different level of the vertical part of the spouted bed annulus (ϕ=40°, $\delta_{w_{Max}}$=20°, $\delta_{s_{Max}}$=4°)

Figure 52 Velocity characteristic mesh (ϕ=40°, $\delta_{w_{Max}}$=20°, $\delta_{s_{Max}}$=4°)

Figure 53 Dimensionless horizontal (u) and Vertical (v) velocity distributions at the bed wall for the vertical part of the annulus

Figure 54 Dimensionless horizontal (u) and vertical (v) velocity distributions at the spout wall for the vertical part of the annulus

Figure 55 Horizontal variation of the horizontal velocity component at different depth of the vertical part of the annulus

Figure 56 Horizontal variation of the vertical velocity component at different depth of the vertical part of the annulus

Figure 57 The computed solid particle streamlines in the vertical part of the annulus

Figure 58 Photograph of a two-dimensional spouted bed

Figure A-1 Stresses and the corresponding Mohr circles (After Walters, 1973)

circle W represents stresses at the bed wall
circle M represents stresses at any point
circle S represents stresses at the spout wall

Figure A-2.1 Stresses on an element at the discontinuity

Figure A-2.2 Mohr circle and position of the shock surface

Figure A-2.3 Characteristics mesh and the shock surface

ABSTRACT

By use of principles and rules of plasticity and soil mechanics, similar to those applied to the flow of bulk solids in bins, the mechanism of solid particle motion in the dense region of a flat bottomed two dimensional spouted bed was investigated. For this computation the material was assumed to be an isotropic, frictional, cohesionless, incompressible rigid-plastic solid.

The first part of this study is the determination of the boundary of the dead zone used on the method of slices as employed in soil mechanics to study the stability of slopes. The results of the analysis are in good agreement with the experimental evidence.

The second part of this study consists of determination of stress and velocity fields for the material contained in the dense moving region. Only the case of plain strain is considered, but the analysis can easily be extended to the case of axial symmetry. The stress analysis is similar to that applied to the flow of bulk solids in bins. While the method of characteristics is capable of determining the stress field, an approximated technique furnishing an analytical solution is suggested to computing the velocity field. In the region of discontinuities

where the method of characteristics becomes quite complicated, an approximated procedure is used. It is beleived that the results of this procedure approximate well the true values, especially for regions far from the discontinuities.

The determination of velocity field by the method of characteristics leads to the identification of lines of maximum shear strain rate (shear lines). These lines were used in computing the velocity distributions. While a quantitative comparison of the particle velocity requires a rigorous experimental procedure, the results of the model show qualitative agreement with the observations and the literature data. The calculated solid streamlines favorably identify the real path of the elements of the particles. The analysis is presented for the vertical part of the dense region of the spouted bed. It is believed, based on the results of this analysis, that the material in the vertical part is in the state of critical equilibrium so that the inertial terms are negligible. In the converging part of the dense region, however, the particle accelerate, intertial terms become important and the full momentum equations must be considered.

CHAPTER ONE

1.0 INTRODUCTION

The spouted beds have emerged in recent years as an effective gas-solid contacting systems for certain applications. Spouted beds may be used as a chemical reactors, although they were originally invented by Mathur and Gishler primarily for the drying of wheat. The system then viewed as a preferable alternative to fluidization when the solid particles were too uniform or too coarse for a stable fluidization. It was soon realized that the characteristics of particle motion is different in the two systems.

While many investigators have analysed the behavior of spouted beds both experimentally and theoretically, the mechanics of particle motion is not yet well understood. The major obstacle is the lack of connection of the subject with a well established and recognized field. It has been suggested that the solid motion in a dense region of a spouted bed may be similar to the flow of bulk solids in bins. While this suggestion has gained more grounds, the problem of flow of bulk solids itself has to rely on the fields of rheology, plasticity, and soil mechanics. These fields must then be well understood if one attempts to use

the analogy between the solid motion in the dense region of a spouted bed and a bin.

A steadily operating spouted bed with a flat bottom shows (see Figure 1) three distinct regions: the dilute phase (spout), the dense region (annulus), and the dead zone.

This work presents a theoretical analysis of particle motion in the dense region of a two dimensional spouted bed. The analysis leads to the determination of stress and velocity fields in a bi-dimensional spouted bed and is based on the principles of plasticity and soil mechanics. The present analysis can readily be extended to the case of a cylidrical spouted bed.

Although the spouted beds have been the subject of extensive ananlysis (International Symposiums on Spouted Beds 1974 and 1983, Mathur and Eptein 1974c, Mathur and Gishler 1955a, Morgan and Littman 1982), both theoretical and experimental, no rigorous mathematical model describing the mechanics of particle motion has yet been developed. It is then the purpose of this work to recognize and develop a set of rules and techniques applicable to the solid motion in a spouted bed.

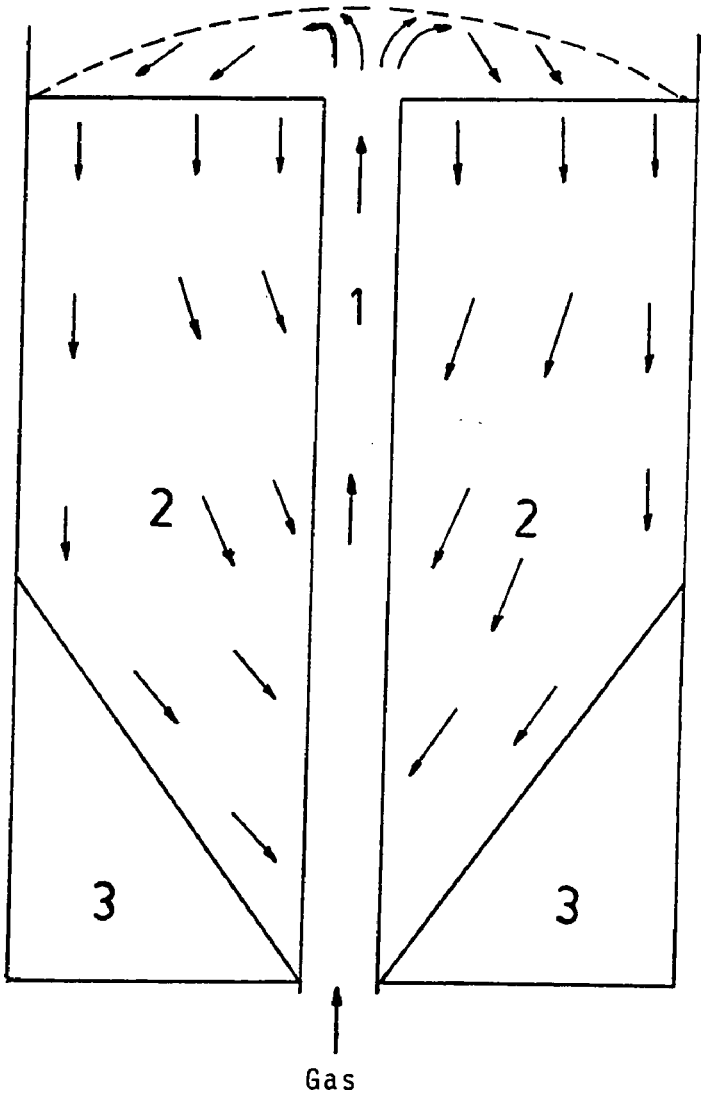

Figure 1 Schematic diagram of a flat based spouted bed

a) spout
b) annulus
c) dead zone

1.1 The Spouting Phenomena

The phenomena of spouting was first introduced by Mathur and Gishler (1955a) in 1955 as a technique for contacting gases with coarse solid particles. The technique was introduced because it was found that the applications of fluidization were limited to relatively fine solids, and fluidized beds of coarse materials show a marked tendency toward slugging (Singiser et al 1966). Although the advantages of the fluidization of solids lead to the introduction of the spouting of solids, it was soon realized that the behavior of the two systems were quite distinct. The spouting phenomena appeard to achieve the same purposes for coarse solids as fluidization does for fine solids, but with a different mechanism, and the phenomena seemed to make it more suitable for certain applications that will be discussed in this chapter. It was also found that the spouting technique could effectively work for solids as fine as 20 to 35 mesh (particle diameter) which could also be fluidized.

The spouting can be obtained by allowing a high velocity jet of fluid enter at the bottom of a packed bed of solids. The bed is usually a cylindrical column having a conical bottom and a gas is normally used as the spouting medium. In passing a gas through a bed of packed

solids the following steps will occur. At very low flow of gas the particle bed behaves like a packed bed and the gas will simply pass upward through the solids bed without disturbing the particles. At higher gas velocities particles around the nozzle entrance will start to oscillate teeter; increasing the gas velocity will cause a noticeable readjustment of particle and formation of a gas pocket in the entry region with active particle circulation. A further increase in gas flow causes a high velocity jet or spout forming a stream of solids to rise rapidly as a central core. The bed and solid particle configuration as well as the velocity of gas determines wheather a jet or a spout will form. The jet may break further up into bubbles or cause a slugging bed to form, while the spout carries the particles to somewhat above the bed level to form a fountain shape of particles. These solids fall back onto the dense region between the spout and the vessel wall where they move slowly downward and radially inward (toward the spout) as a loosely packed bed. Some of the gas penetrates into the dense region and travels upward, countercurrently with the solid particles. Solids cross flow from the dense region into the spout occur all along the bed height. This cross flow is more visible in the upper portion of the bed due to the higher energy of gas entering the bed. Figure 2 illustrates spouting of

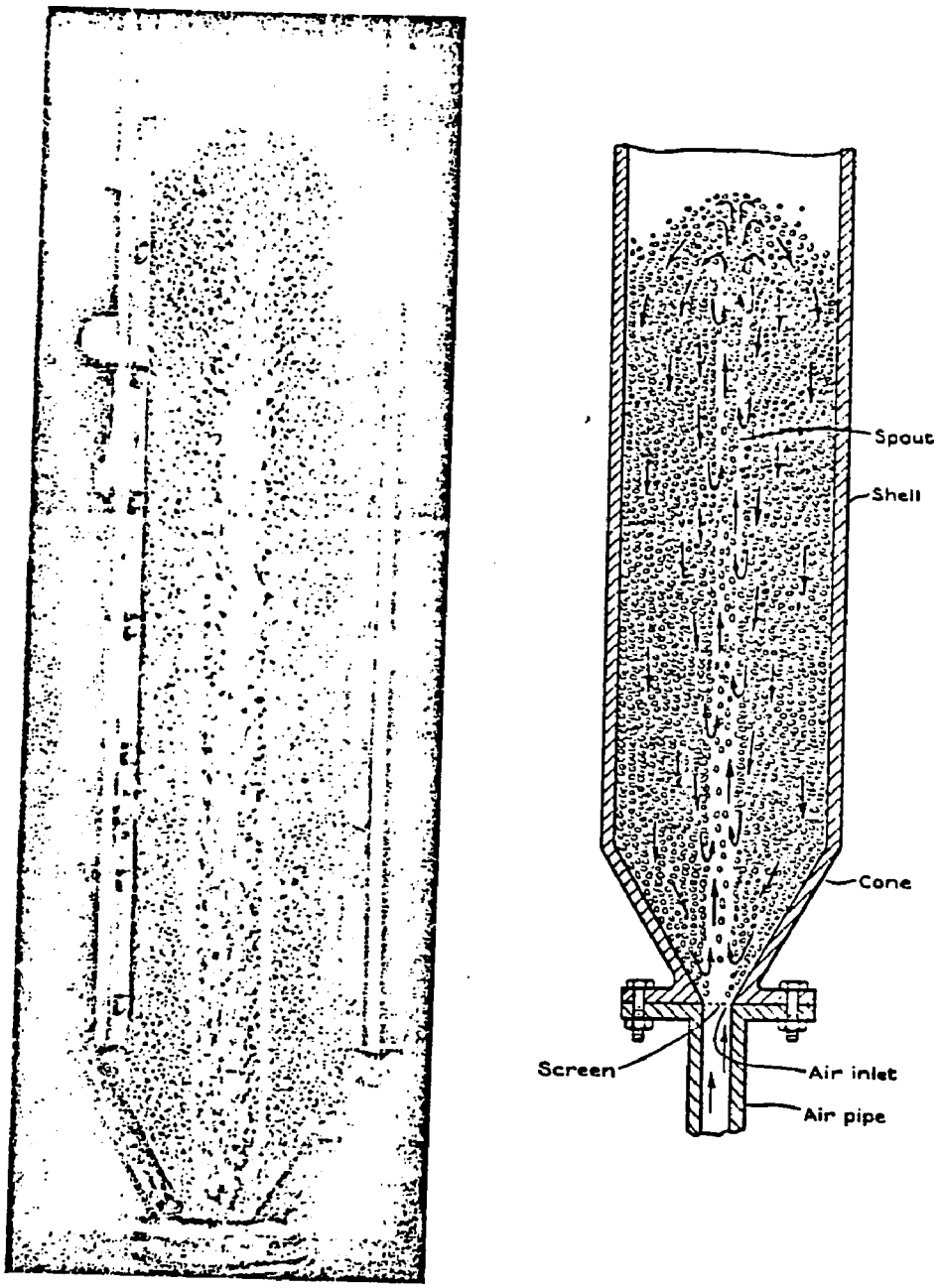

Figure 2 Spouted wheat bed in a 6" sectional column

wheat in a semi-cylindrical column as shown by Mathur and Gishler (1955a).

1.2 The Effect of Gas Flow on Bed Condition

The flow regime of the bed is mostly determined by the gas flow through the pressure drop across the bed. A typical pressure drop curve given by Mathur and Gishler (1955a) is shown in Figure 3 and can be described as follows: starting from point A and increasing the gas flow, the pressure drop rises directly to point B. This portion of curve corresponds to the percolation of gas through the stationary particles and packed bed like behavior of the bed. Further increase in gas flow causes the pressure drop to decrease sharply to point C. This reduction of pressure drop indicates to the formation of a short internal spout at the bottom of the bed. The height of this internal spout increases with increase in gas flow so that for gas flow corresponding to point C a noticeable expansion of the solid bed takes place due to the solid displacement in the central core. Increasing the gas flow from point C to point D causes movement of particles at the top of the bed. A sharp decrease in pressure drop is observed by increasing the gas flow further to point E where the spout breaks through the top of the bed. After that the pressure drop is seen remains constant where the gas flow is in-

creased beyond the point E where a steady spout has been achieved. If the gas flow is now reduced, the bed operates under a steady spout condition for gas velocities lower than that at point E until we reach point E'. This is because the particle in the central core do not need an "excess energy" to disintegrate and the interparticle contacts had been broken when the spout formed. Point E' corresponds to the minimum gas velocity for which spouting is possible. Reducing of gas flow beyond this point causes a sharp increase in pressure drop owing to the collapse of the spout. Point D' indicates to the dissappearance of the internal spout and the whole bed behaves as a packed bed beyond this point. Once the gas flow is stopped the bulk solid in the bed consolidates (gains strength) and a different gas velocity will be required to form the spout again due to newly acquired yield strength (consolidation and interlocking). The pressure drop curve for the decreasing gas flow is lower than that for the increasing gas flow because the density of the packing has been reduced by introducing the gas at the bottom of the bed.

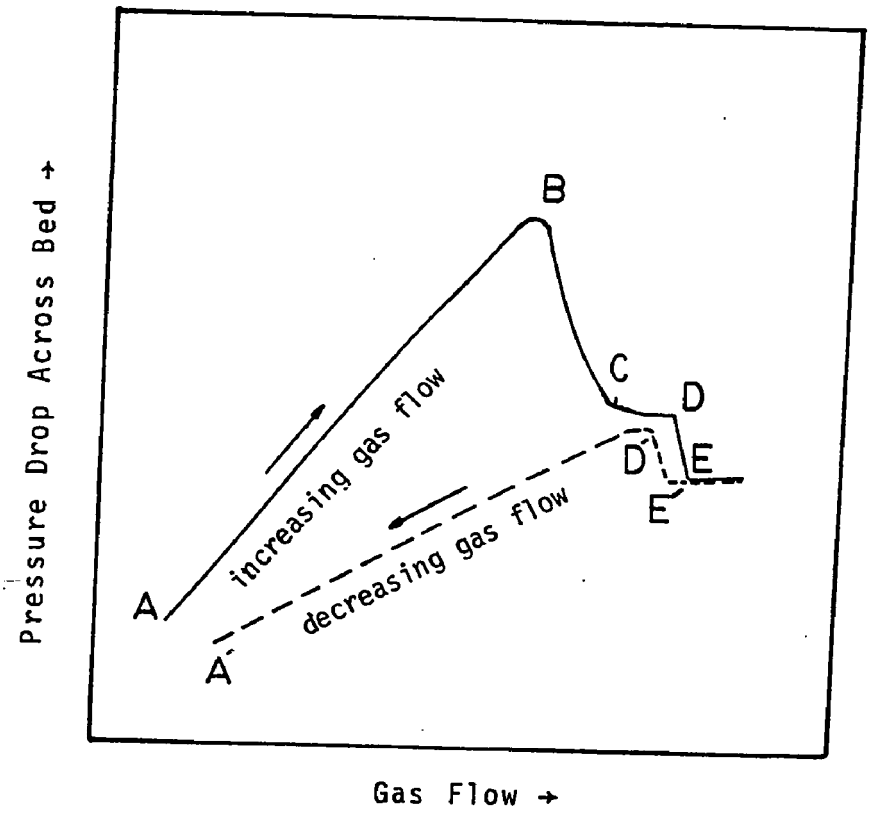

Figure 3 Effect of gas flow on pressure drop in a bed of solids (Based on Mathur and Gishler, 1955)

1.3 Literature Survey

The spouted bed technique was first introduced by Mathur and Gishler (1955b) as a method for the drying of wheat. In 1951 Western Canada produced a large wheat crop after a wet fall and the moisture content of the wheat was well above that considered safe for storage. At the Lakehead terminal elevators alone, about 110 million bushels were dried (Peterson 1962). The incident created a good market for a small compact high capacity continous driers for farms or small elevators. Mathur and Gishler proposed the spouted bed technique in 1954 following preliminary experiments on fluidizing wheat. The experiments were done on a one foot diameter spouted bed wheat drier and the results were published by them in 1955 after being presented to the Society of Chemical Industry, London in 1954. The variables studied by them were: feed moisture content, feed rate, bed depth and inlet air temperature. The first commercial spouted bed were installed in Canada in 1956.

Soon after the introduction of the spouted bed as a technique for wheat drying, different analyses made to study the behavior of the spouted beds, although the applications were somewhat limited to drying processes. The main advantage of employing the spouted bed technique for

drying processes had been suggested to be the possibility of high drying rates by using a relatively high inlet gas (air) temperature as a spouting medium without causing damage to the solid particles (wheat). In 1955 Mathur and Gishler (1955b) proposed the spouted beds as a technique for contacting gases with coarse and uniformly sized solid particles which are not amenable to fluidization. In 1957 Cowan, Peterson and Osberg studied the applicability of spouted beds for drying of wood chips, used in paper making industries, usually containing 150 percent moisture (dry basis). They concluded that using the spouted bed technique to reduce the moisture to 50 percent (d.b.) would save up to $6.00 per ton of dried chips in the cost of transportation (few hundred miles by rail, from the site to the mill), credited against the cost of drying. Klassen and Gishler (1958) compared the heat transfer from the column wall to bed in spouted, fluidized, and packed systems. The results of their comparison indicated to a sharp increase in the heat transfer coefficient at the point of transition from a packed bed to a moving bed. Comparison between fluidized bed and spouted bed, on the other hand, showed that the maximum heat transfer coefficient was from 25-75% higher in a fluidized bed than for a spouted bed under similar flow conditions. This was due to greater turbulance of the particle in fluidized bed

compared to smooth, regular, laminar like motion of the particle at the wall in a spouted bed. Ghosh and Osberg (1959) continued Klassen and Gishler studies on heat transfer in water spouted beds. Similar analysis by Malek and Lu (1964) indicated that under similar conditions the heat transfer coefficient between the column wall and the bed is from 10 to 66% higher for a fluidized bed than for a spouted bed, but the mass flow rate of gas (air) required for spouting varied from 35-55% of that for obtaining the maximum heat transfer in a fluidized bed.

Late in 50's and during 60's attentions had been very much focused on the flow pattern of gas and solid, factors governing the spouting phenomena, developing correlations describing the variables controlling the spouted bed, as well as experimental and semi-theoretical evaluation of spouted bed parameters. In 1959 Thorley, Saunby, Mathur and Osberg made a rigorous analysis of air and solid flow in a spouted wheat bed. They studied the effect of orifice size, cone angle, bed height and air flow on the performance of a spouted bed, and developed correlations for the maximum spoutable bed depth, minimum spouting velocity, and particle flow lines. Becker (1961) also investigated the laws governing the spouting of coarse particles and after defining some variables developed cor-

relation leading to the maximum spoutable bed depth based on the particles Reynolds number. Malek, Madonna and Lu (1963) estimated spout diameter of a spouted bed for eight materials in two semi-circular columns using air as the spouting medium. The results of their estimation showed that the spout diameter is proportional to the square root of the mass flow rate of air, and based on that they proposed a generalized equation for estimating spout diameter under various conditions. Malek and Lu (1965), two years later, studied the spouting pressure drop and maximum spoutable bed height in three different columns using seven materials and air as the spouting medium, and proposed that the spouting pressure drop depends on the air density, solid and bed properties, and is independent of the column and the orifice diameter. They also proposed an equation for the maximum spoutable bed height based on the experiments and related that factor to the column orifice and particle diameters, density and shape factor of particles, and air density. The result of their analysis had an average deviation of 11% from those by Becker (1961). Smith and Reddy (1964) made a systematic experimental study on the characteristic behavior and the spoutability of mixed particle size material (mean diameter from .0134 to .104 inches and density from 65.8 to 246.3 lb/ft^3). They developed a new correlation for

the minimum spouting velocity and found that Mathur-Gishler (1955a) correlation was not very successful in predicting their experimental findings. Singiser, Heiser and Prilling (1966) applied the concept of spouted bed technique as an air-suspension tablet coater and found not only the system would reduce overall costs, but it also results more uniform production. Mamuro and Hattori (1968) analysed the behavior of fluid flow in a spouted bed both theoretically and experimentally. They proposed a model of the balance of forces acting to the dense region and based on that obtained equations for fluid velocity and pressure drop. They claimed that the fluid flow data obtained by them and Becker (1961), and the pressure drop data by Malek et al (1965) proved that the proposed model was useful to explain the characteristics of the spouted beds. Maximum spoutable bed depths(MSBD) for mixed particle size beds were analysed by Reddy, Fleming and Smith (1968). They found experimentally that the MSBD reaches a peak at a critical particle Reynolds number of about 70, while their theoretical prediction based on the Smith-Reddy correlation (1964) estimated critical Reynolds number of 68 for MSBD. They also concluded that in contrast to Becker's correlation (1961) the MSBD is independent of the inlet diameter and the column geometry.

In 1969, Lefroy and Davidson studied the mechanism of spouted beds exclusively. They experimentally found that the fluid pressure variation just outside the spout is well described by a quarter cosine wave, when they used a flat based semi-cylindrical 30.5 cm diameter bed. Using the spout pressure distribution as a boundary condition, they calculated the pressure distribution in the dense region and concluded that for beds having a height/diameter ratio greater than two it would be reasonable to assume a uniform pressure across a horizontal section. They also used particle and fluid force balances at the spout associated with a yield criterion employed in soil mechanics to describe equilibrium of the spout wall. Lefroy and Davidson (1969) were the first investigators that employed a soil mechanics yield criterion, although in very primitive form, to the spouted beds. They proposed a mechanism for particle entrainment and employed that mechanism in a particle and fluid momentum balance to develop approximate equations for maximum spoutable bed height and spout diameter. They also were first in applying a force balance to develop an equation for the spout diameter. Bridgwater and Mathur (1972) derived a theoretical equation for spout diameter from a force balance analysis which took into account the solid stresses based on hopper flow of solids, in addition to

the hydrodynamic forces. Their analysis applied to a region away from both the upper free surface and conical bottom (deep bed approximation employed in hopper flow). They also used the concept of stresses born by the solids (effective stresses in soil mechanics) and the simple law of friction to develop their model.

In the 4th joint Chemical Engineering Conference AIChE-CSChE, Vancouver, Canada, September 9-12 in 1973, for the first time in an international conference two sessions were completely been programmed to the spouted bed techniques. In the past, papers on spouted beds were usually been included in sessions or symposia on fluidized beds. However, by that time, spouted beds had reached a stage of development where spouting was recognized as a fluid-solid system in its own right. Eleven papers by nine countries other than Canada were presented in the symposium which was divided into characterization of the dynamics of spouted beds with emphasis on residence time distribution of the gaseous phase and the variations introduced by liquid phase spouting, and examples of industrial applications on spouted beds. The paper by Mathur and Epstein (1974a) on developments in spouted bed technology indicated that applications of spouted beds had gone far beyond the drying process. In this paper seven-

teen industrial applications of spouted bed were reported with a brief description of each application, under the broad categories of physical operations (diffusional and thermal) and chemical processes (solids as reactives and solids as heat carrier or catalyst), including: drying of granular material, granulation, reaction granulation, tablet coating, gas cleaning, solids blending, shale pyrolysis and charcoal activation.

McNab and Bridgwater (1974) constructed a mathematical model for the analysis of the stresses in the annular space of a cylindrical spouted bed applying the principle of soil mechanics. They were the first investigators who considered the annular material as a loosely packed assembly of particles with its behavior described by effective stress applying the Mohr-Coulomb failure criterion employed in soil mechanics. The model extensively used the principle of soil mechanics and the rules governing the flow of bulk solids in hoppers to approximate the position of the spout wall. They used the deep bed approximation, applied to the hoppers, together with a constant effective weight of material to uncouple the height and radius effect. The deep bed approximation assumes that a region exists in a hopper far from both the upper free surface and the base in which all stresses are independent of height.

Mathur and Epstein in 1974(b) attempted to assess the general applicability of the different correlations of spouted bed variables, developed to date, by performing many experimental work. They concluded that Becker's equation (1961) for MSBD gave good agreement with the obtained data over a wider range of experimental conditions than any of the other equations. Same authors at the same year condensed most of the works done to date and published the only book (Mathur and Epstein 1974c), yet, titled "Spouted Beds".

Lim and Mathur (1974) were the first to attempt to develop a theoretical model of a spouted bed chemical reactor involving gas phase reaction with solid particles as catalyst or heat carrier. They used a generalized one dimensional hydrodynamic model to describe the gas phase flow pattern, necessitated by the kinetic model. Later, in 1976, these workers used helium tracer experiments to conclude that the residence time distribution of gas in the annulus is better described by considering the radial gradients effect and curved streamlines originating on the spout boundary. The same workers (1978), based on the same concept, developed a mathematical model to calculate flow path and residence time distribution of solid particles in the annulus from particle velocity-at-wall data. They also

developed a model for the motion of solid particles in the spout using an improved version of the Thorley force balance (1955). Calling the curved streamlines the "streamtube model" and the vertically upward gas flow the "one dimensional model", Piccinini, Grace and Mathur (1979) measured chemical conversion of ozone decomposition on an iron oxide catalyst. A simple first order kinetic reaction was assumed and the experimental results showed good agreement with predictions from both streamtube and one dimensional models. However, their data were not adequate to discriminate between the two models and provide a confident theoretical basis for the design of spouted bed reactors.

The theory of Mamuro Hattori (1968) was extended by Grbavcic et al. (1976) to predict the fluid flow pattern, minimum spouting velocity, and the spouting pressure drop for beds having a height lower than the maximum spoutable height (H_m). They found the new extended theory in good agreement with their experimental data for both gas and water spouted beds and also developed a correlation for H_m in a water spouted bed which was found to fit the literature data of gas spouted systems. In 1978 Epstein, Lim and Mathur made a critical examination of the approaches used by different investigators for the prediction of fluid

flow distribution and pressure drop in spouted beds, and rationally modified some of the models to increase their acceptability and conform to experimental observations. They found that Mamuro-Hattori force balance model (1968) is deficient in neglecting the shear forces at the spout and column walls. Suciu and Patrascu (1978) used a high speed camera to measure particle velocities along the cylindrical length of a column and based on the experimental results developed a correlation which related the particle velocity in the dense phase to the minimum spouting velocity and relative bed height (H/H_m). In 1979 McNab and Bridgwater applied the Walker's method for bins to propose a theory for effective solid stresses in the annular region of a cylindrical spouted bed. They employed the concept of distribution factors, as used by Walker for bins, to relate stresses at the spout wall and the vessel wall to the mean effective stress on a horizontal plane. Effects of factors such as bed height, fluid pressure gradient, frictional conditions at spout and vessel walls, and the angle of internal friction of the solid particles on the stresses were also examined. However, they did not pursue a complete solution which requires solution to partial differential equation arising from force balances, because of the computational difficulties. King and Harrison (1980) made some experimental work on spouting at

elevated pressure and suggested a correlation similar to the Mathur and Gishler (1955b) for minimum spouting velocity at elevated pressure. Littman et al. (1977, 1979, 1981) in a series of theoretical and experimental work attempted to predict the maximum spoutable bed height for spherical and non-spherical particles. Morgan and Littman (1980) derived a general relationships for the minimum spouting pressure drop ratio, $\Delta P_{ms}/\Delta P_{mf}$, and a new spout-annulus interfacial condition which approximately satisfied the quarter cosine relationship. Littman et al. (1981) developed an axisymmetric fluid flow model in the annulus part of a spouted bed based on non-Darcy flow, and new spout-annulus interface as well as the top of the annulus boundary conditions. Their experimental results showing that as the inlet flow rate is increased above the minimum, the local annular velocities do not change and the average spout diameter increases.

In sum, although extensive research studies have been directed toward the behavior of spouted beds, the fundamental aspects of the mechanisms of particle motion have not been investigated in depth and are poorly understood. Few attempts have been directed to this fundamental question and even those have been hampered by the complexity of the nature of the problem. It is hoped that the outcome

of this research study be able to bridge this gap and led to a fundamental picture of spouted beds.

CHAPTER TWO

2.0 BASIC RULES IN SOIL MECHANICS, PLASTICITY AND FLOW OF BULK SOLIDS

This chapter is intended to state tne basic principles and define the terms used in soil mechanics, plasticity and flow of bulk solids that were employed in developing the models.

2.1 Definitions and Concepts

2.1.1 Principal stresses

At any material point subject to stress there are three mutually prependicular planes on which there are no shear stresses. These planes are called Principal Stress Planes. The axes normal to these planes are called principal axes and their directions principal directions. The stresses normal to the principal stress planes are called principal stresses and are denoted by σ_1, σ_2 and σ_3. These are discussed in most textbooks of strength of materials such as Crandall and Dahl (1959). The largest of these stresses is called major principal stress σ_1, the smallest is called minor principal stress σ_2, the third is called the intermediate principal stress σ_3. Because of uncertainity of influence of the intermediate principal stress upon the strength and stress-strain properties of soil (Lambe & Whitman 1979), most of the

work done are primarily in terms of σ_1 and σ_2.

2.1.2 Mohr circle

It is possible to describe the state of stress at a point using the static equations if the major and the minor principal stresses are specified both in magnitude and direction (in the case of two-dimensions). Figure 4-a shows σ_1 and σ_2 together with normal and shear stresses in an arbitrary direction. The static equations derived in most strenght of materials textbooks (e.g., Crandall and Dahl, 1959, pp130-138) and represented by equations (2.1.2-1) and (2.1.2-2) provide a complete (two dimensional) description of the state of stress. These equations describe a circle, as shown in Figure 4-b.

$$\sigma_\theta=\sigma_1\cos^2\theta+\sigma_2\sin^2\theta = \frac{\sigma_1+\sigma_2}{2} + \frac{\sigma_1-\sigma_2}{2}\cos2\theta \qquad (2.1.2\text{-}1)$$

$$\tau_\theta = (\sigma_1-\sigma_2)\sin\theta\cos\theta = \frac{\sigma_1-\sigma_2}{2}\sin2\theta \qquad (2.1.2\text{-}2)$$

Shear stress is positive when counterclockwise and angle is measured counterclockwise from the axis direction. Any point such as A represents the stress on a plane whose normal is oriented at an angle θ to the direction of the major principal stress. For any given point A, the center of the circle is located at a distance corresponding to

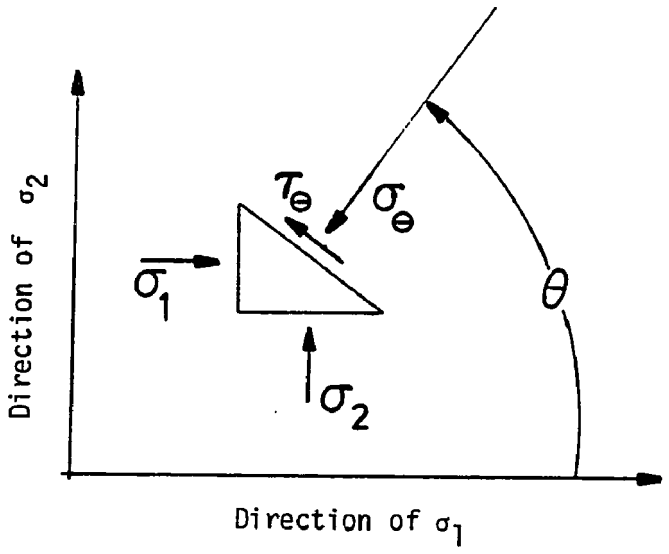

(a)

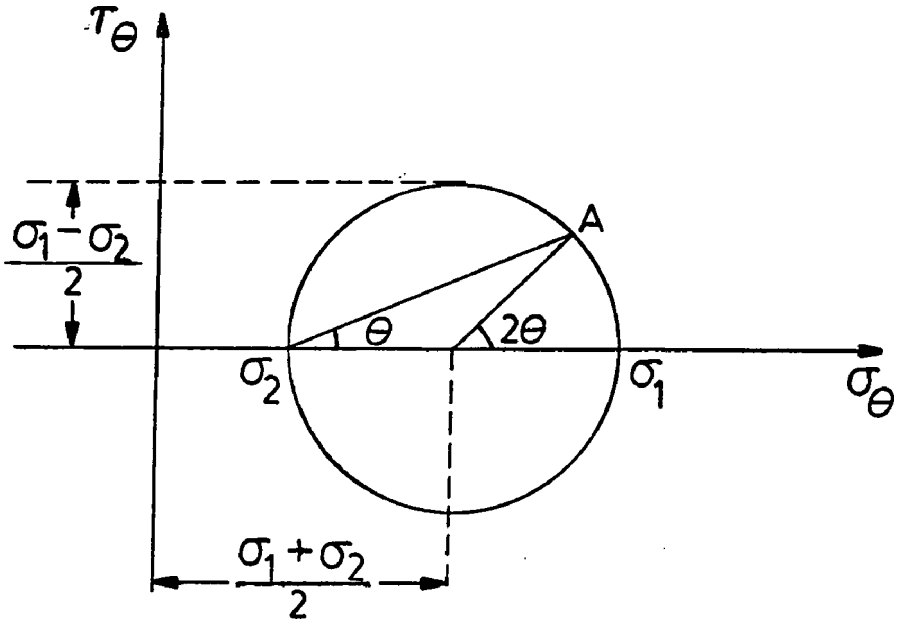

Figure 4 Mohr circle of stress representation

a) equations for state of stress at a point
b) Mohr circle for state of stress at a point

the mean of the principal stresses σ from the origin of $(\sigma_\theta, \tau_\theta)$ coordinate and its radius represents the maximum shear stress at point A. This graphical representation of the state of stress is known as the "Mohr Circle" and it has extensive applications in soil mechanics.

In order to simplify the Mohr circle application the pole of the diagram, point P, is defined as the intersection of the circle with a line through the point representing σ_1 (or σ_2) and parallel to the major principal plane (or minor principal plane). Having determined the pole of the diagram, the stresses in any direction can be found using the pole by simply drawing a line parallel to the plane on which the stresses act. For example, in Figure 5 the horizontal stress σ_x is obtained by drawing the line PE parallel to the vertical axis, the plane on which σ_x acts. Similarly the vertical stress σ_y is obtained by drawing PF parallel to the horizontal axis. Notice that line EF is a diameter of the circle.

2.1.3 Effective stress

The concept of effective stress employed extensively in soil mechanics basically treats a saturated soil as a two-phase continuum. The principle of effective stress as used in soil mechanics and described by Lambe & Whitman

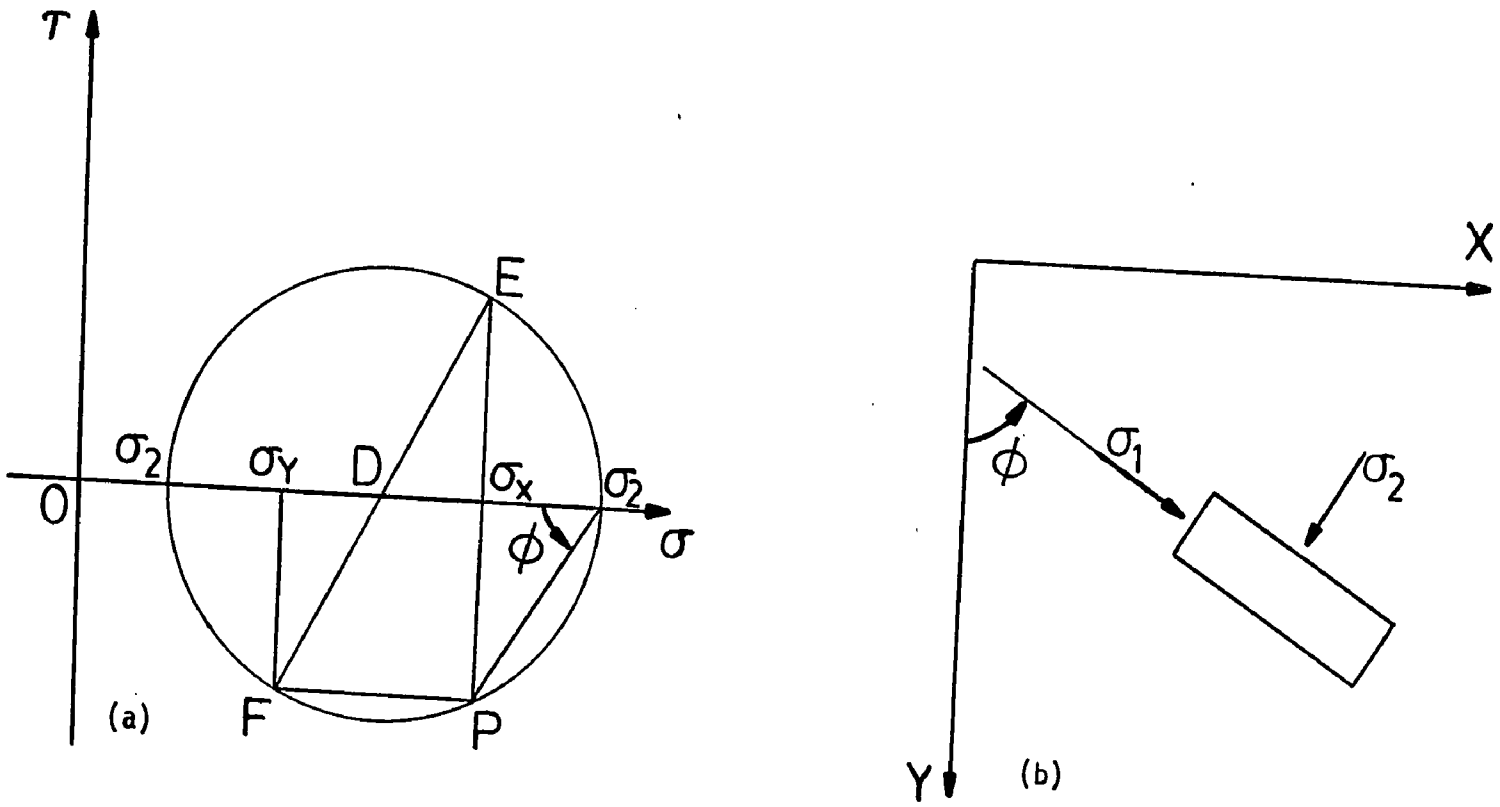

Figure 5 Determination of pole of a Mohr circle
a)Mohr stress circle
b)a physical element

(1979) or Schofield & Wroth (1968) states that the total stress normal to any plane in the soil is the sum of the (water) pore-pressure and the effective stress which controls certain aspects of soil behavior, mainly compression and strength. Experiments by many investigators (Lambe & Whitman, 1979) have shown that effective stress is closely related to the stress transmitted through the mineral skeleton and is equal to the net stress born by the particles. For this reason the effective stress is often called intergranular stress.

2.1.4 Strains and principal strains

Applying forces to a medium not only produce stresses but also displace its particles. The normal strains are defined as the limit of the elongation per unit length of a line element as its length tends to zero. If the displacements in three directions are denoted by l_x, l_y and l_z the normal strains will be

$$\epsilon_x = \frac{\partial l_x}{\partial x}, \quad \epsilon_y = \frac{\partial l_y}{\partial y}, \quad \epsilon_z = \frac{\partial l_z}{\partial z} \qquad (2.1.4\text{-}1)$$

where the normal strains are taken to be positive in compression.

The deformation also causes, in general, a change between two line elements. If the line elements are in the

directions of x and y the decrease of the originally right angle is called a shear strain:

$$\gamma_{xy} = \frac{\partial l_y}{\partial x} + \frac{\partial l_x}{\partial y} \qquad (2.1.4\text{-}2)$$

and similarly:

$$\gamma_{zx} = \frac{\partial l_x}{\partial z} + \frac{\partial l_z}{\partial x}, \qquad \gamma_{yz} = \frac{\partial l_z}{\partial y} + \frac{\partial l_y}{\partial z}$$

If the displacement are changed to the velocities in the three directions u,v and w in the preceding discussion the strain rates are written as

$$\dot{\epsilon}_x = \frac{\partial u}{\partial x}, \qquad \dot{\epsilon}_y = \frac{\partial v}{\partial y}, \qquad \dot{\epsilon}_z = \frac{\partial w}{\partial z} \qquad (2.1.4\text{-}3)$$

$$\dot{\gamma}_{xy} = \frac{\partial v}{\partial x} + \frac{\partial u}{\partial y}, \quad \dot{\gamma}_{yz} = \frac{\partial w}{\partial y} + \frac{\partial v}{\partial z}, \quad \dot{\gamma}_{zx} = \frac{\partial u}{\partial z} + \frac{\partial w}{\partial x}$$

At any strained point there exist three mutually orthognal directions which remain orthognal after deformation. These directions are called principal directions of strain and denoted by ϵ_1, ϵ_2, ϵ_3.

2.1.5 Plane strain

If a system of rectangular coordinates x, y, z can be chosen for the plastic flow of a material so that the velocity components u and v are independent of z, and w

vanishes identically flow is called plane. Under these circumstances the deformation takes place only on plane xy, and it can be written:

$$\begin{matrix} \dot{\epsilon}_x, & \dot{\epsilon}_y, & \dot{\gamma}_{xy} \\ \dot{\epsilon}_z = & \dot{\gamma}_{yz} = & \dot{\gamma}_{zx} = 0. \\ \tau_{yz} = & \tau_{zx} = 0. \end{matrix} \quad \text{independent of } z \qquad (2.1.5\text{-}1)$$

and condition of incompressibility reduces to

$$\dot{\epsilon}_1 + \dot{\epsilon}_2 = \dot{\epsilon}_x + \dot{\epsilon}_y = 0. \qquad (2.1.5\text{-}2)$$

or in terms of velocity components

$$\frac{\partial u}{\partial x} + \frac{\partial v}{\partial y} = 0. \qquad (2.1.5\text{-}3)$$

2.2 Stress-Strain Behavior of a Soil Mass

The true behavior of stress-strain of a soil mass is quite complicated. The stress-strain relation mainly depends on the loading conditions such as loading, unloading and reloading as well as the type of loading, i.e. isotropic compression, confined compression, triaxial compression or direct shear. The relation is also different for various type of soil. Extensive theoretical and experimental work have been done by many investigators (Lambe & Whitman, 1979) to explain both the mechanism of deformation of granular soils and characteristics of the stress-strain relationship. Only a brief background for the type of relation used in the models is provided here.

The investigators in soil mechanics have concluded that the soil will behave in a first approximation as an elastic material with the proper choices of the Young's modulus E, shear modulus G and Poisson's ratio ν corresponding to the particular loading. The stress-strain relation for an elastic material can be written as

$$\varepsilon_x = \frac{1}{E}\left[\sigma_x - \nu(\sigma_y+\sigma_z)\right]$$

$$\varepsilon_y = \frac{1}{E}\left[\sigma_y - \nu(\sigma_z+\sigma_x)\right]$$

$$\varepsilon_z = \frac{1}{E}\left[\sigma_z - \nu(\sigma_x+\sigma_y)\right]$$

$$\gamma_{xy} = \frac{\tau_{xy}}{G} \qquad (2.2\text{-}1)$$

$$\gamma_{yz} = \frac{\tau_{yz}}{G}$$

$$\gamma_{zx} = \frac{\tau_{zx}}{G}$$

Clearly, when applying to a soil mass good judgment is needed for choosing values of the modulus and Poisson's ratio. Figure 6 shows results of a triaxial compression test upon a well graded sand from Libya (Lambe & Whitman 1979). This Figure shows a typical stress-strain curve of

a soil mass.

2.3 Shear Strength and Mohr Coulomb Failure Law

Investigation since 1773 have indicated that granular soil is "frictional" and the resistance to sliding at each contact point is proportional to the normal force at that point. The behavior of granular soil deviates from being purely frictional because of the effect of the consolidation stress upon the grain interlocking. This interlocking contributes to the overall resistance. Increasing the consolidation stress decreases the interlocking by flattening the particles contact points. Even though this action produces a denser specimen, it makes it easier for shear deformations to occur.

The state of stress at the peak point of the stress-strain curve, point P of Figure 6, usually defines the strength of a soil. Otto Mohr (see Lambe & Whitman, 1979) who first wrote about general strength theory in 1882 proposed the concept of representing the strength of a soil mass by Mohr circles representing the state of stress at the peak points of different consolidation stresses. These Mohr circles are called critical Mohr circles. Figure 7 shows six critical Mohr circles with the Mohr envelope. The physical meaning of the Mohr envelope can be

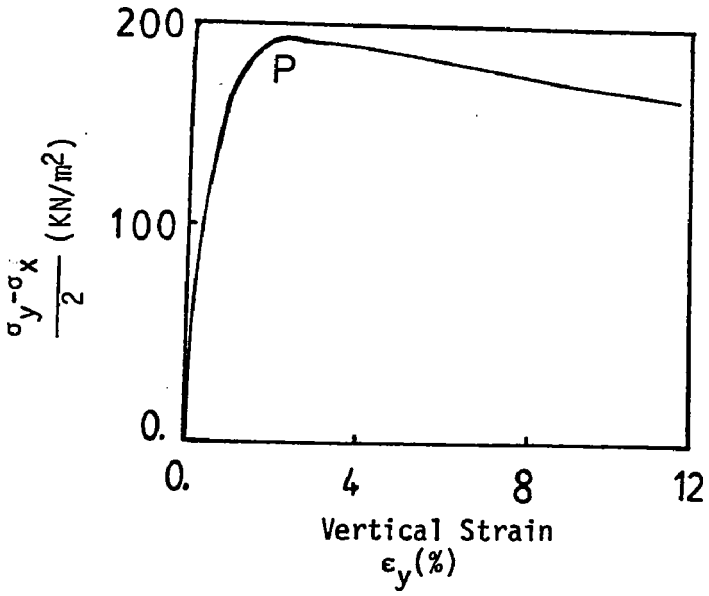

Figure 6 Results of a triaxial compression test upon a well graded calcareous sand from Libya (Lambe & Whitman, 1978)

described as follows:

1- The state of stress whose Mohr circle lies completely below the Mohr envelope corresponds to a soil that will be stable under that state of stress.

2- If the state of stress changes such that its corresponding Mohr circle become just tangent to the Mohr envelope then the soil has developed a full strength on some plane through its mass. This plane is called failure plane and makes an angle of θ_{cr} with the major principal plane. Figure 8 shows a failure plane and the corresponding Mohr circle representation with the shear and normal stresses on the failure plane. These stresses are called the limiting or yield stresses.

3- The state of stress within a soil mass whose Mohr circle intersects the Mohr envelope of that soil is not admissible. It would be impossible to impose such a state of stress without causing an unlimited strains, i.e. failure.

The concept of limiting stress condition developing on the failure plane was first introduced by Coulomb in 1773 as the "critical equilibrium theory". He applied the

theory to determine the pressure of a fill bounded by a horizontal plane on a vertical retaining wall. His solution was based on the assumption that there should exist a plane surface of rupture, and based on this he introduced the "theory of slip" (see Schofield & Wroth, 1968). Rankine in 1857 presented the concept of slip surfaces and found the condition of limiting equilibrium.

The limiting stress condition represented by the Mohr envelope in general is a curved line and may be written in a functional form as

$$\tau_{ff} = f(\sigma_{ff}) \qquad (2.3\text{-}1)$$

where τ_{ff} and σ_{ff} are the failure shear and normal stresses acting on the failure plane. However, for most practical calculations regarding the stability of a soil mass, the functional form of the Mohr envelope is approximated by a straigh line. Thus the strength is expressed by the Mohr-Coulomb failure law:

$$\tau_{ff} = \sigma_{ff}\tan\phi + c \qquad (2.3\text{-}2)$$

where ϕ is the angle of internal friction or angle of shearing resistance and c is the cohesion or cohesion intercept. Equation (2.3-2) approximating the Mohr envelope by a straight line of slope ϕ and intercept c is widely

used for granular soil and at the same time is one of the most controversial equations employed in soil mechanics. The degree of approximation depends on the range of σ_{ff} of interest. Experiments have shown that the Mohr envelope curvature is greatest for dense granular soils and decreases as a soil becomes looser (Scott, 1963).

The soil is called cohesionless if the Mohr envelope passes through the origin of the Mohr diagram. A specimen of such a soil will not stand as a cylinder if the confining (consolidating) pressure is zero. Using the Mohr-Coulomb failure law for a cohesionless soil, the strength can be expressed simply by:

$$\tau_{ff} = \sigma_{ff}\tan\phi \qquad (2.3\text{-}3)$$

Equation (2.3-3) had been used by Coulomb (Schofield & Wroth 1968, Ch.8 and 9) for a cohesionless soil in his first paper in 1776, and since then has been applied to granular soils by many investigators in soil mechanics. Coulomb's original assumption cosidered the soil as a rigid homogeneous material which could rupture into separate blocks. He then applied equation (2.3-3) to the rupture plane.

Equation (2.3-2) expresses the strength of a cohesive soil by two parameters ϕ and c suggesting that both cohe-

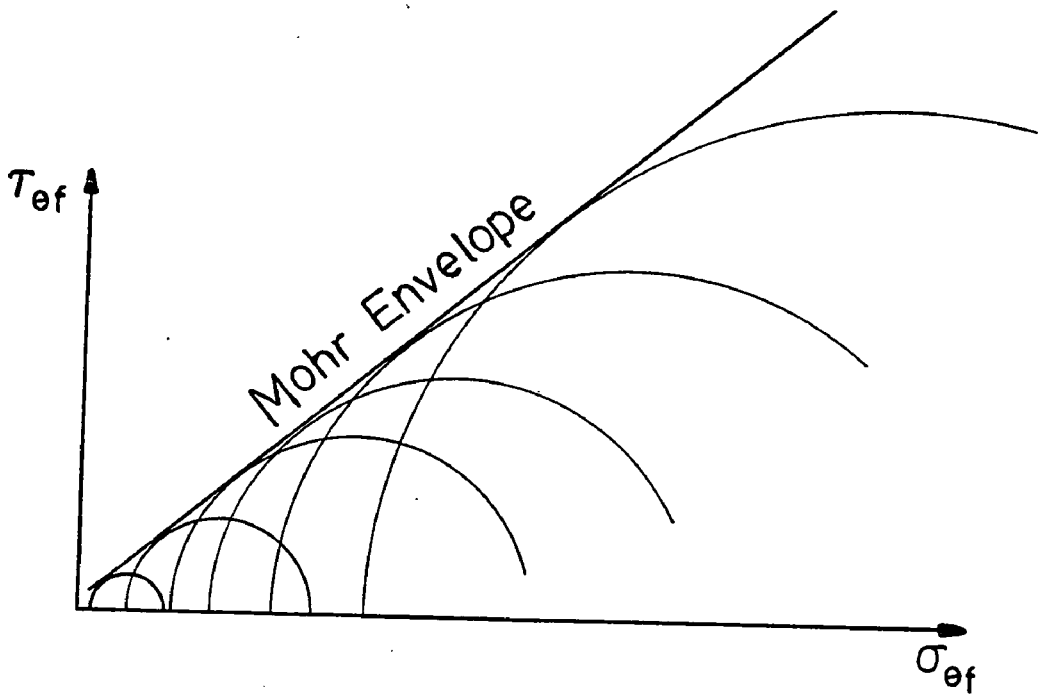

Figure 7 Critical Mohr circles and the Mohr envelop

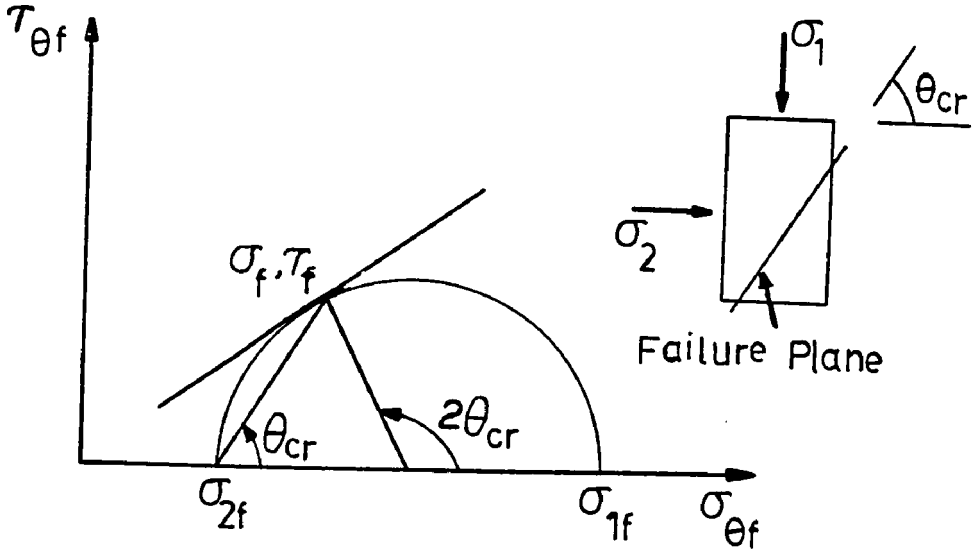

Figure 8 Stresses at failure

sion and friction must be overcomed during slip along the rupture surface. Equation (2.3-3) on the other hand indicates that to express the strength of cohesionless soil only one parameter ϕ need to be specified and only friction must be overcomed during slip along the rupture surface. Figure 8 shows the state of stress at failure for a cohesionless material which the strength (yield function) has been expressed by the Mohr-Coulomb failure criterion. From this Figure it can be easily shown that

$$\frac{\sigma_{1f}}{\sigma_{2f}} = \frac{1 + \sin\phi}{1 - \sin\phi} \qquad (2.3\text{-}4)$$

Equation (2.3-4) was first recognized by Rankine who considered soil as a continuous body. Rankine studied soil without cohesion or pore-pressure and asserted that when the ratio of principal stresses reaches its peak value, given by equation (2.3-4) the obliquity of the stress vector on any plane could not exceed the angle of friction ϕ. Schofield and Wroth (1968) generalized Rankine's equation using Mohr circle of effective stress. They introduced the parameter $H=c.\cot\phi$ and obtained (Figure 9),

$$\frac{\sigma_{1f} + H}{\sigma_{2f} + H} = \frac{1 + \sin\phi}{1 - \sin\phi} \qquad (2.3\text{-}5)$$

and named it the Mohr-Rankine criterion for peak effective stress ratios in soil about to fail. The importance of

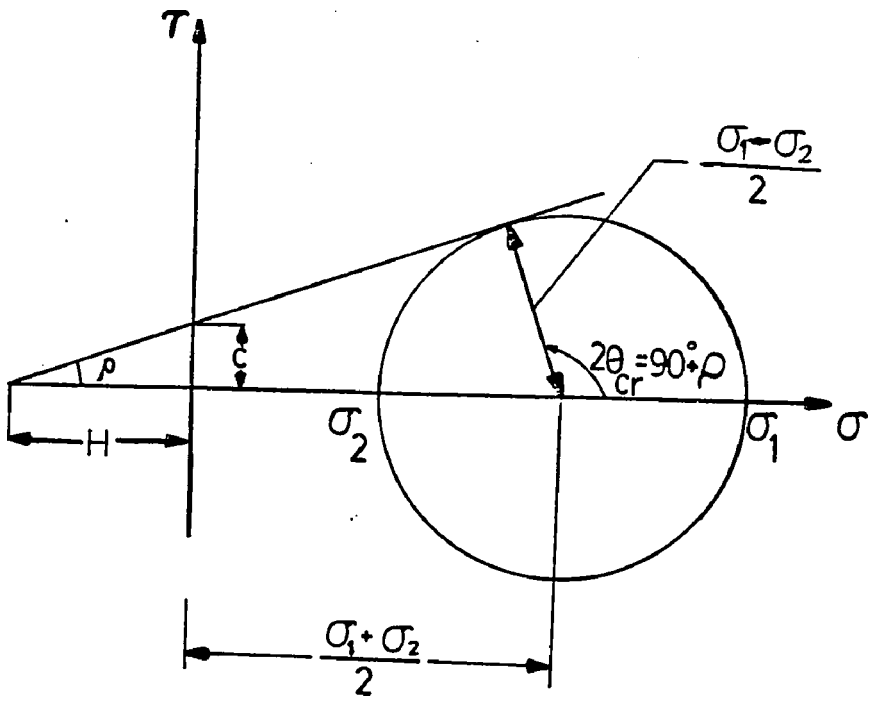

Figure 9 Relations between ρ and principal stresses at failure "The Mohr-Rankine Criterion"

the Rankine's analysis lies on the Coulomb's original assumption of a soil about to fail. Like Coulomb, Rankine considered soil as an elastic plastic continuous medium which became a basis for the later suggestion of Drucker, Gibson, and Henkel (1957) that soil behavior can be described by a theory of plasticity.

It is of greatest importance to notice that the failure plane, or slip line, described here, in general is not the plane upon which shear strains become concentrated when the soil fails. The difference between the two planes have been studied by workers such as Rowe (1963). The physical and mathematical interpretation of these planes is considered in detail in Chapter 5.

2.4 Flow of Bulk Solids, Soil Mechanics and Plasticity

The motion of solid particles in the annular region of a spouted bed is very similar to the flow of bulk solids in bins and hoppers (Bridgewater and Mathur, 1972). The word flow here refers to a slowly deforming medium. We discuss here the rules governing flow of bulk solids in bins as well as similarities and dissimilarities of these rules with the principles of soil mechanics and plasticity. It is also intended to recognize the fundamental differences between flow of bulk solids and fluids flow.

At the end of the nineteenth century when there was a need to store large quantities of grain, the first major studies related to the storage of bulk solids were performed by Janssen (see Hancock and Nedderman, 1974) and Airy (1897). These studies were mainly concerned with the wall pressures affecting the structural design of silos and bins. Since then the problem of proper structural design of silos and hoppers as well as the subject of flow of bulk solids have been studied extensively by many workers. A complete list of references may be found in the publications of Jenike and Johanson (1968), Jenike (1964), and in the review articles by Nedderman et al. (1982) and Tuzun et al. (1982). Specifically the extensive studies of Jenike (Jenike and Jenike et al., 1960, 1961, 1962, 1964) led to the postulation of a flow-no flow criterion of bulk solid and design of storage bins and channels.

Although many of the concepts employed in the theory of bulk solids flow are similar to those found in soil mechanics and plasticity, when applied to bulk solids these concepts undergo important modifications. Like soil, the bulk solids are considered as rigid-plastic material, but the magnitude of the stresses are 100 to 1000 times smaller than those encountered in soil mechanics. Thus,

some of the phenomena not observable in soil mechanics plays a critical role in flow of bulk solids. For instance, the yield loci (or Mohr envelope) can well be approximated by a straight line and while the curvature of this loci is normally undetectable in soil mechanics, it is quite pronounced in flow of bulk solids and its recognition led to the introduction of a new yield locus. This "Effective Yield Locus" proposed by Jenike and Shield (1959) is conceptually different of the yield locus encountered in soil mechanics. Moreover, standard soil mechanics test do not detect the low values of cohesion and a solid possessing a cohesion of 50 pound per square foot (2.394 kPa) is considered to be cohesionless whereas, according to Jenike (1964), bulk solids with that value of cohesion, an angle of internal friction of 30^{o} and a density of 100 pounds per cubic foot form a stable dome across a 3 foot diameter channel that prevents the flow from starting.

When the flow of solid is mentioned one is inclined to assume-by association- that the solid behaves much like a liquid since the word flow is more often associated with fluids than with solids. Such an assumption is incorrect. The mechanical characteristics of solids and liquids differ so much that no easy analogies can be drown. These

differences can be summarized as:

I- Solids have a static angle of friction greater than zero so that they can transfer shearing stresses under static conditions, whereas liquids can not support shearing stresses under static conditions. That is why liquids form level surfaces but solids form piles.

II- In fluids flow the shearing stress is proportional to the rate of shear and independent of the mean pressure, but for a slowly deforming bulk solid the developed shearing stress can usually be considered independent of the rate of shear and dependent on the mean pressure.

III- Many solids when consolidated exhibit cohesive strenght and retain a shape under load, characteristics that are not observed in a liquid.

These are fundamental differences between solid and liquid behavior when flowing, and as Jenike (1964) has suggested a bulk flowing solid has to be considered as a plastic and not a visco-elastic continuum.

2.4.1 Yield locus, effective yield locus, plastic potential and normality

The yield function for a bulk solid assumed to be rigid-plastic, isotropic, frictional, cohesive and compressible in the plastic region is discussed in this section. From it the yield function for a non-cohesive and incompressible bulk solid is then obtained to develop the mathematical model for the flow of solids in the annular region of the spouted bed.

The convention adopted in flow of bulk solids, as in soil mechanics, assumes pressure and compressive strain rates as positive, tension and expansive strain rates as negative.

--Yield locus, yield surfaces

The strength of a bulk solid is described by its yield function. This description named and used by Jenike et al. (1960) as modified rigid-plastic Coulomb solid can be stated as follows: a rigid-plastic solid is one for which there exists a limiting stress function such that stresses lower than those determined by the function cause no deformation, whereas stresses equal to the limiting stresses cause either failure or plastic flow. Stress conditions exceeding the limiting stresses are not permissible.

The proper choice of a yield function had been a major obstacle in the solution of the problems of continuous plastic flow for isotropic, non-work-hardening (perfectly plastic) solids which exhibit an angle of friction greater than zero until late 50's, while this type of problems had been successfuly solved for the case of zero angle of friction (Hill, 1950, Prager and Hodge, 1951, Shield, 1955a). The yield function was a generalization of the criterium of either Von Mises or Tresca (Figure 10a) into a function dependent on the hydrostatic stress. In the principal stress space such a generalization transformed the cylinder of Mises or the prism of Tresca (Figure 10b) into, respectively, a cone or a pyramid (Figure 10c) which were assumed to extend without a bound in the direction of hydrostatic pressure. As a result, the principle of plastic potential, or normality (Jenike and Johanson 1962), required the solid to dilate continously during flow while at the same time retaining its strength properties. Dilation causes loss of strength. Experimental evidence by shear and triaxial tests indicate to the fact that a bulk solid may flow without a change of density (constant volume) as well as with an increase of density (decreasing volume), and that the history of stress and strain do not affect the yield surface in any significant way during flow (Jenike 1961).

a-

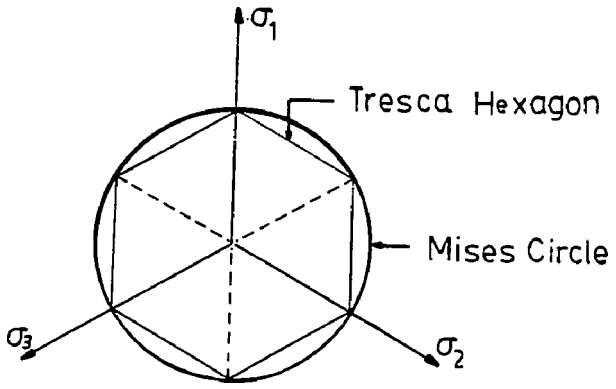

Yield loci of Tresca and Mises

b-

Yield surfaces in stress space

c-

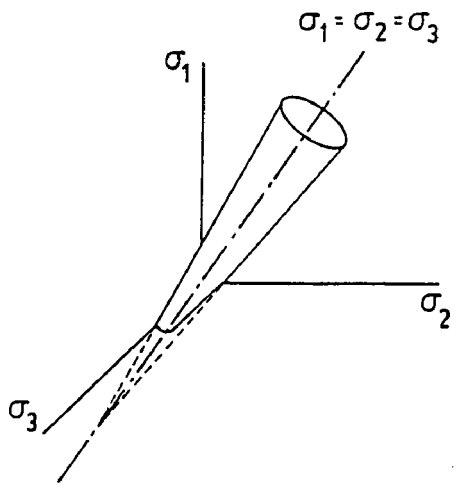

Mises type of extension of Coulomb criterion

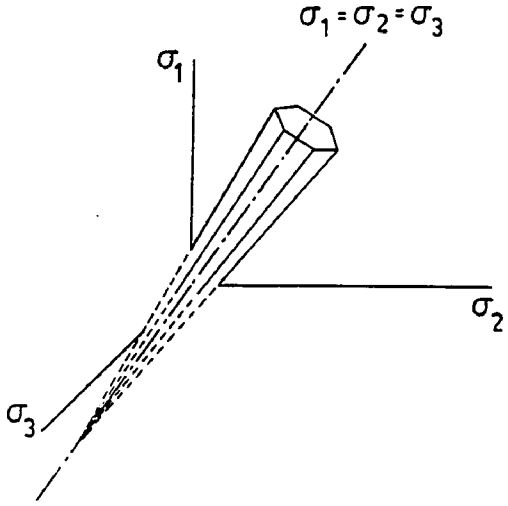

Tresca's type of extension of Coulomb criterion

Figure 1.

A yield surface was proposed by Jenike and Shield (1959) to overcome the discrepancy between the prediction of the theory and physical realities. The yield surface is based on the Shield's pyramid (Shield, 1955b). The planes of the sides of this pyramid in the space of principal stresses are given by

$$\sigma_1(1-\sin\rho)-\sigma_2(1+\sin\rho)-2\cos\rho = 0 \qquad (2.4.1\text{-}1)$$

and the pyramid can be constructed by cyclic renumbering of the variables σ_1 and σ_2. The Shield's pyramid underwent three modifications: the pyramid was bounded on the pressure side, after a suggestion by Drucker (1951), by a flat hexagonal base peripendicular to the octahedral axis; the size of the pyramid was a function of the density; and the vertex of the pyramid was rounded off. The flat base can be represented by

$$\sigma = 1/3\ (\sigma_1+\sigma_2+\sigma_3) \qquad (2.4.1\text{-}2)$$

Figure 11 shows the evolution of the yield surface in the principal stress space. The abscissa $\sigma_1\sqrt{2}=\sigma_2\sqrt{2}$ is in the σ_1, σ_2 plane and bisects the angle between the σ_1, σ_2 axes so that $\sigma_1\sqrt{2}$ is the magnitude of the vector sum or the distance along the line at 45° to the σ_1-axis and σ_2-axis in the plane of $\sigma_3=0$. This evolution was visualized as follows: in its uncompacted state the material is under zero pressure and the yield surface is a point at

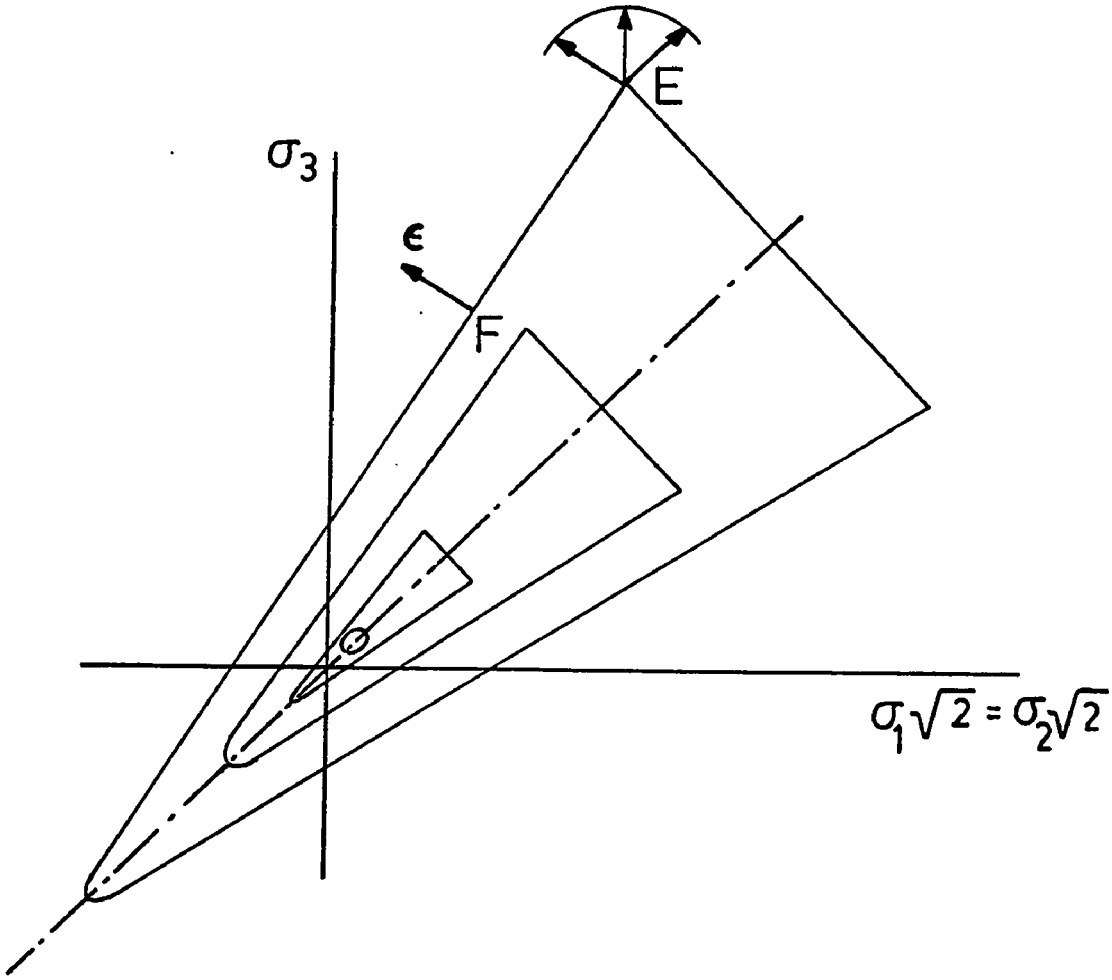

Figure 11 Evolution of the yield surface pyramid

the origin O, Figure 11. As pressure is applied the material consolidates, the yield surface develops due to progressively increasing hydrostatic pressure σ provided that the stress vector lies within the pyramid.

The bulk solid is rigid and remains rigid for any state of stress within the yield surface appropriate to the consolidating pressure σ. Yield can only occur when the stress point lies on the yield surface (yield stress). A change in volume (density) is measured by the normal component of the strain rate vector. During consolidation process the normality locates the strain rate vector $\dot{\epsilon}$ at the flat base of the pyramid which expands in size as the density and consolidating pressure increase. For a stress represented by a point on the side of the pyramid, the normality condition requires solid expansion which is opposite to consolidation and the yield surface diminishes in size as the flow progresses. When a corner point such as E of Figure 11 corresponds to a state of stress, normality gives certain limits for the $\dot{\epsilon}$ vector, but does not specify it uniquely and the solid may expand, contract, or flow with no change in volume. This is the condition achieved for continous deformation of solids in hoppers.

The concept of the adapted Shield's pyramid thus im-

plies to the existance of an infinite number of yield loci corresponding to different consolidating pressure for a given solid, each of them terminating at a point E, Figure 12. Point E corresponds to a point at the intersection of the base plane with the side planes of the pyramid. The yield locus can be approximated by a straight line, given by (2.3-2), at the point of tangency with the Mohr circle in the σ, τ coordinate. Figure 12 shows two yield locus associated with their Mohr circle. Superimposing the direction of normal and shear compressive strain rates with σ and τ (coaxiality condition), the principle of normality restricts the angle ϕ_v of ϵ to a range of $-90deg<\phi_v<\rho$ at the point E which corresponds to the flow condition.

--effective yield locus(EYL)

Steady flow in channels has been characterized by a continous deformation without change in the stress at a given point (Jenike 1964). During this type of flow within the regions of non-zero velocity the plastic region is uniformly at yield with yield planes passing through every point of the region. Experiments carried out by Jenike on hundreds of bulk solids have demonstrated that steady state flow occurs only for certain stress conditions, and, that, the ratio between the major and the minor con-

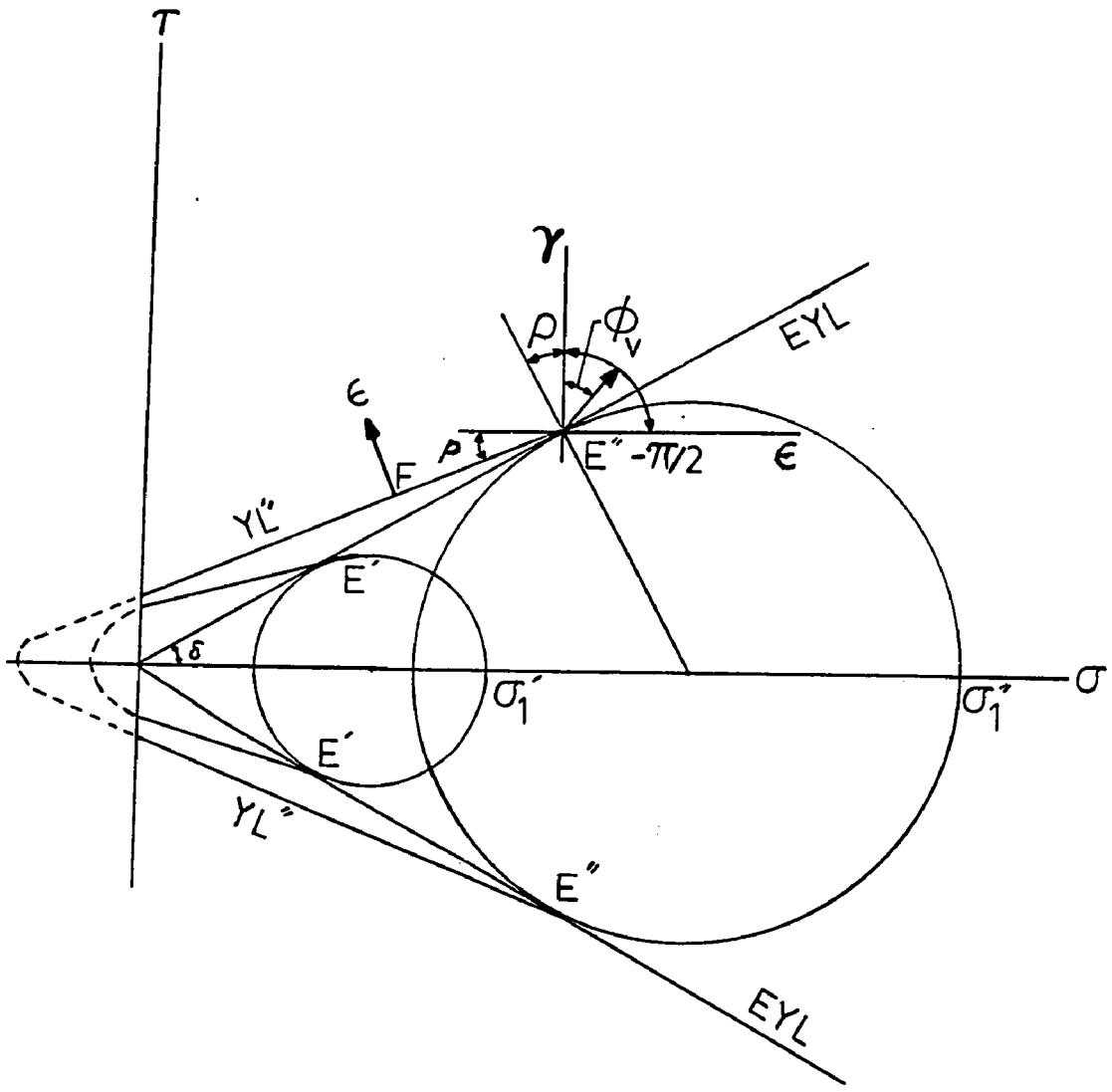

Figure 12 Yield loci and the direction of ε

solidating pressures remains almost constant for a solid with a constant moisture content and temperature:

$$\frac{\sigma_1}{\sigma_2} = \frac{1+\sin\delta}{1-\sin\delta} \qquad (2.4.1\text{-}2)$$

This relation is due to the Jenike and Shield (1959) and has been referred to as the "Effective Yield Function". The angle δ named the effective angle of friction is, in general, a function of the temperature and moisture content of the solid. Under conditions of flow and constant temperature and moisture δ is constant. The angle δ has been measured to be between 30^{o} and 70^{o} for various solids. Under normal circumastances δ is small for fine and dry and large for coarse and wet solids (Jenike 1964).

The effective yield function (2.4.1-2) can be represented by a straight line through the point of zero stress in the (σ,τ) coordinates. This line is characterized by angle δ and has been termed the "Effective Yield Locus, EYL". Results of the shear test procedure proposed by Jenike (1960) indicated that EYL, given by (2.4.1-2), is tangent to all Mohr stress circles representing a steady flow. Figure 12 shows the geometrical representation of EYL. The EYL transforms into σ_1, σ_2, σ_3 coordinates as the plane

$$\sigma_1(1-\sin\delta) - \sigma_2(1+\sin\delta) = 0 \qquad (2.4.1\text{-}3)$$

which passes through the σ_3 axis and makes an angle $\beta=\tan^{-1}(1-\sin\delta/1+\sin\delta)$ with the axis σ_1. By permutating the subscripts of the variables in equation (2.4.1-3) six such planes can be constructed each passing through one of the axes and making an angle β with one of the other axes. These six planes form a surface, Figure 13, named the "Effective Yield Pyramid", after Shield (1955b). Stress conditions for steady flow are represented by points lying on the surface of this pyramid. The effective yield pyramid with its vertex at the origin has a hexagonal cross-section, but unlike the yield pyramid extends into the direction of hydrostatic pressure without a base. Since the principal stresses chosen so that $\sigma_2<\sigma_3<\sigma_1$ then the pyramid side AFO need only be considered, remembering that these sides are similar. Along OA $\sigma_1=\sigma_3>\sigma_2$ and along OF $\sigma_3=\sigma_2<\sigma_1$.

--plastic potential function and the normality condition in steady flow

The classical formulation of theory of plasticity considers a class of materials which the yield function $f(\sigma_{ij})$, (2.4.1-1), also serves as the plastic potential for flow. The plastic potential or normality states that (Updike, 1981)

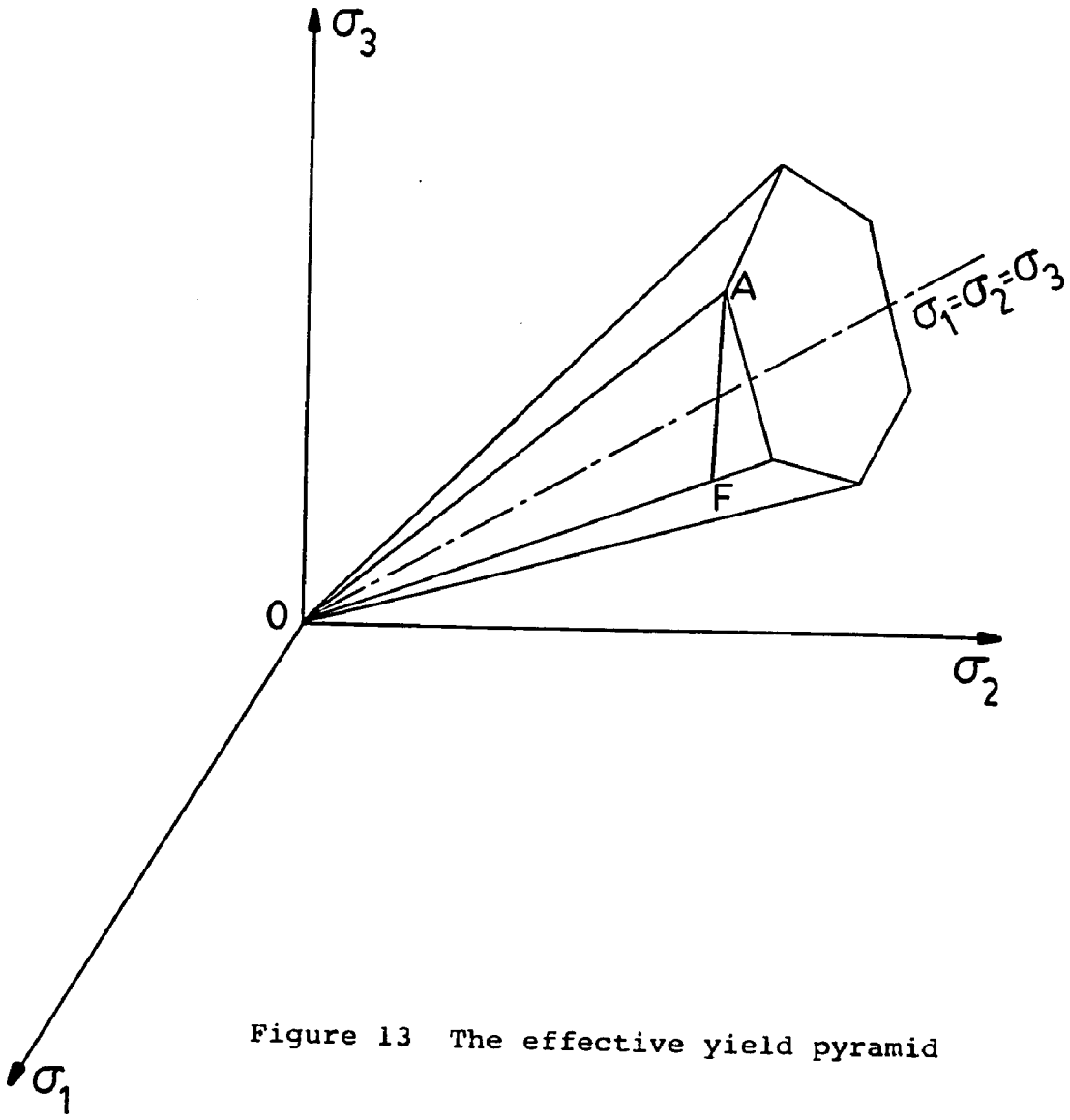

Figure 13 The effective yield pyramid

The plastic strain rate vector is outward, normal to the yield curve which is non-concave.

This statement can be expressed as

$$\dot{\epsilon}_i = \lambda \frac{\partial f}{\partial \sigma_i} \; ; \qquad \lambda \geq 0 \qquad (2.4.1\text{-}4)$$

In particular, considering one side of the yield pyramid given by equation (2.4.1-1), then the three components of the strain rate vector are:

$$\dot{\epsilon}_1 = \lambda \frac{\partial f}{\partial \sigma_1} = \lambda(1-\sin\phi), \quad \dot{\epsilon}_2 = \lambda \frac{\partial f}{\partial \sigma_2} = -\lambda(1+\sin\phi),$$

$$\dot{\epsilon}_3 = \lambda \frac{\partial f}{\partial \sigma_3} = 0 \qquad (2.4.1\text{-}5)$$

This vector, $\lambda[(1-\sin\phi),-(1+\sin\phi),0]$, is normal to the given plane. At the sharp edges or corners of the yield pyramid of the yield function $\dot{\epsilon}_i$ is defined only to within the limits imposed by the intersecting surfaces (Drucker et al., 1957).

The continuity of the solid may be expressed by

$$\dot{\epsilon}_1+\dot{\epsilon}_2+\dot{\epsilon}_3 = \dot{\epsilon}_x+\dot{\epsilon}_y+\dot{\epsilon}_z = \frac{1}{\gamma} \frac{d\gamma}{dt} \qquad (2.4.1\text{-}6)$$

in which γ is the solid density. If γ is assumed to be constant, the resulting condition

$$\dot{\epsilon}_1 + \dot{\epsilon}_2 + \dot{\epsilon}_3 = 0 \qquad (2.4.1\text{-}7)$$

restricts the strain rate vector to the octahedral plane. The strain rate vector $\lambda[(1-\sin\phi),-(1+\sin\phi),0]$ normal to the side of the yield pyramid does not satisfy this condition. One now sees the necessity of modification of the yield pyramid by closing its end with an octahedral plane and creating corner points like E of Figure 12, where the $\dot{\epsilon}$ vector has enough freedom to satisfy the condition (2.4.1-7). It is important to note that the plastic potential implies normality with respect to the yield surface not to the effective yield surface.

--case of plane strain, incompressible, cohesionless materials

The case of plane strain is characterized by deformation in one plane only, that is in the (σ_1, σ_2) plane such that velocity is zero in the direction of σ_3 and $\epsilon_3=0$. This condition together with (2.4.1-7) forces the direction of the strain rate vector such that normality limitation can only be satisfied at the point F, Figure 13. The vertical line AF in this Figure is the intersection of a given EYL function and the plane of the YL function. Thus, for incompressible plane strain material normality limits the stresses to $\sigma_2=\sigma_3<\sigma_1$.

In general, the bulk density of a solid is assumed to

be a function of the major consolidating pressure, as well as of the time t, the temperature T, and the moisture content H:

$$\gamma = \gamma(\sigma_1, t, T, H) \qquad (2.4.1\text{-}8)$$

Under the condition of flow, the bulk density of solid can be assumed to be of the form

$$\gamma = \gamma(\sigma) \qquad (2.4.1\text{-}9)$$

A barotropic equation of state has been found experimentally by Jenike (1964) to be

$$\gamma = \gamma_o(1+\sigma)^{\beta} \qquad (2.4.1\text{-}10)$$

where γ_o and β are constant under conditions of flow. Results of the tests show that for σ measured in pounds per square foot β does not exceed 0.10. The value of β for Foundry Sand and Light Soda Ash has been found to be 0.009 and 0.017, respectively (Jenike, 1964).

Different solids gain different strength under equal pressure. Some of the solids like gravel and dry sand are cohesionless so that they gain practically no strength within the typical range of pressure (150 to 2500 pounds per square foot). To cause such solids to shear, it is sufficient to overcome their angle of internal friction ϕ. In these solids slip takes place when $\tau = \sigma\tan\phi$. This is

Coulomb friction. For free flowing solids like gravel and dry sand the yield locus coincide with effective yield locus and thus $\rho=\delta$. For these materials the YL can well be appreoximated by a straight line through the origin of (σ,τ) coordinate characterized by δ, as EYL, and the vertex of the yield locus pyramid will be at the origin of $(\sigma_1,\sigma_2,\sigma_3)$ axis. Since these types of solids do not gain strength under applied pressure, there is no evolution of the yield pyramid as the applied pressure increases. The yield pyramid in this case retains its original size, there is only one yield loci, and flow develops under the achieved consolidating pressure.

--isotropy in steady flow

In the plastic region where the material deform slowly different points may have different yield functions. However, material properties are assumed isotropic, i.e. independent of direction. It has been shown that this usually implies the directions of principal stress and strain rate coincide (Jenike and Johanson, 1962). Superimposing these directions, the coaxiality condition is expressed by

$$\frac{2\tau_{xy}}{\sigma_x-\sigma_y} = \tan 2\phi = \frac{\gamma_{xy}}{\epsilon_y-\epsilon_x} \qquad (2.4.1\text{-}11)$$

where ϕ is the angle measured counterclockwise from the Y direction to the direction of major principal stress and strain rate, Figure 5. Equation (2.4.1-11) expresses the coaxiality condition which is often linked to that of isotropy (Tuzun et al., 1982). Jackson (1983) has recently discussed the principles of normality and coaxiality, and has used the coaxiality condition to develop the velocity field solution for a granular material flowing in a hopper.

CHAPTER THREE

3.0 BASIC EQUATIONS

In this chapter we present the conservation and constitutive equations that will be used to compute the stress and velocity fields. We first consider the fluid pressure distribution in the annulus and its effect on the solid density. The equation of the motion are then reduced for the slowly plastically deforming material in the annulus to obtain the basic equations describing the motion of solids. Finally, the boundary conditions are discussed in the light of physical realities of the problem.

Compressive stress and strain are taken to be positive. Shear stress is taken to be positive in the counterclockwise direction. The angles are measured in the counterclockwise direction from the axis.

In the vertical portion of the annulus the material is compressed vertically and extend radially toward the spout, the major pressure is vertical and a divergent flow developes. An active state of stress then exists for this portion. In the conical region, on the other hand, the material is compressed horizontally and the flow is convergent. A passive state of stress then exists for this portion. Observations and photographs confirm the conver-

gent and divergent flow in the vertical and conical regions respectively. A switch from active to passive then exists at the vertical/conical junction of the annulus similar to that at the bin/hopper junction (Savage and Yong, 1969, Horne and Nedderman, 1978a).

Because of the symmetry the computations are done on only one half of the annulus region. Throughout the analysis b_o^*, $\rho_p g(1-\epsilon_o)b_o^*$, and $W/\rho_p(1-\epsilon_o)b_o^*$ are used as the length, pressure, and velocity reference quantities.

3.1 Effect of the Gas

3.1.1 Spout pressure distribution

Lefroy and Davidson (1969) using the experimental data have concluded that in any spouted bed the pressure just outside the spout can be approximated by:

$$P^* = \Delta P^* \cos[(\pi/2)(1- y^*/H^*)] \qquad (3.1.1\text{-}1)$$

Using equation (3.1.1-1) and the fact that at the maximum spoutable bed depth, H_m^*, the pressure gradient was enougn to fluidize the bed at the top, ΔP^* has been found:

$$(\Delta P^*)_{H_m^*} = 2H_m^* \rho_p g(1-\epsilon_o)/\pi \qquad (3.1.1\text{-}2)$$

Replacing ΔP^* from equation (3.1.1-2) into equation (3.1.1-1) yields the pressure distribution just outside the spout at the maximum spoutable bed condition:

$$P^* = (2/\pi)\rho_p g(1-\epsilon_o)H_m^* \cos[.5\pi(1- y^*/H_m^*)] \qquad (3.1.1\text{-}3)$$

Lefroy and Davidson generalized equation (3.1.1-3) so that it would be applicable to all values of H^* and not just H_m^*, by introducing a factor B such that:

$$B = \frac{\Delta P_s^*/H^*}{(\Delta P_s^*)_{H_m^*}/H_m^*} \qquad (3.1.1\text{-}4)$$

where obviously B<1. Using the factor B, the pressure distribution just outside the spout is given by:

$$P^* = (2/\pi)B\rho_p g H^*(1-\epsilon_o)\cos[(\pi/2)(1- y^*/H^*)] \qquad (3.1.1\text{-}5)$$

McNab and Bridgwater (1977) used five different models in their attempt to correlate the value of B for 64 experimental observations of spouted bed pressure drop. They found a result that was found by Epstein, Lim and Mathur (1978) to give close agreement with the experimental data:

$$B = \sin\left(\frac{\pi H^*}{2H_m^*}\right) \qquad (3.1.1\text{-}6)$$

3.1.2 Annulus Pressure Distribution

Due to the pressure gradient in the spout the air flowing in the spout leaks into the porous annular region where it flows upward countercurrently to the slowly des-

cending particles. Many investigators have developed correlations for the prediction of the flow and pressure distribution of fluid in the annulus of a spouted bed. Models developed by both Mamuro and Hattori (1968) and the Grbavcic et al. (1976) assume unidirectional Darcy flow in the annulus. Epstein and Levine (1978) reworked the Grbavcic et al. theory to account for the turbulent non-Darcy flow in the annulus. Littman et al. (1981) have solved numerically the continuity equation combined with the vector form of the Ergun equation and appropriate boundary conditions to find the flow and the pressure distribution. To check the calculations, they measured the pressure distribution in the annulus and spout experimentally and found good agreement between the proposed model and the experimental evidence.

In our case we assume laminar flow with interstitial region and Darcy's law is applied to calculate the pressure distribution of the air in the annulus. This law states that

$$u_f = - K_x \frac{\partial P}{\partial x} \quad , \quad v_f = - K_y \frac{\partial P}{\partial y} \qquad (3.1.2\text{-}1)$$

K_x and K_y are the Darcy's permeabilities in the x and y directions, respectively. The prediction by Darcy's law is

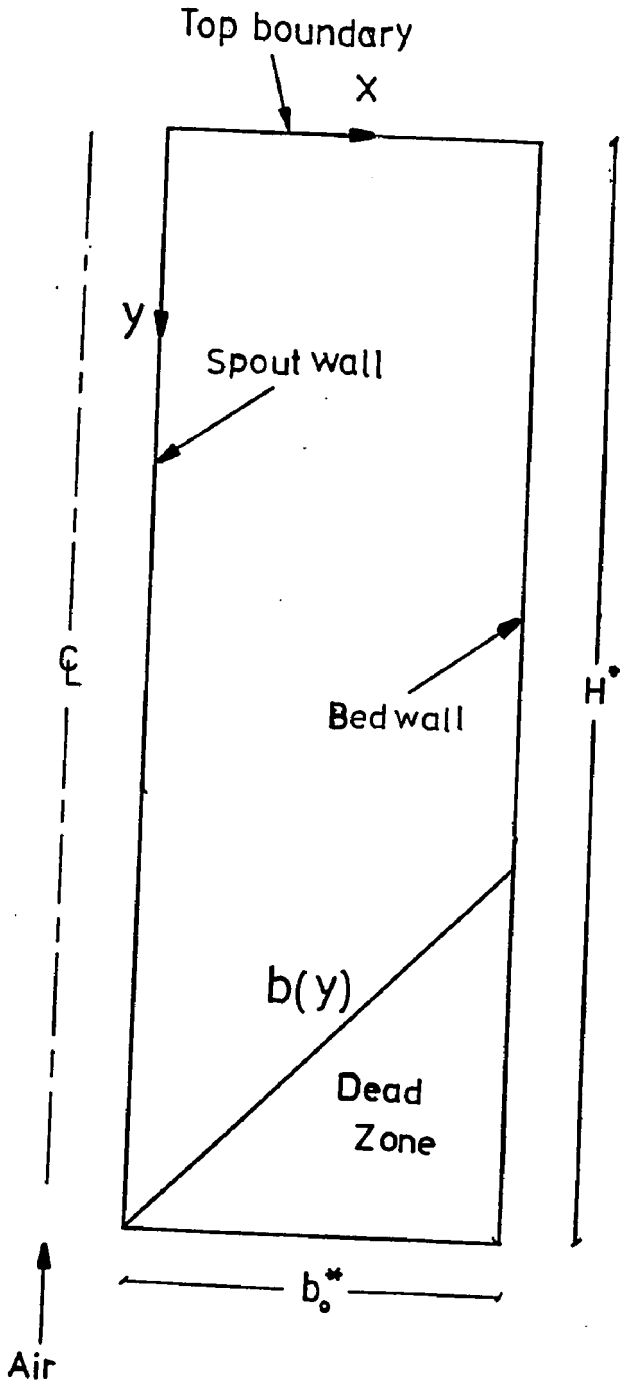

Figure 14 One half of the two dimensional spouted bed and the boundaries of annulus

particularly good when the particle Reynolds number is less than 10 (Leva et al., 1951). However, proper allowance for the effect of the particle Reynolds number is complex and Darcy's law is assumed as suggested by Lefroy and Davidson (1969). Using the continuity equation of the fluid and assuming that Darcy's constants are independent of direction (isotropic material), one obtains Laplace's equation for the pressure distribution in the annulus:

$$\frac{\partial^2 P^*}{\partial x^{*2}} + \frac{\partial^2 P^*}{\partial y^{*2}} = 0 \qquad (3.1.2\text{-}2)$$

Using the dimensionless quantities, the dimensionless governing equation and the boundary conditions are:

$$\frac{\partial^2 P}{\partial x^2} + \frac{\partial^2 P}{\partial y^2} = 0 \qquad (3.1.2\text{-}3)$$

$$y=H \quad \partial P/\partial y = 0 \;; \quad x=1 \quad \partial P/\partial x = 0$$
$$y=0 \quad P=0 \;; \quad x=0 \quad P=(2/\pi)HB\sin[(\pi/2)(y/H)]$$

The solution to equation (3.1.2-3) is given by:

$$P(x,y) = \frac{2}{\pi} HB\sin\left(\frac{\pi y}{2H}\right) \frac{\cosh[(\pi/2H)(1-x)]}{\cosh(\pi/2H)} \qquad (3.1.2\text{-}4)$$

in which B is obtained from (3.1.1-6). Figure 15 shows the ratio of the wall pressure, P_w to spout pressure, P_s for different H. For beds having height to half width ratio greater than 2, it may be assumed a uniform pressure across a horizontal section. This assumption introduces

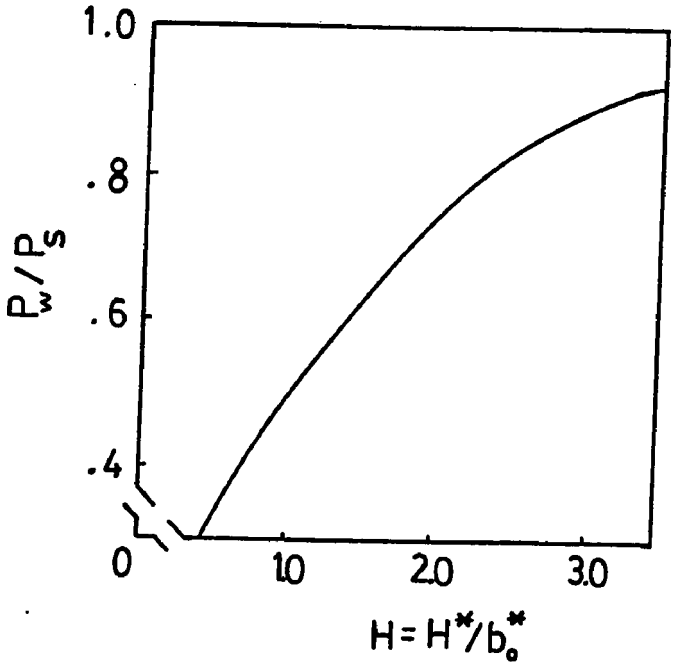

Figure 15 Ratio of wall pressure to spout pressure as a function of the dimensionless depth of the material

at most 11% deviation for H=3 and 24% for H=2, but greatly simplifies the computations. The deviation from the average gas pressure across a horizontal section is 8% for H=3 and 16.5% for H=2. Since the case of H=3 is mainly considered throughout the analysis, the air pressure distribution is assumed to be given by

$$P = (2/\pi)HB\sin(\pi y/2H) \qquad (3.1.2\text{-}5)$$

3.2 The Effective Density

The effective weight per unit volume of the material in the annulus is defined as:

$$\rho_e = (\rho_p-\rho_f)(1-\epsilon_o) - \frac{1}{g}\frac{dP^*}{dy^*} \qquad (3.2\text{-}1)$$

In cases where the fluid density ρ_f is much smaller than the particle density ρ_p,

$$\rho_p - \rho_f \simeq \rho_p \qquad (3.2\text{-}2)$$

The effective density can then be written:

$$\rho_e = \rho_b - \frac{1}{g}\frac{dP^*}{dy^*} \qquad (3.2\text{-}3)$$

and in the dimensionless form

$$\frac{\rho_e}{\rho_b} = 1 - \frac{dP}{dy} \qquad (3.2\text{-}4)$$

The pressure gradient term dP/dy is obtained from

(3.1.2-5) thus,

$$\frac{\rho_e}{\rho_b} = 1 - B\cos\frac{\pi}{2H}y \qquad (3.2\text{-}5)$$

3.3 The Equations of Motion for the Solid

3.3.1 Stress field

The equations describing the solid motion in the annulus are described in this section. These equations are developed for two dimensional cartesian coordinates. The attention was restricted to the case of plane strain. The bulk solid was assumed to be an isotropic, frictional, cohesionless, incompressible, rigid-plastic material obeying the yield functions described in section (2.4.1). The yield function of (2.4.1-2) can be written in terms of the stress components and, using the Mohr diagram, Figure 16-a, as

$$[(1/4)(\sigma_x-\sigma_y)^2 + \tau^2_{xy}]^{1/2} = (1/2)(\sigma_x+\sigma_y)\sin\delta \qquad (3.3.1\text{-}1)$$

Points E and E' in Figure 16-a correspond to the yield stresses and lines PE and PE', connecting the pole of the diagram to the points of tangency, are the slip lines. The angle between two sliplines is bisected by the direction of major consolidating pressure. This angle can be related to the angle δ using the right triangle OED:

$$2\psi = \pi/2 - \delta \qquad (3.3.1\text{-}2)$$

The physical planes are shown in Figure 16-b. It is now observable that sliplines make angles $\phi \pm \psi$ with the y axis.

Refering all stresses in Figure 16-a to the point O, a new stress variable presented by distance OD can be defined as

$$\sigma = \frac{\sigma_1 + \sigma_2}{2} = \frac{\sigma_x + \sigma_y}{2} \qquad (3.3.1\text{-}3)$$

such that the three stress components are written in terms of two variables σ and ϕ:

$$\sigma_x = \sigma(1-\sin\delta\cos 2\phi) \qquad (3.3.1\text{-}4)$$
$$\sigma_y = \sigma(1+\sin\delta\cos 2\phi) \qquad (3.3.1\text{-}5)$$
$$\tau_{xy} = \sigma\sin\delta\sin 2\phi \qquad (3.3.1\text{-}6)$$

These relations satisfy the yield function identically.

The equations of motion of the continuum for the two dimensional cartesian coordinates are:

$$\rho\left(u^*\frac{\partial u^*}{\partial x^*}+v^*\frac{\partial u^*}{\partial y^*}\right) = -\left(\frac{\partial \sigma_x{}^*}{\partial x^*}+\frac{\partial \tau_{xy}{}^*}{\partial y^*}\right) - \frac{\partial P_f{}^*}{\partial x^*} \qquad (3.3.1\text{-}7)$$

$$\rho_b\left(u^*\frac{\partial v^*}{\partial x^*}+v^*\frac{\partial v^*}{\partial y^*}\right) = \rho_b g - \left(\frac{\partial \sigma_y{}^*}{\partial y^*}+\frac{\partial \tau_{xy}{}^*}{\partial x^*}\right) - \frac{\partial P_f{}^*}{\partial y^*} \qquad (3.3.1\text{-}8)$$

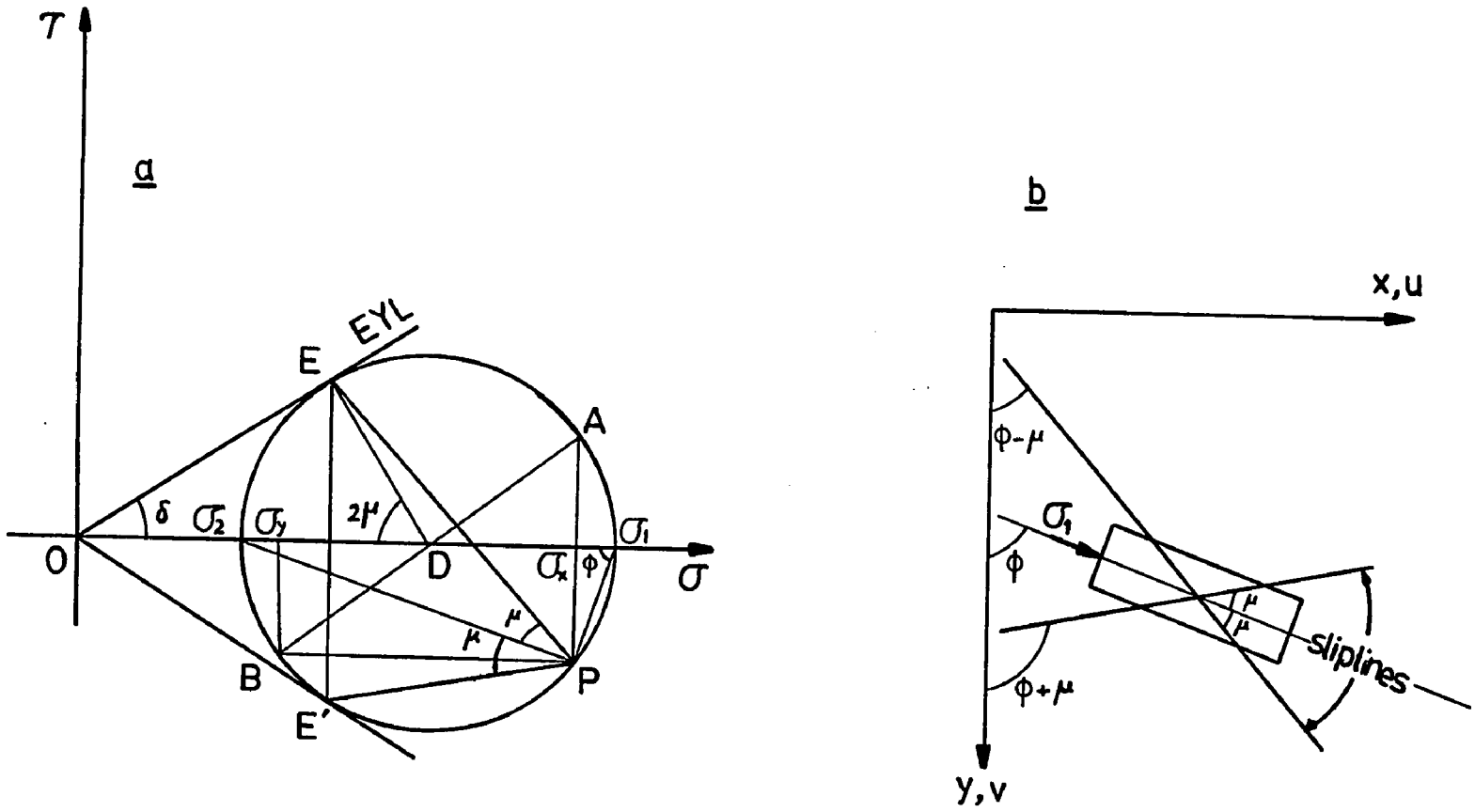

Figure 16 Relations between principal stress and sliplines

a) Mohr stress circle
b) physical plane

The motion of solid particles in the annulus is slow, such that the inertial forces can be considered in a first approximation negligible and the equations reduce to the equations of equilibruim:

$$\frac{\partial \sigma_x^*}{\partial x^*} + \frac{\partial \tau_{xy}^*}{\partial y^*} = 0 \qquad (3.3.1\text{-}9)$$

$$\frac{\partial \sigma_y^*}{\partial y^*} + \frac{\partial \tau_{xy}^*}{\partial x^*} = \rho_e g \qquad (3.3.1\text{-}10)$$

In the equation (3.3.1-10) the fluid pressure term is combined with ρ_b to give ρ_e defined by (3.2-1) where we have neglected the horizontal component of the pressure gradient. Making equations (3.3.1-9) and (3.3.1-10) dimensionless and using relations (3.3.1-4, 5, 6) the limit equilibrium equations written in terms of σ and ϕ are:

$$(1-\sin\delta\cos 2\phi)\frac{\partial \sigma}{\partial x}+\sin\delta\sin 2\phi\frac{\partial \sigma}{\partial y}+2\sigma\sin\delta\sin 2\phi\frac{\partial \phi}{\partial x} +2\sigma\sin\delta\cos 2\phi\frac{\partial \phi}{\partial y} = 0 \qquad (3.3.1\text{-}11)$$

$$\sin\delta\sin 2\phi\frac{\partial \sigma}{\partial x}+(1+\sin\delta\cos 2\phi)\frac{\partial \sigma}{\partial y}+2\sigma\sin\delta\cos 2\phi\frac{\partial \phi}{\partial x} -2\sigma\sin\delta\sin 2\phi\frac{\partial \phi}{\partial y} = 1-\frac{dP_f}{dy} \qquad (3.3.1\text{-}12)$$

where P_f is given by (3.1.2-5). The governing equations

for stresses described here subject to [illegible] boundary conditions define a well posed solution for the stress field. Notice that the two equilibrium equations [illegible] with the yield condition may be used to determine the stress components. However, employment of the two variables σ and ϕ reduces the three governing equations to the two equations (3.3.1-11) and (3.3.1-12), thus making them more suitable for a particular numerical technique.

The system (3.3.1-11,12) is hyperbolic and will be solved using the method of characteristics. All stresses mentioned here are the effective stresses.

3.3.2 Velocity field

The equations determining the velocity field are those of incompressibility and coaxiality

$$\frac{\partial u}{\partial x} + \frac{\partial v}{\partial y} = 0 \qquad (3.3.2\text{-}1)$$

$$\frac{\dfrac{\partial v}{\partial x} + \dfrac{\partial u}{\partial y}}{\dfrac{\partial v}{\partial y} - \dfrac{\partial u}{\partial x}} = \tan 2\phi \qquad (3.3.2\text{-}2)$$

Equation (3.3.2-2) is obtained using (2.4.1-11) and (2.1.4-3).

With well-posed boundary conditions on the velocity components these equations can be solved if ϕ is known. Since ϕ is determined by the stress field solution, this condition ties the velocity and stress fields together. However, the velocity field is independent of the magnitude of σ, and the stress boundary conditions do not determine the velocity boundary conditions (Johanson, 1964).

The system (3.3.2-1,2) is hyperbolic and it is also solved using the method of characteristics.

3.3.3 Boundary conditions

The stresses and velocities along the boundaries of the annulus region are discussed here. The region boundaries are (Figure 14):

- Top boundary

The top boundary of the annulus is assumed to be traction free. If in addition to being traction free the surface also satisfies the EYL condition for steady flow, the stress state is defined by point O in Figure 16 and is therefore, stress free. The Mohr circle for this condition degenerates to a point $\sigma=\tau=0$, however, the direction of principal stress ϕ can be determined as a function of the angle of inclination ψ of the stress free boundary. The

physical assumptions are:

1- There is no load on the free surface.
2- The material is in the plastic state.
3- The material at the boundary is in equilibrium.

The angle ω can then be obtained, as shown by Jenike and Johanson (1962), by noting that

$$\sigma = 0 \quad \text{or} \quad \frac{\partial \sigma}{\partial x}dx + \frac{\partial \sigma}{\partial y}dy = 0 \qquad (3.3.3\text{-}1)$$

and that $dy/dx=-\tan\omega$. This condition together with equation (3.3.1-11) for $\sigma=0$ can be solved for ω and ϕ_t giving that for the homogeneous system of linear algebraic equations to have a solution, it must be:

$$\sin(2\phi_t - \omega) = -\sin\omega/\sin\delta \qquad (3.3.3\text{-}2)$$

the pertinent root of which is

$$2\phi_t = \omega + \sin^{-1}(-\sin\omega/\sin\delta) \qquad (3.3.3\text{-}3)$$

The top boundary is assumed to be horizontal, i.e. $\omega=0$, and thus the conditions on the stress parameters across this boundary are:

$$\sigma = 0$$
$$\phi_t = 0 \text{ or } \pi/2 \qquad (3.3.3\text{-}4)$$

Notice that the two solutions for ϕ_t correspond to the active and passive state of stress, respectively.

The two conditions for the velocity components across

this boundary are:

$$u = 0$$
$$v : \text{uniform} \qquad (3.3.3\text{-}5)$$

The first condition assumes that there is no horizontal motion of particles on this boundary and the particles enter the annulus vertically. The second condition assumes a uniform distribution of the vertical velocity component. This component can be related to the total solid circulation W as:

$$v^* = \frac{W}{\rho_p(1-\epsilon_o)b_o^*} \qquad (3.3.3\text{-}6)$$

that written in dimensionless variable is:

$$v = 1 \qquad (3.3.3\text{-}7)$$

across the top boundary.

- Bed wall

Jenike (1961) has found experimentally that when the solid flows on rigid side walls the normal and shear stresses along the wall lie approximately on a straight line as shown in Figure 17a by the "Wall Yield Locus", WYL. The angle δ_w is said to be the angle of friction between the rigid wall and the solid under steady flow.

At the bed wall the direction of the major principal stress ϕ_w can be found as a function of δ and δ_w simply

from the Mohr's circle of stress construction for the material at the wall. Such a construction is shown in Figure 17a, which corresponds to an active state of stress (point K). From this Figure:

$$\sphericalangle MWK = \cos^{-1}(MW/r) = \cos^{-1}(\sin\delta_w/\sin\delta)$$
$$\sphericalangle MWQ = \pi/2 - \delta_w$$

Thus,

$$\phi_w = [\pi/2 - \cos^{-1}(\sin\delta_w/\sin\delta) - \delta_w]/2 \qquad (3.3.3\text{-}8)$$

Equation (3.3.3-8) is the only relation that must be satisfied at the bed wall.

The only condition that must be satisfied at the bed wall as far as the velocity field is concerned is that u must vanish, and the material flow along the wall:

$$u_w = 0 \qquad (3.3.3\text{-}9)$$

- Boundary of dead zone

The boundary of dead zone separates the plastically deforming solids from the stationary (rigid) material forming the dead zone. Thus, this boundary is considered as a rigid-plastic boundary and therefore is a wall, composed of the solid particles, by its definition (Jenike, 1961). Being a wall, the direction of major principal stress is then given by a Mohr circle of stress construc-

tion similar to Figure 17a corresponding to the passive case (piont L) providing that $\delta_w=\delta$, as well as considering the inclination of the boundary:

$$\phi_b = \tan^{-1}[db(y)/dy] + (\pi/2 - \delta)/2 \qquad (3.3.3\text{-}10)$$

in which b(y) describes shape of the dead zone boundary (Figure 14). Equation (3.3.3-10) is the only condition that must be satisfied along the boundary for the stress field.

The foregoing consideration about the boundary of dead zone implies that this boundary to be considered as a line of discontinuity in the velocity field (Prager, 1948). The equilibrium condition requires that the velocity vector normal to a line of discontinuity become continous across this line. Applying this requirement, the geometry of Figure 14 necessitates that:

$$\frac{u_b}{v_b} = \frac{db}{dy} \qquad (3.3.3\text{-}11)$$

since the velocity normal to the boundary on the dead zone side is zero. Relation (3.3.3-11) provides the only condition to be held along the boundary for the velocity field.

- spout annulus interface

The spout annulus interface is assumed to be a hydrodynamically induced wall without necking and rippling movement. It is also assumed that the stress state of solids at the spout wall can be approximated by a straight line as shown in Figure 17b by the "Spout Yield Locus", SYL. The angle δ_s is said to be the angle of friction between the fluid flowing in the spout and the solid under steady flow. There are different assumptions about the numerical value of this angle in the literature. Bridgewater and Mathur (1972) have assumed zero angle of friction at the spout wall (implying no shear stress), while McNab and Bridgwater (1974, 1979) reasoned that the extraction of material from the spout wall and movement up the spout means that some shear and normal stress must exist. They have suggested the range of 0-δ for the magnitude of δ_s. The numerical value of δ_s is not taken to be zero in this work to make the computations as general as possible.

At the spout wall the direction of the major principal stress Φ_s can be found from the Mohr's circle of stress construction for the material at the spout wall, Figure 17b. From such a construction

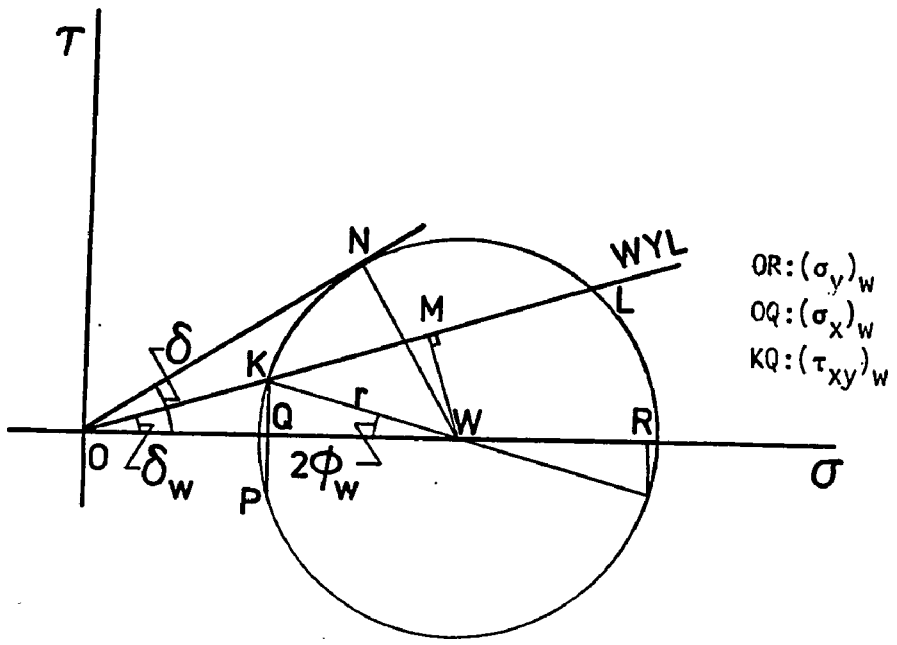

Figure 17a Mohr circle of stress construction for material at the bed wall (active state)

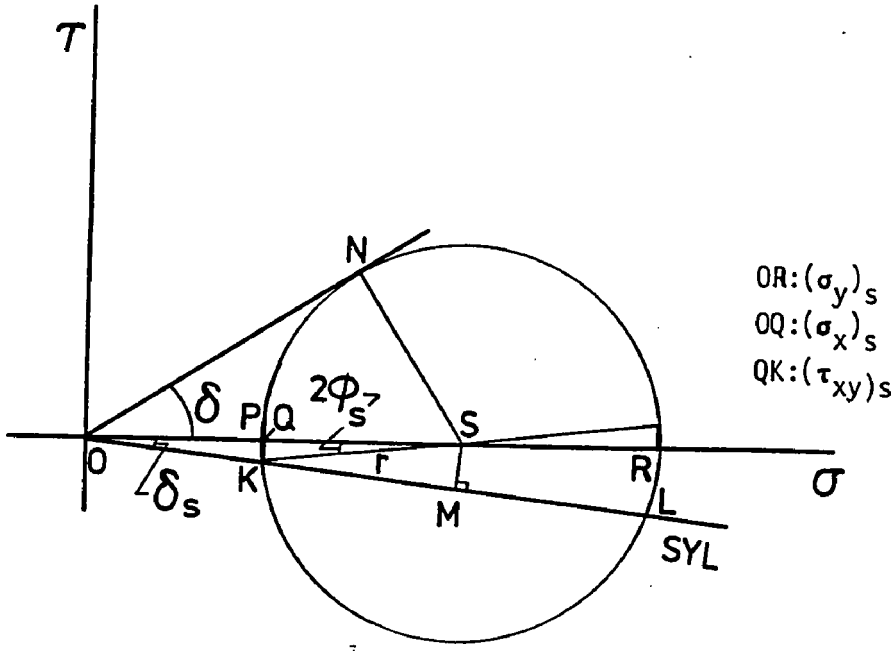

Figure 17b Mohr circle of stress construction for material at the spout wall (active state)

$$< MSK = \cos^{-1}(MS/r) = \cos^{-1}(\sin\delta_s/\sin\delta)$$
$$< MSR = \pi/2 - \delta_s$$

Thus,

$$\phi_s = [\pi/2 - \delta_s \mp \cos^{-1}(\sin\delta_s/\sin\delta)]/2 \qquad (3.3.3\text{-}12)$$

where the upper sign (-) corresponds to the active state of stress applied to the vertical portion of the annulus and the lower sign (+) corresponds to the passive state of stress applied to the conical portion of the annulus. This equation is the only condition that must be met at the spout wall for the stress field.

The boundary condition for the velocity field is one of the uncertainity since the actual mechanism of particle entraintment is not yet known. Thorley et al. (1955) have traced particle flow lines by observation against the flat wall of a 61cm diameter half-column. Later, Mathur and Epstein (1974c) have used their data to evaluate the total solid circulation W approximated by particle velocity at the bed wall. The experimental data by Mathur and Gishler (1955a) have indicated to a linear variation of W with height in the cylindrical portion of the annulus. There was no approximation the could be developed for the lower portion (conical region) of the bed.

The following condition is used in this work as a boundary condition at the spout wall for velocity:

$$u_s = \frac{1}{H} \qquad (3.3.3\text{-}13)$$

This condition presents a uniform variation of u_s which satisfies the overall mass (solid) balance.

Figure 18 shows the annulus region with the conditions discussed along the boundaries.

The governing equations and the boundary conditions described in this chapter define a unique stress and velocity field solution. The way these equations were set up make them suitable for the method of characteristics. There is only one condition available along each boundary, for each field, except at the top boundary. The method of characteristics can integrate the governing equations with the corresponding conditions.

The conditions at the top boundary, in general, do not match with the condition at the bed or spout wall at the point of intersections. Similarly, the variables are double valued at the intersection point of the bed wall and the boundary of dead zone. These points may be the origination of a fan of characteristics (normally in the

active state) or a shock surface (normally in the passive state) that is discussed in Chapter 5. Although these types of numerical difficulties are encountered in applying the method of characteristics, it is remarkable that the method not only gives an exact numerical solution but it provides sliplines, shearlines, and other important information. The technique of applying this method is discussed in Chapter 5 for solution of stress and velocity fields.

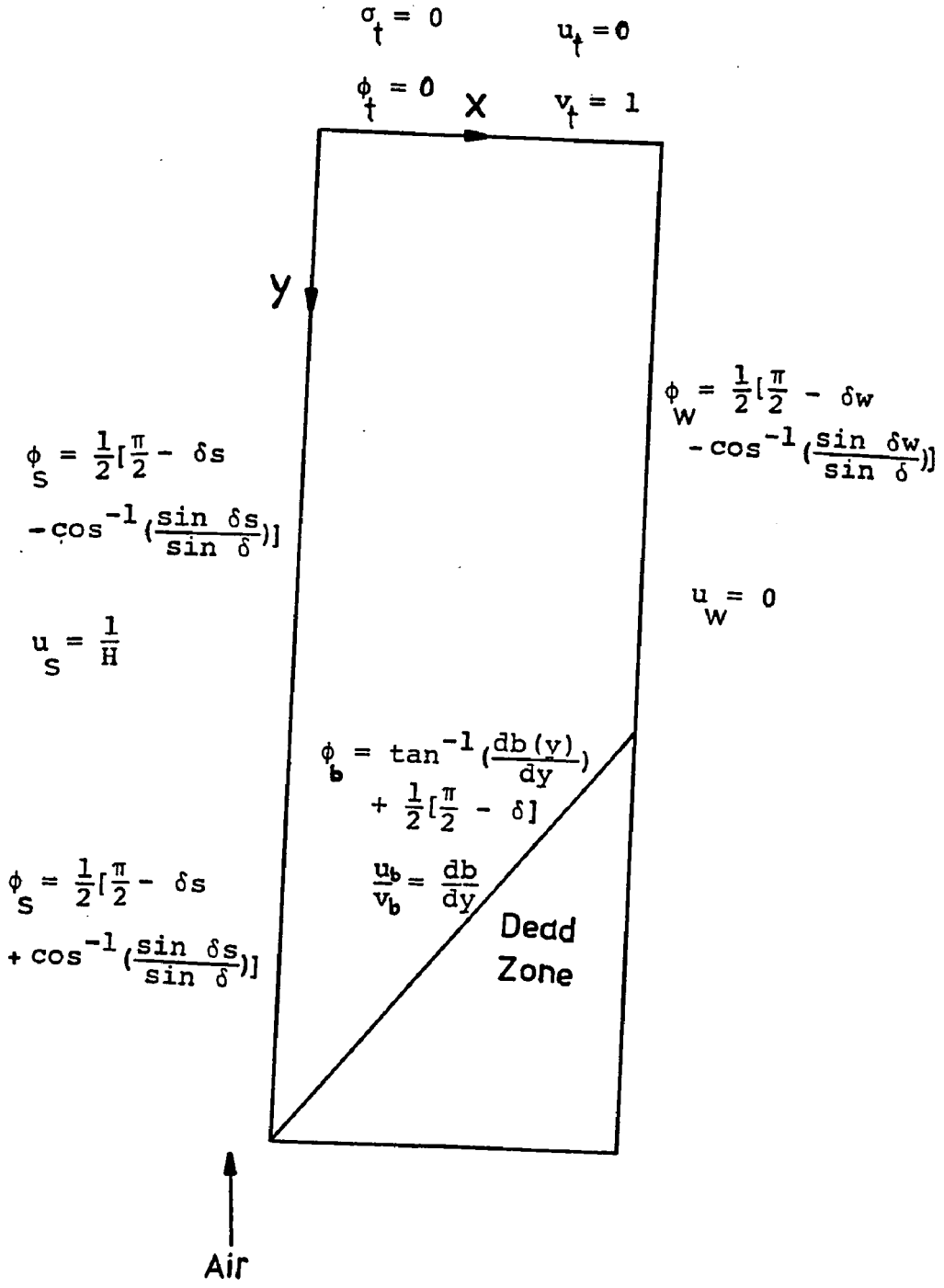

Figure 18 The annulus region of spouted bed with the boundary conditions for the stress and velocity fields along its boundaries

CHAPTER FOUR

4.0 EXPERIMENTAL OBSERVATIONS AND BOUNDARY OF DEAD ZONE

Some experimental observations and a mathematical model based on the method of the slices for the shape and formation of the dead zone are presented and discussed in this chapter.

The experimental work was primarily done for observation, determination of the maximum spoutable bed depth H_m, and verification of the results of the method of slices. This method was employed to determine the boundary of dead zone. The method of slices has basically been developed for the problem of slope stability to compute the factor of safety for a potentially sliding mass.

4.1 Experimental Observations

4.1.1 Apparatus

A two-dimensional plexiglass column was used for the experimental observations. The bed had a rectangular cross section of 2.4x15.2cm. A piece of plexiglass with the same dimensions of the bed cross section and a height of 10.16cm was used as the gas distributor, and placed at the bottom of the bed. The distributor had a centrally drilled .635cm (1/4 inch) diameter orifice at the base which was

nected at 1.9cm from the base to a channel (slit) of 2.4x.635cm. The channel allowed a uniform two-dimensional jet enter the bed. The channel was covered with a coarse mesh at the top to prevent particles draining into the channel and orifice. Air was used as the spouting medium, and, to reduce the static electric effect between the particles and the plexiglass sheet the air was humidified in a bubbling tank. All the solid particles used were non-cohesive.

4.1.2 Observations

To evaluate effect of different parameters on the spouting phenomena three types of solid particles were used. The properties of these particles are shown in Table 1. In the absence of sophisticated experimental equipments, the angle of internal friction was measured according to the simple method of Zenz (1975).

The bed was filled with three different heights for each material such that the ratios of the material height to half of the bed width (from the edge of the channel to the bed wall) H, at the spouting state, were 1, 2, and 3. For the material used with H>3.5 the spouting was not either achievable or very stable and the spouting gave way either to aggregative fluidization or slugging.

Table 1: Solid Particles Used for Experiments

Material	$D_{ave.}$ (mm)	ρ_p (g/cm^3)	δ (Degree)
Glass Beads	1.10	2.42	30
Copolymer Seed	.988*	2.43	37
Alfalfa Seed	1.67*	1.18	40

* Mean Diameter

As the height of material (bed depth) increased, the range of the gas flow for spouting became narrower until at the maximum spoutable bed depth equal to 3 there was practically only one velocity at which the bed could be spouted. The maximum spoutable bed depth which is an index of spouting stability (Mathur and Epstein, 1974b) was much shorter in two-dimensional than in three dimensional spouted beds. This fact, which is a consequence of the role played by surface instability of the spout, has been reported by Volpicelli et al. (1967) using a two-dimensional spouted bed. Empirical equations have been developed by many investigators for H_m and are extensively discussed by Mathur and Epstein in their book (1974c). All of these equations were obtained for three dimensional cylindrical and semi-cylindrical beds. The only available information for two-dimensional beds, known to us, is that obtained by Volpicelli et al. (1967). They found H=1-3 for stable spouting. The effect of particle density on H_m and spout stability has been considered by many investigators but the published information is contradictory. The experiments have indicated that it is possible to achieve a stable spout for deeper beds with Alfalfa Seeds (ρ_p=1.18 g/cm^3) than with Glass Beads (ρ_p=2.42 g/cm^3). The correlation for calculating H_m proposed by Malek and Lu (1965) implies that spouting stability is adversely af-

fected by particle density, but Fleming (see Mathur and Epstein, 1974c) and many other investigators (Reddy et al., 1968) could not confirm that there exist any limit on particle density beyond which spouting is impossible, nor there is any clear evidence to show whether spouting stability is affected by particle density. The present results, on the other hand, are affected by the particles' shape, size and surface characteristics which are different for seeds and beads.

Phase diagrams for two-dimensional spouting are similar to those obtained by Gishler and Mathur for cylindrical columns, Figure 3, however, the shape of spout and its movement are quite different in the two systems. In a two-dimensional bed the spout is necked, Figure 19, and depending on the air flow rate oscillates or stays tilted to the left or right while, in a cylindrical bed not only the spout annulus interface is an almost vertical line but the spout is very stable. The photographs taken from two-dimensional flat bed and cylindrical bed, Figure 20, show the spout shape.

The regular downward solid motion in the annulus was disrupted by increasing the air flow rate. This disruption switched the spouting action to slugging. It is believed

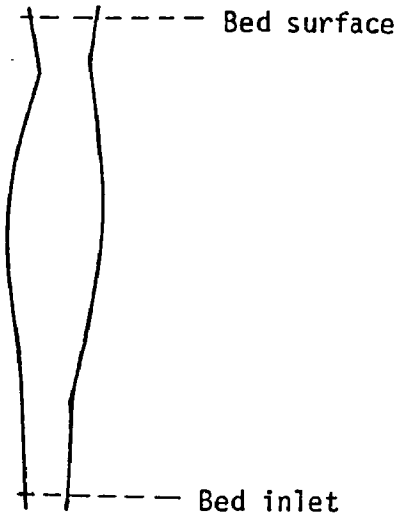

Figure 19 Observed spout shape for a two-dimensional bed

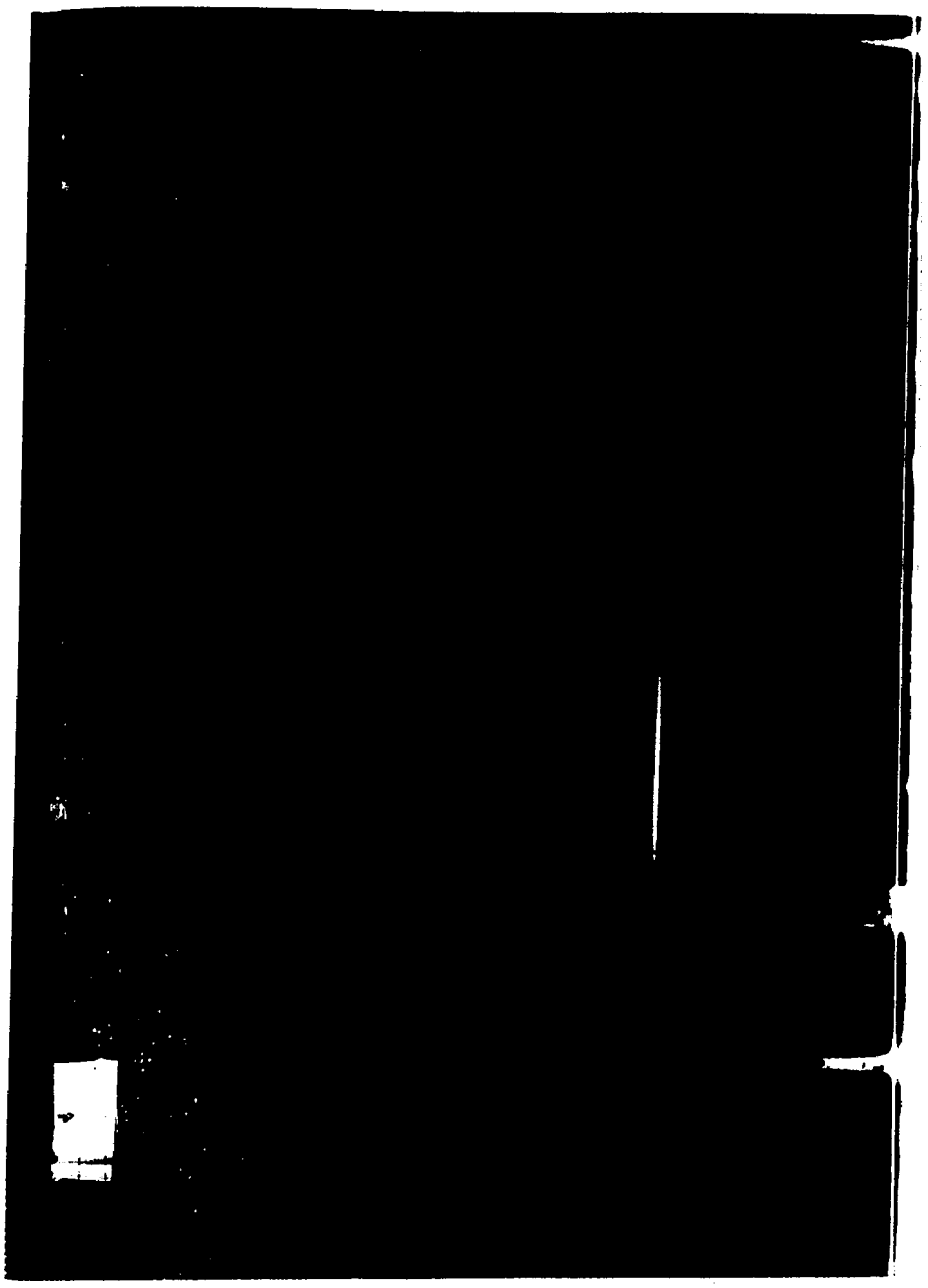

a) cylindrical spouted bed

Figure 20 Spout shape

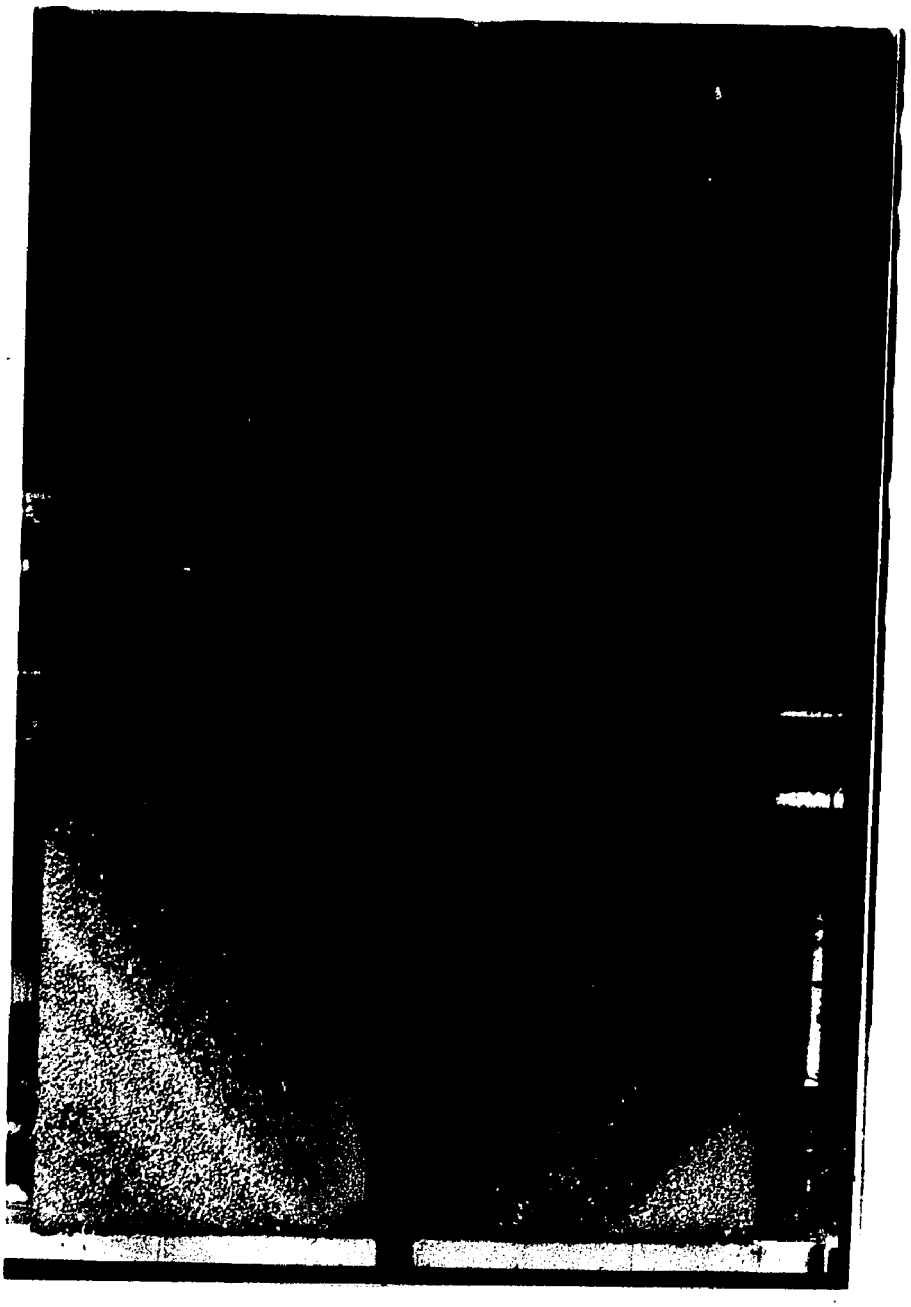

b) Two-dimensional spouted bed

that the transition from spouting to slugging is related to surface instability and is controlled by the entrainment rate of particles at the spout mouth. Disturbances developed at the spout and moved upwards like ripples. The analysis of high speed motion pictures by Volpicelli et al. (1967) showed that particles moved sinusoidally as they fell down on the side of the spout. Observations of the present bed showed a pulsating flow of particles in the dense region. This pulsation which causes the choking of spout may be related to the stability problem, since pulsation was not observed regularly in cylindrical beds.

In conclusion, it is believed the role played by surface instability controls many aspects of the dynamics of a two-dimensional spouted bed. The fact that maximum spoutable bed depths were much smaller in two-dimensional than in three dimensional spouting may be an indication of the presence of this instability mechanism.

4.2 Determination of the Boundary of Dead Zone Using the Method of the Slices

The boundary of dead zone in the annular region is here obtained theoretically by the condition of limiting equilibrium together with the method of slices. The method of slices is a modification of circular-arc method employed in soil mechanics for the stability analysis of slopes. This method is particularly useful when non-homogeneity exist in the soil mass, where the mass may slip along a non-circular slip surface; since analysis based solely upon circular slip surface may significantly overestimate the "factor of safety" (Bishop, 1955).

We believe that the condition of limit equilibrium together with the method of slices provide a satisfactory basis for estimating the boundary of dead zone. In soil mechanics, Janbu (1957) was probably the first who applied this basis in evaluating the factor of safety for a potentially sliding mass. However, in this work the major concern was the determination of the shape of the failure surface, not the estimation of factor of safety for an assumed slip surface which is usually done in the slope stability problems. The factor of safety assumed to be 1, and basic governing equations applied were those used in the slope stability analysis by the method of slices

employed by many workers (Janbu, 1957, Morgenstern and Price, 1965).

4.2.1 The equations of equilibrium

It was assumed that the material was in a state of incipient failure throughout its mass; that is, in so far as the material in the dead zone was concerned the whole mass above the dead zone boundary was on the verge of collapse. The relation between the normal and tangential forces (stresses) acting on the failure surface of the potentially sliding mass is given by the coulomb friction law:

$$\tau_f = \sigma_f \tan\delta \qquad (4.2.1\text{-}1)$$

Also, according to this law the shearing resistance between the material and wall could be written as

$$\tau_w = \sigma_w \tan\delta_w \qquad (4.2.1\text{-}2)$$

The equations were written by dividing the annular region into a number of finite slices by vertical lines with coordinates x_0, x_1, ..., x_n. This division was carried out so that within each slice the portion of the failure surface was linear, and it was assumed that each slice is a column of material acting independent of the other columns. Figure 21-a presents a one half of a spouted bed with the position of the slices. The objective was to

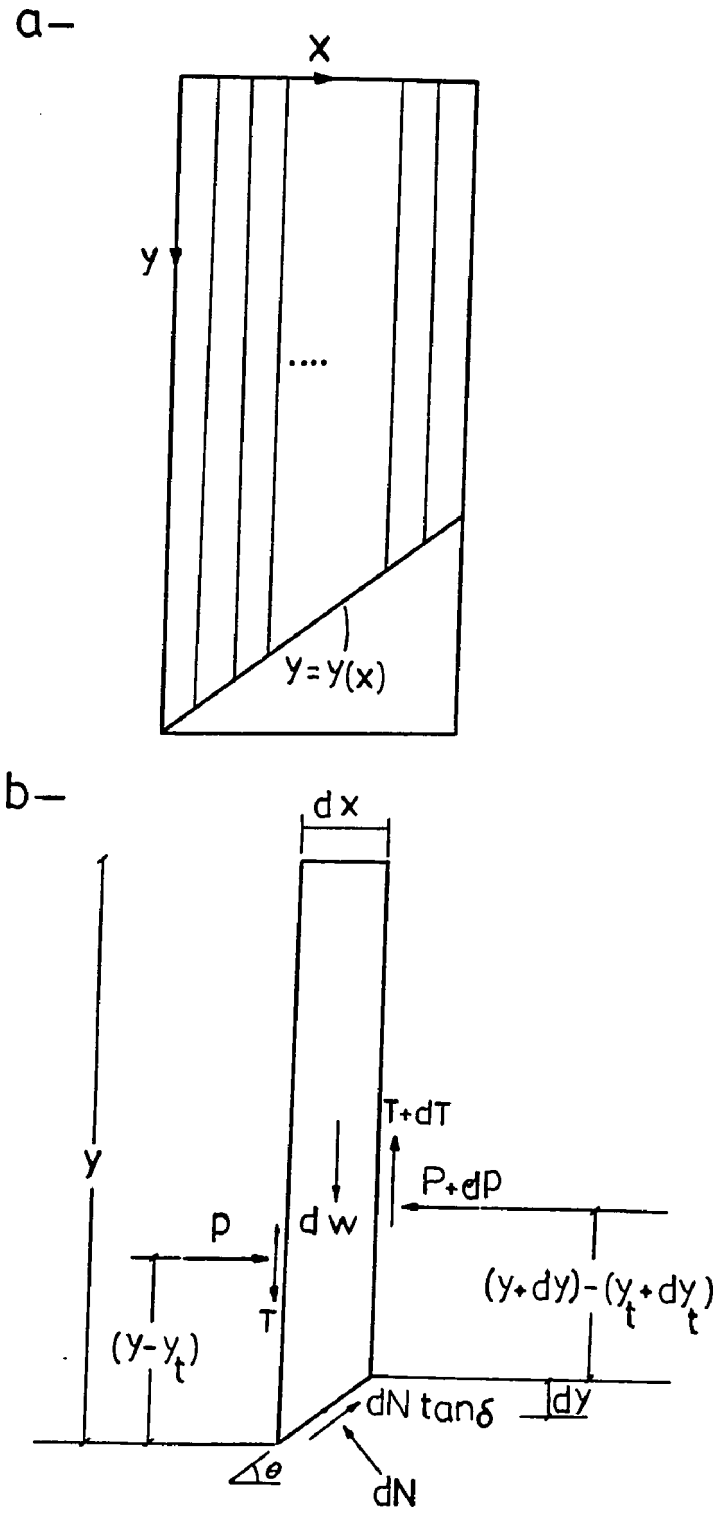

Figure 21 Method of slices

a) semi-spouted bed with position of slices
b) forces acting on a slice

evaluate the angle of the slip line for each individual slice so that all the equilibrium conditions were satisfied. A typical slice is shown in Figure 21-b along with the associated forces. In this Figure:

P = the lateral force (thrust) on the side of the slice,
dP = the change of magnitude of the lateral force,
dW = the effective weight of the slice,
dN = the normal force on the base of the slice,
T = the vertical shear force on the side of the slice,
dT = the change of magnitude of the vertical shear force,
y_t = the equation of the position of the horizontal force,

θ = the inclination of the base of the slice respect to the horizontal axis.

All the variables correspond to the dimensionless quantities.

For equilibrium in the x direction,

$$dN \tan\delta\cos\theta = dN \sin\theta + dP \qquad (4.2.1\text{-}3)$$

and for equilibrium in the y direction,

$$(\tan\delta\sin\theta + \cos\theta)dN = dW - dT \qquad (4.2.1\text{-}4)$$

Eliminating dN from equations (4.2.1-3,4) it can be readily shown that:

$$dP = \tan(\delta-\theta)(dW - dT) \qquad (4.2.1\text{-}5)$$

The condition that there be no rotation of the slice can be satisfied if the sum of the moments about the center of the base of the slice is equal to zero. Taking moments about the midpoint of the base of the slice, it can be

written:

$$P[y-y_t-(-dy/2)] - Tdx/2 - (P+dP)[y+dy-y_t-dy_t +(-dy/2)] - (T+dT)dx/2 = 0 \qquad (4.2.1\text{-}6)$$

After simplifying and proceeding to the limit it can be readily shown that:

$$T + y\frac{dP}{dx} = \frac{d}{dx}(Py_t) \qquad (4.2.1\text{-}7)$$

The effective weight of the slice dW, using equation (3.2-5), can be written as:

$$\frac{dW}{dx} = [1 - B\cos(\frac{\pi}{2H}y)]y \qquad (4.2.1\text{-}8)$$

The factor B may be obtained from (3.1.1-6). Substituting dW and also noticing that in the specified coordinate system $\tan\theta=-dy/dx$, equation (4.2.1-5) can be written as

$$\frac{dP}{dx} = \frac{\tan\delta+(dy/dx)}{1-\tan\delta(dy/dx)}\{-\frac{dT}{dx} + [1-B\cos(\frac{\pi}{2H}y)]\,y\} \qquad (4.2.1\text{-}9)$$

It was assumed that the line of thrust passes through the lower third points of each slice. This assumption corresponds to a hydrostatic pressure distribution and has also been used by Janbu (1957) to determine the earth pressure coefficients for a chosen slip surface by the method of composite surfaces. Thus, equation (4.2.1-7) can

be written as

$$T + y\frac{dP}{dx} = \frac{2}{3}\frac{d}{dx}(Py) \qquad (4.2.1\text{-}10)$$

The two governing equations (4.2.1-9) and (4.2.1-10) involve three unknown functions P, T and y, that is, the system is statically indeterminate as long as the actual stress conditions were not explored. However, to render the problem statically determinate two approaches might be used. In order to obtain a complete, exact and unique solution it is necessary to use a stress-strain relationship which is not as yet known or practical. The alternative is to make a set of assumptions that reduce the problem to statically determinate problem and in this case there will be a range of possible solutions rather than a unique solution. Following the Morgenstern and Price (1965) method a function f(x) was assumed relating the side forces P(x) and T(x) as

$$f(x) = \frac{T(x)}{P(x)} = \tan[\alpha(x)] \qquad (4.2.1\text{-}11)$$

The function f(x) describes the pattern by which $\alpha(x)$ varies from interface to interface. If f(x) [or $\alpha(x)$] is specified the problem is statically determinate so that P and y may be found from a solution to the governing equations that satisfies the appropriate boundary conditions.

The function f(x) can take any prescribed form in principle and one must exercise judgment and intuition in the assumption of this function. Having made an assumption regarding f(x) and having the result of the computations for any given case, all the computed quantities must be examined to check whether they seem reasonable in the light of intuition (Whitman and Bailey, 1967).

The two governing equations (4.2.1-9) and (4.2.1-10) can be written in finite difference form and solved for each slice applying proper boundary conditions for a given f(x) to obtain Δy and ΔP. The boundary conditions are:

For the first slice, x=0 : $\alpha=0$, y=H, $P_s=J_g+J_s$ a

For the last slice, x=1 : $\alpha=\delta_w$ (4.2.1-12b)

The total force at the spout was assumed to be the sum of force J_g applied by the gas and force J_s exerted by the solid interaction at the spout wall. The net horizontal gas force is given by the horizontal pressure drop, as given by the Lefroy and Davidson (1969) gas pressure distribution. J_g can then be obtained employing this distribution and taking the average of this force. It must be mentioned that this value is approximated by 12% since the ratio of the wall to spout pressure in Figure 15 is shown to be 0.88. However, the results of the computation

are shown to be not too sensitive to this approximation. J_s was obtained using stress distribution by the method of differential slices (section 5.1) for the vertical part along with a linear stress distribution for the conical part yielding zero solid stress at the bottom of the bed. Using the described approximated spout force requires a sensitivity analysis concerning the effect of this force on the outcome of the computations.

4.2.2 Calculation procedure and results

The calculations started by fixing the number of slices. It was assumed that the potentially sliding body in the annulus may be divided into a number of finite slices of identical thickness by vertical lines. The governing equations (4.2.1-9) and (4.2.1-10) were then solved in their finite difference form. This was done by substituting the differentials (d) by the differences (Δ). The resulted algebraic system of equations were then solved for the first slice using proper conditions, based on a guessed H_D (height of the dead zone at the bed wall), to obtain Δy and ΔP by means of a successive approximate procedure. This procedure was based on a fast convergence technique. Having determined Δy and ΔP for the first slice computations were then continued for the second slice applying proper conditions for that slice. The

method was followed for each slice repeatedly until the last slice. Having obtained the height of dead zone at the wall the numerical value of P_s was updated and the computations were repeated.

Several functions were attempted to describe the pattern of changing $\alpha(x)$. Figure 23 shows two of such functions. These two functions were found to give reasonable results in the light of intuition; i.e., the height of dead zone increased as δ or δ_w increased. Employment of function 23-a yielded particularly acceptable results for a range of δ in the light of experimental evidence. These results are shown in Figure 24. The dead zone strongly depends on the angle of friction. Solids possessing a large angle δ form a much steeper boundary. Function 23-b, on the other hand, yielded reasonable results only for $30^{o}<\delta<40^{o}$. These are shown in Figure 25. Comparison of Figures 24 and 25 indicates that f(x) has some bearing on the shape of the boundary, but the height of the boundary at the bed wall is reasonably unaffected by f(x). However, to make a general conclusion about the effect of f(x) on the boundary more functions must be tried.

The influence of N, the number of slices, on the boundary was also examined. The results indicated that

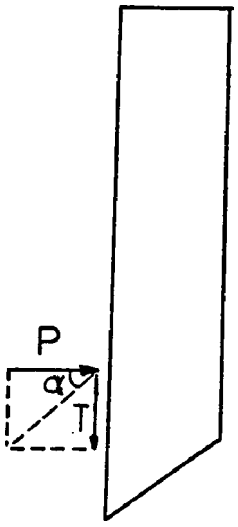

Figure 22 Side forces and angle α

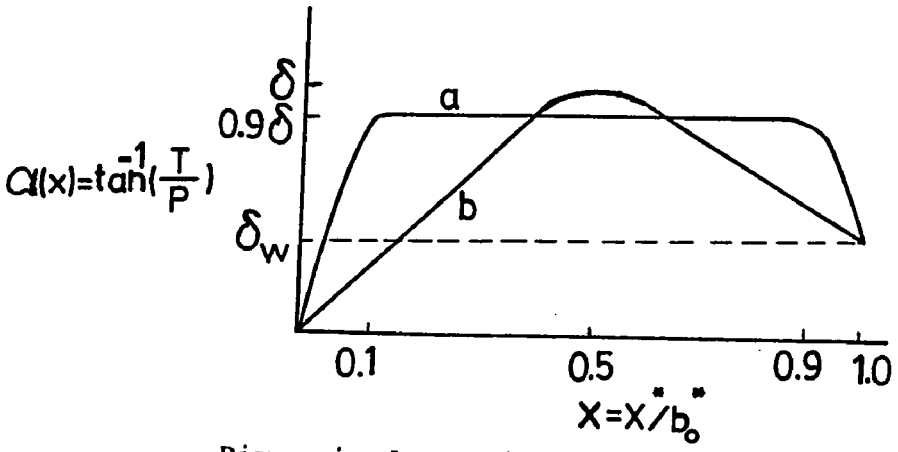

Figure 23 Functions α employed in the method of slices

changing N from 100 to 10 changes the height of the boundary only by one percent. Predictions were not consistent for the values of N less than 10. In order to keep the computations at its minimum and at the same time obtain an acceptable results, it is suggested that the slice number taken to be equal to 10. This analysis was done using Functions 23-a and 23-b. The outcome of the analysis may differ for other functions. Results of the analysis also indicated that the height of the material at the bed wall is not sensitive to the value of P_s. Doubling P_s or making it half changes the H_D within 5% for different materials.

Figure 26 shows percent of the bed wall occupied by dead zone against the wall friction angle δ_w for different materials. This Figure shows that rougher walls cause the material form steeper boundaries. The effect of δ_w on the height of the boundary at the wall H_D for different material, on the other hand, can be related to the roughness ratio. This ratio has been defined by Janbu (1957) as $\psi=\tan\delta_w/\tan\delta$. Changing δ_w from 10^o to 20^o causes an increase in H_D by 6% for $\delta=20^o$ and .45% for $\delta=50^o$. The reason for this difference in the percent of H_D for the two materials may be explained by the roughness ratio. Although δ_w in both cases changes equally (10^o), the 10^o change in δ_w in the case of $\delta=20^o$ means increasing ψ to 1,

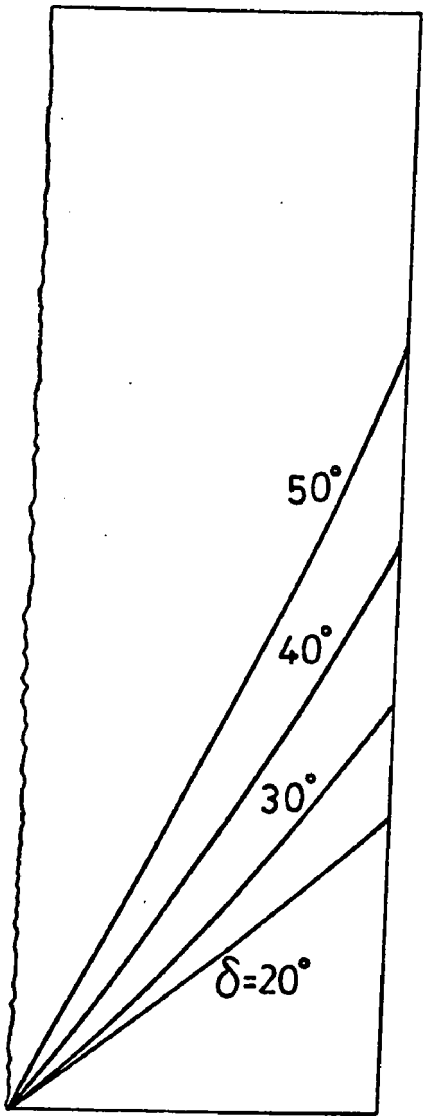

Figure 24 Boundary of dead zone
(Function 23-a)

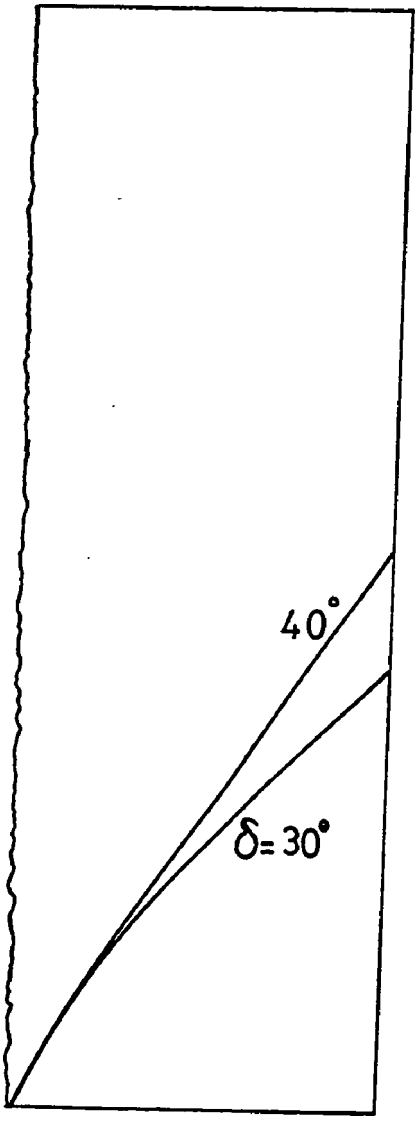

Figure 25 Boundary of dead zone
(Function 23-b)

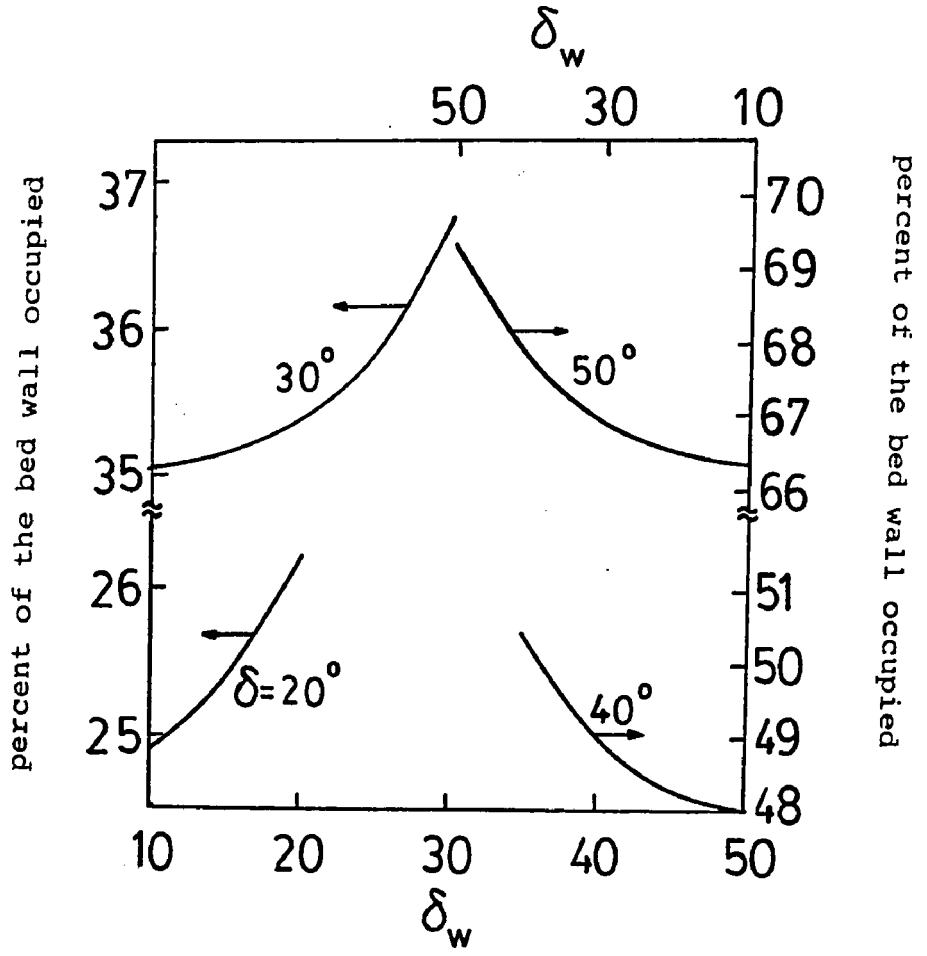

Figure 26 Percent of wall occupied by the dead zone for different δ and δ_w

while in the case of $\delta=50^{\circ}$ Ψ is increased to .3054. The effect of δ_w on the H_D is more pronounced when Ψ approaches to one. When the wall roughness is increased, H_D increases for less frictional material more than that for more frictional material. Changing δ_w from 10° to δ causes a 6% and a 4.77% increase in H_D for δ of 20° and 50°, respectively.

The predictions by the method of slices were tested experimentally. Figure 27 shows the comparison for three different H and three different materials for each H. Both the experimental and the theoretical results show that the boundary of dead zone can be well approximated by a straight line. The experimental data were obtained by operating the bed at its minimum spouting (air) velocity corresponding to each H. The MOS overpredicts the boundary for case of H=1. The agreements are much better for cases of H equal to 2 and 3, especially for $\delta=40^{\circ}$.

We may conclude that the method of slices is capable of predicting the boundary of the dead zone. Although the solution may not be unique, but physical intuition can help in the choice of the right solution. This solution is generally distinguished by the physics of the problem, or, if possible, experimental evidence.

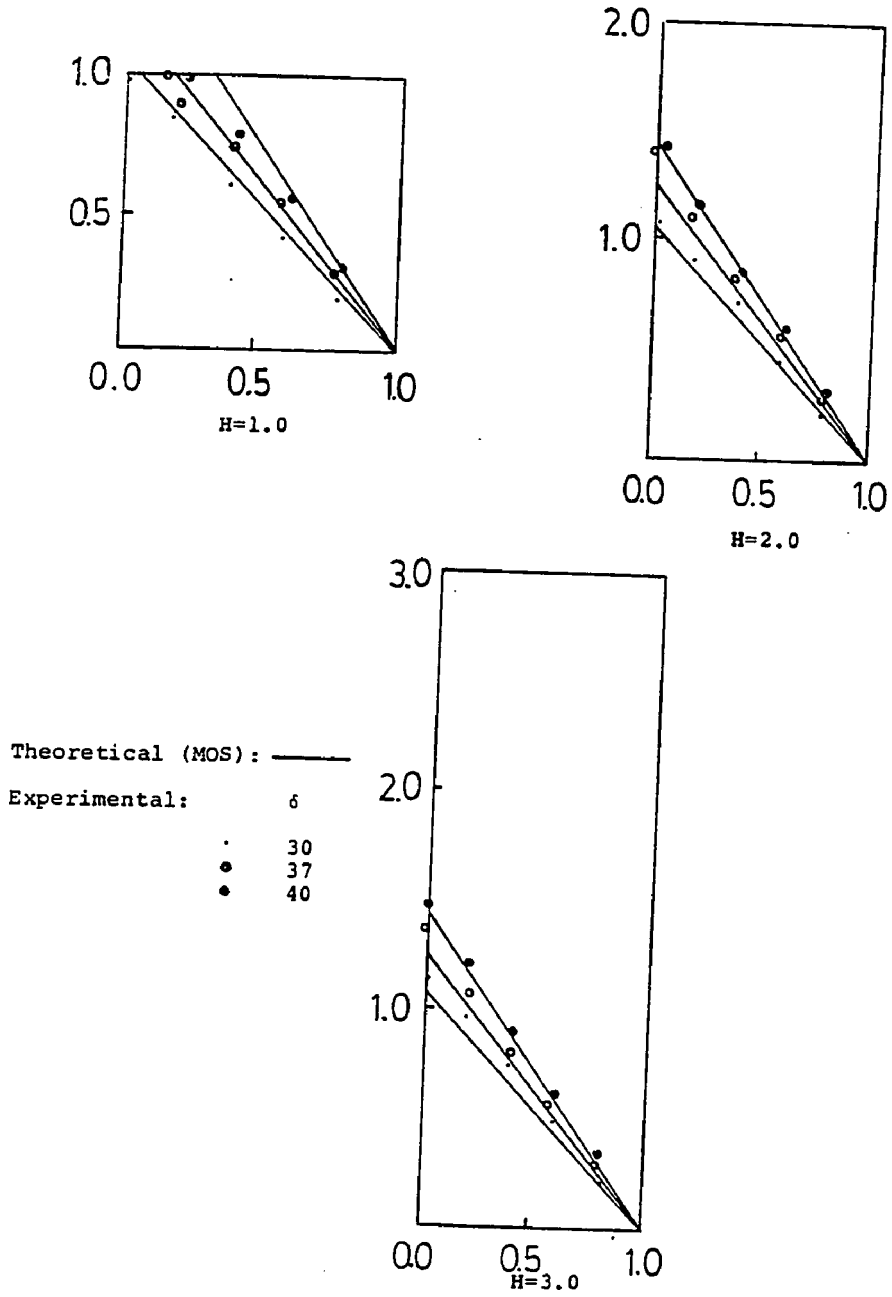

Figure 27 Comparispon of the boundary of dead zone with the model

CHAPTER FIVE

5.0 ANALYSIS OF STRESS AND VELOCITY FIELDS

The solution of mathematical models developed for the motion of the solid particles in the dense region are described in this chapter.

An active state of stress was assumed in the vertical part of the annulus where the material is being compressed vertically and expand horizontally toward the spout. The flow in this portion is divergent. In the conical region the material is being compressed horizontally. The observations and photographs indicate that the flow in this portion is convergent. Thus, a passive state of stress must exist in the conical region.

A stress analysis was made applying the method of differential slices (MOS) previously employed in bins and hoppers by Walker (1966). The method considers the forces acting on a horizontal differential element, and uses distribution factors to calculate the stress distributions. The normal and shear stress at the walls obtained by this method for a vertical bunker without many computations and numerical difficulties comparing to the other methods. However, it was not attempted to employ this method for the conical part because of the uncertainity about the

validity of constant distribution factors in this part, as discussed in 5.1. This method is discussed in section 5.1.

A more precise solution can be obtained applying the method of integral relations (MOI). This method is analogous to the Karman-Pohlhausen integral method commonly used in fluid mechanics for the analysis of boundary layers. The method of integral relations is able to predict the stress distributions in both the vertical and conical sections of the annulus whenever a limit equilibrium solution exists. Although this method involves somewhat lengthy calculations, it provides an approximate analytical solution for the stress distribution that is particularly useful in the computation of the velocity field as is discussed in section 5.4. This method is discussed in section 5.2.

A detailed computation of the stress field was also made using the method of characteristics (MOC). This method provides a systematic numerical approximation to the exact solution can be used as a basis to evaluate the approximated methods such as the method of integral relations. It is, however, rather cumbersome and it was attempted to ease these difficulties by introducing some ap-

proximations when applicable. The stress analysis by the method of characteristics is discussed in section 5.3.

All stresses discussed in this chapter are effective stresses.

The velocity field was also obtained by the method of characteristics. To obtain the velocity field, the orientation of the major stress ϕ is needed. This orientation was obtained employing the method of integral relations since an analytical expression of ϕ is given by this method. Applying the method of characteristics for this purpose would have required a point by point interpolation since ϕ was known only at the grid points. The velocity field is discussed in section 5.4.

5.1 The Method of Differential Slices (MOS)

The formation of the dead zone divides the annulus region into two parts: the vertical section and the converging (conical) section. In the vertical section the material is bounded by the bed wall and the spout wall whereas the material in the conical section is bounded by the dead zone boundary and the spout wall. The boundary of dead zone was shown that could be described by a straight line in 4.2. While the material yield throughout the particle volume the particles of the vertical section adjacent to the bed wall must yield at that wall, and the particles of the conical section have to face the particles at rest in order to yield. Thus, when particles move from the vertical section to the conical section the frictional resistance switches from particle-wall to particle-particle at the boundary of dead zone.

An approximate stress analysis using Walker's (1966) method was developed for the vertical section. Walker's method is based on Janssen's analysis (see Hancock and Nedderman, 1974). Janssen developed his original analysis for a cylindrical bunker by using a differential slice in determining the wall stresses. His original analysis contains two important assumptions: first, the stresses are independent of radial position; and second, the radial and

vertical stresses are principal stresses in the ratio of

$$K = \frac{1+\sin\delta}{1-\sin\delta} \qquad (5.1\text{-}1)$$

Assuming the radial and vertical stresses as principal stresses, the equation (5.1-1) is then a consequence of the yield condition. Although these assumptions greatly simplifies the determination of wall stresses, they provide only approximate values of the stresses. The second assumption, on the other hand, is inconsistent with the basic definition of principal stress. If the radial stress at the wall is a principal stress the wall shear stress must be zero, while Janssen analysis indicates that the wall shear stress asymptotically approaches to a constant. Walker relaxed the Janssen's assumptions by distinguishing between the average value of the axial stress $\bar{\sigma}_y$ and the value at the wall $(\sigma_y)_w$.

The Walker's modification of Janssen's analysis was used to calculate stress distribution for the material in the vertical portion of the annulus. Considering a differential slice shown in Figure 28, the equilibrium equation can be written:

$$\frac{d\bar{\sigma}_y}{dy} - (\tau_{xy})_s + (\tau_{xy})_w = \frac{\rho_e}{\rho_b} \qquad (5.1\text{-}2)$$

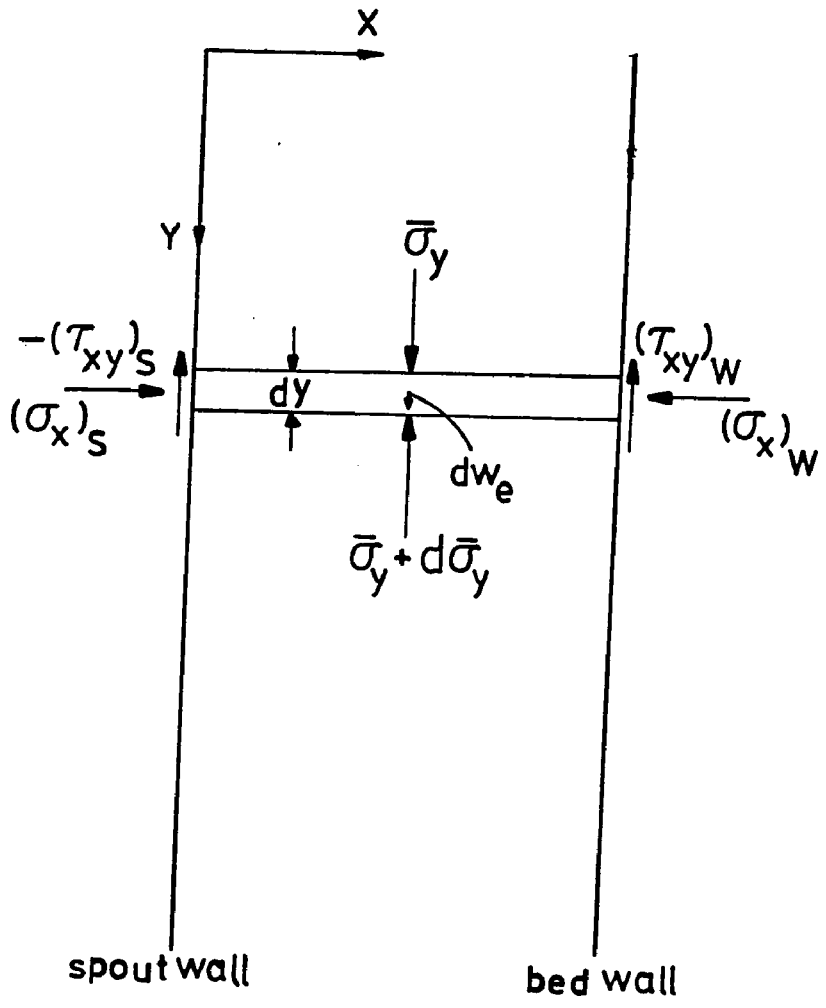

Figure 28 Differential element and force balance

where $\bar{\sigma}_y$ is the dimensionless mean vertical stress over a horizontal section. $(\tau_{xy})_w$ can be related to $(\sigma_y)_w$ by considering the geometry of Figure 17a:

$$OW = r/\sin\delta \quad , \quad MW = OW \sin\delta_w = r \sin\delta_w/\sin\delta$$

$$< KWM = \cos^{-1}(MW/r) = \cos^{-1}(\sin\delta_w/\sin\delta)$$

$$< MWQ = \pi/2 - \delta_w$$

so

$$2\phi_w = \pi/2 - \delta_w - \cos^{-1}(\sin\delta_w/\sin\delta) \qquad (5.1\text{-}3)$$

but

$$(\tau_{xy})_w = KQ = r \sin 2\phi_w$$

$$(\sigma_y)_w = OR = r/\sin\delta + r\cos 2\phi_w$$

Hence,

$$(\tau_{xy})_w = B_w(\sigma_y)_w \qquad (5.1\text{-}4)$$

where

$$B_w = \frac{\sin\delta \sin 2\phi_w}{1 + \sin\delta\cos 2\phi_w} \qquad (5.1\text{-}5)$$

Substituting the value of ϕ_w from (5.1-3) into (5.1-5), B_w can be written:

$$B_w = \frac{\sin\delta_w[\cos\delta_w - (\sin^2\delta - \sin^2\delta_w)^{1/2}]}{1+\sin^2\delta_w + \cos\delta_w(\sin^2\delta - \sin^2\delta_w)^{1/2}} \qquad (5.1\text{-}6)$$

values of B_w are shown in Figure 29 for different values of δ_w and δ as a parameter.

Following the same procedure by considering the geometry of Figure 17b it can be shown that

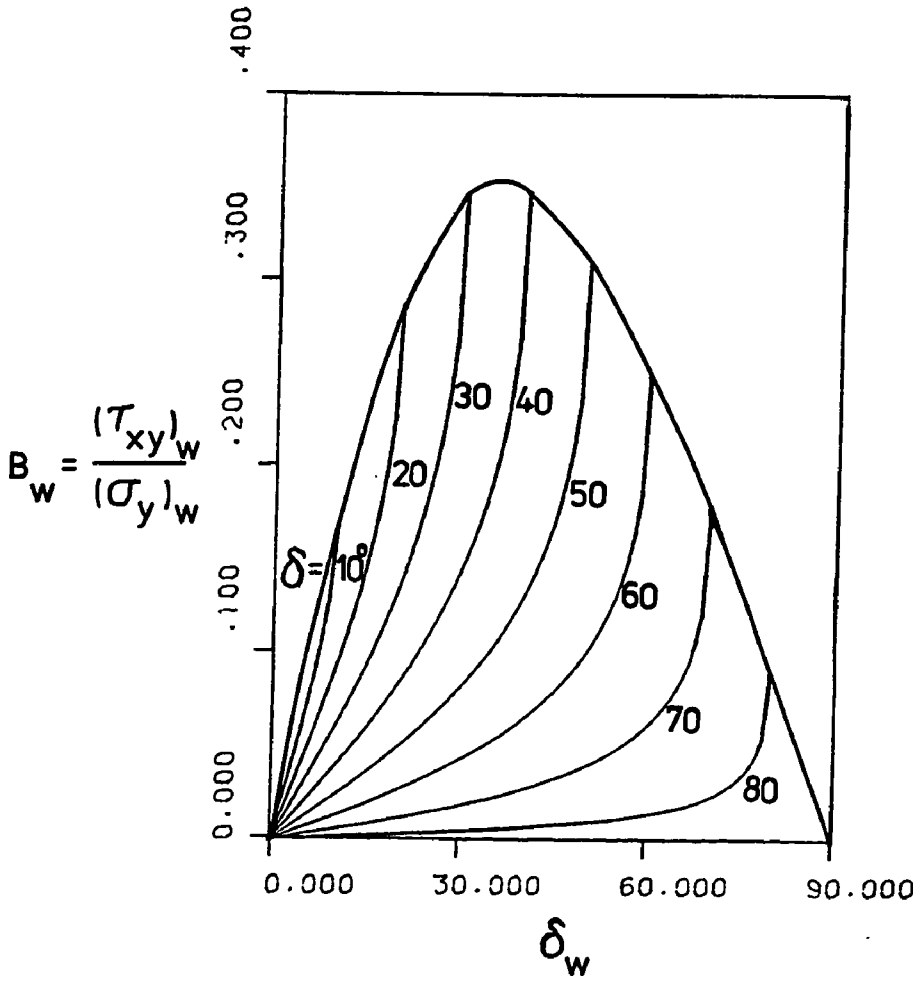

Figure 29 Relation between the vertical and shear stresses at the wall (active case) as a function of the internal (δ) and wall friction angles (δ_w)

$$(\tau_{xy})_s = B_s(\sigma_y)_s \qquad (5.1\text{-}7)$$

$$B_s = \frac{\sin\delta_s[\cos\delta_s-(\sin^2\delta-\sin^2\delta_s)^{1/2}]}{1+\sin^2\delta_s+\cos\delta_s(\sin^2\delta-\sin^2\delta_s)^{1/2}} \qquad (5.1\text{-}8)$$

Figure 30 presents a plot of B_s vs δ_s ($=0.1\delta$).

The average vertical stress $\bar{\sigma}_y$ can be related to the vertical stress at the walls $(\sigma_y)_w$ and $(\sigma_y)_s$ by the Walker's distribution factor D:

$$D_w = (\sigma_y)_w/\bar{\sigma}_y \qquad (5.1\text{-}9)$$

$$D_s = (\sigma_y)_s/\bar{\sigma}_y \qquad (5.1\text{-}10)$$

In general the distribution factor is an unknown function of y. Combining equations (5.1-4, 7, 9, 10), it can be written

$$(\tau_{xy})_w = B_w D_w \bar{\sigma}_y \qquad (5.1\text{-}11)$$

$$(\tau_{xy})_s = B_s D_s \bar{\sigma}_y \qquad (5.1\text{-}12)$$

Substituting the values of shear stresses from (5.1-11,12) and the value of ρ_e/ρ_b from (3.2-6) into the equation (5.1-2), this equation can be written:

$$\frac{d\bar{\sigma}_y}{dy} + K\bar{\sigma}_y = 1 - B\cos\frac{\pi y}{2H} \qquad (5.1\text{-}13)$$

in which $K=(B_wD_w-B_sD_s)$. No approximation has yet been used in obtaining equation (5.1-13), that is, the equation

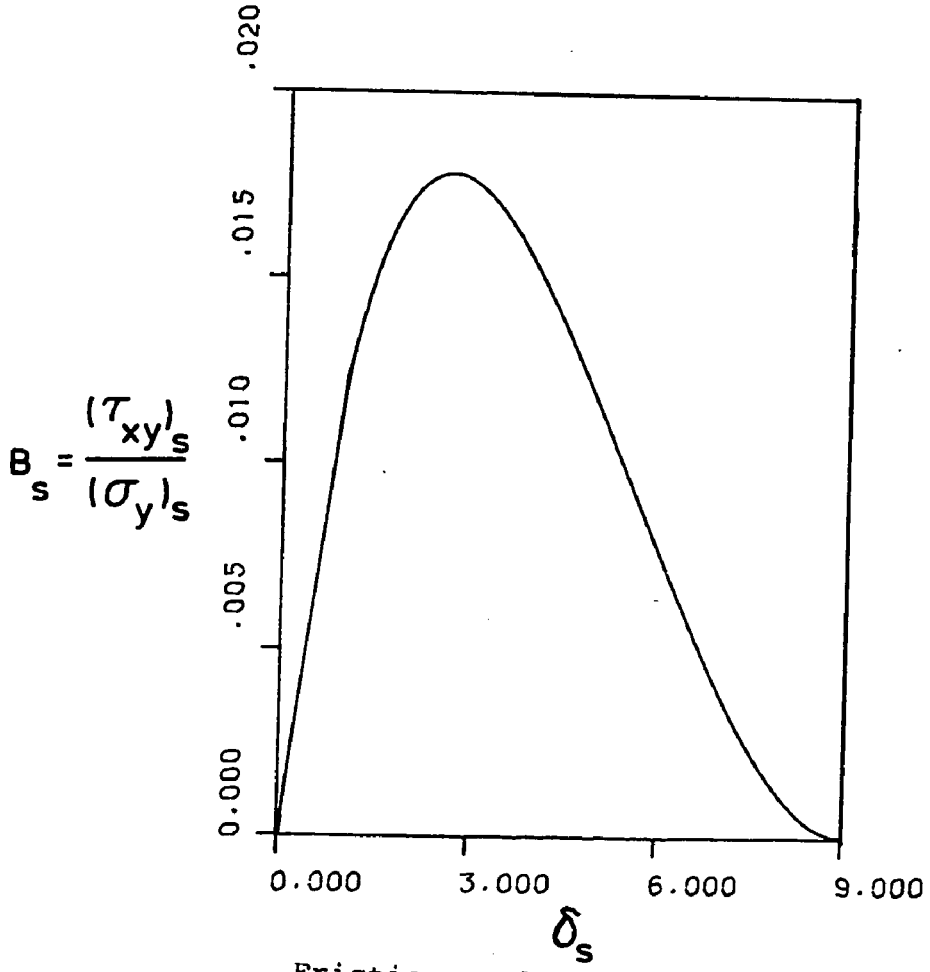

Figure 30 Relation between the vertical and shear stresses at the wall of the spout (active case) with $\delta/\delta_s=10$

is exact. But, it can not be solved since D's are unknown functions. Walker, however, notes that the value of D at great depth can be assumed to be constant and is then easily calculated. The evaluation of D (Walters, 1973b) is based on the assumption that stresses are invariant with height at great depth (the deep bed approximation), and that the horizontal normal stress is independent of x. In a two dimensional situation the equilibrium equations along with the deep bed approximation require that σ_x be independent of x, however, as Walters and Nedderman (1973) point out, in cylindrical systems σ_r is not constant because of the influence of the circumferential stress σ_θ. Thus the values of D presented by Walters (1973b) for the cylindrical bins are not exact. Following Walters, the D's are derived in Appendix 1. The results are shown graphically for all combinations of δ and δ_w in Figure 31 and 32. Walker (1966) mostly considered the case D=1 which he claimed to be a very good approximation for all possible cases. Figure 31 shows that the Walker assumption is not very accurate for the cases where δ/δ_w is close to 1.

Notice that the value of the constant K in equation (5.1-13) could also had been found directly by noticing that

$$\tau_w = (\tan\delta_w)\sigma_x \quad ; \quad \tau_s = (\tan\delta_s)\sigma_x$$

which can be combined with the relation between σ_x and σ_y given by equation (A.1.7) of Appendix 1 to give

$$K = \frac{\frac{\cos^2\delta}{\sin\delta}(\psi_w-\psi_s)(\tan\delta_w+\tan\delta_s)}{\frac{1+\sin^2\delta}{\sin\delta}(\psi_w-\psi_s)-\psi_w\sqrt{1-\psi_w^2}+\psi_s\sqrt{1-\psi_s^2}-\sin^{-1}\psi_w+\sin^{-1}\psi_s}$$

Equation (5.1-13) can now be integrated since D's are constants, subject to the no surcharge boundary condition:

$$y=0 \quad ; \qquad \bar{\sigma}_y=0 \qquad (5.1\text{-}14)$$

and the solution is given by:

$$\bar{\sigma}_y = \frac{1}{K}(1 - e^{-Ky}) + \frac{B}{K^2+(\frac{\pi}{2H})^2}[Ke^{-Ky} - K\cos\frac{\pi y}{2H} - \frac{\pi}{2H}\sin\frac{\pi y}{2H}] \qquad (5.1\text{-}15)$$

The other stresses can be written:

$$(\tau_{xy})_w = B_w D_w[\bar{\sigma}_y] \qquad (5.1\text{-}16\ a)$$

$$(\tau_{xy})_s = B_s D_s[\bar{\sigma}_y] \qquad (5.1\text{-}16\ b)$$

$$(\sigma_y)_w = D_w[\bar{\sigma}_y] \qquad (5.1\text{-}16\ c)$$

$$(\sigma_y)_s = D_s[\bar{\sigma}_y] \qquad (5.1\text{-}16\ d)$$

$$\sigma_x = \frac{B_w D_w}{\tan\delta_w}[\bar{\sigma}_y] \qquad (5.1\text{-}16\ e)$$

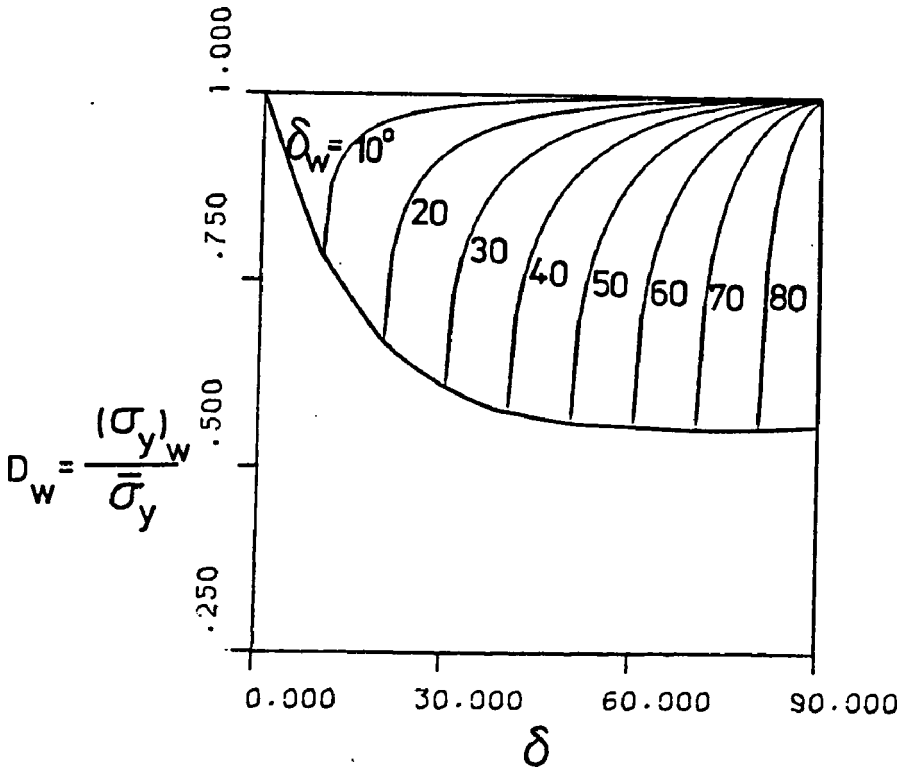

Figure 31 Distribution coefficients (D_w) relating the vertical normal stress at the wall $(\sigma_y)_w$ to the average normal stress σ_y across the width of annulus vs. the angles of internal (δ) and wall (δ_w) friction

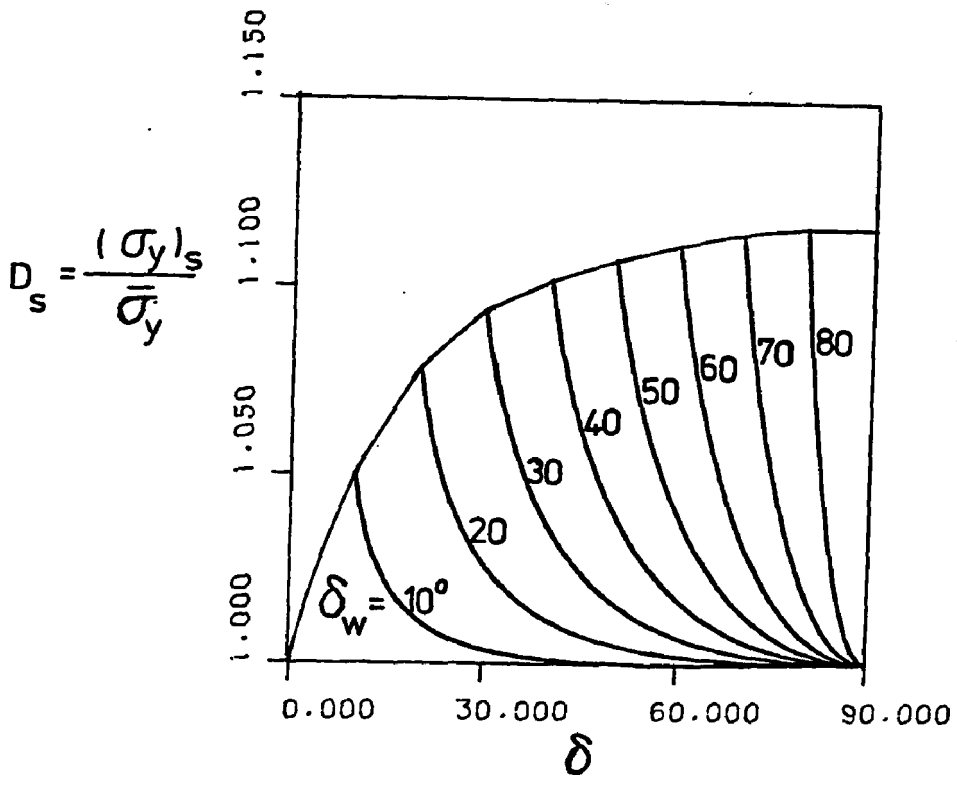

Figure 32 Distribution coefficients (D_s) relating the vertical normal stress at the spout wall $(\sigma_y)_w$ to the average normal stress σ_y across the width of annulus vs. the angles of internal (δ) and spout wall (δ_s) friction

in which $[\bar{\sigma}_y]$ corresponds to the mean vertical stress distribution given by equation (5.1-15). Figure 33a represents the stresses graphically for two cases of fluid flow and no fluid flow. The case B=0 corresponds to an annular hopper with no gas flow and the other case, B=1, corresponds to a spouted bed at maximum spouting height. For simplicity the existence of the dead zone has been ignored to obtain the approximate depth where the deep bed approximation can be applied. From Figure 33a it seems that for a two dimensional bed, with no flow of gas in the annulus (constant density), the deep bed approximation would be applicable at greater depths (for the present analysis this depth seems to be at least four times of the annulus width). If the gas flow is considered (case of a spouted bed) the deep bed approximation will not be applicable for any bed depth. This can be seen from the analytical solution, equation (5.1-15). McNab and Bridgwater (1974) have applied the deep bed approximation to a cylindrical spouted bed (with the assumption of constant density) to locate the position of the spout wall. The results of the present analysis show that this approximation is invalid for spouted beds where the effective density varies with height. They (McNab and Bridgwater, 1979) have done very similar analysis to the present one for the effective solid stresses in the an-

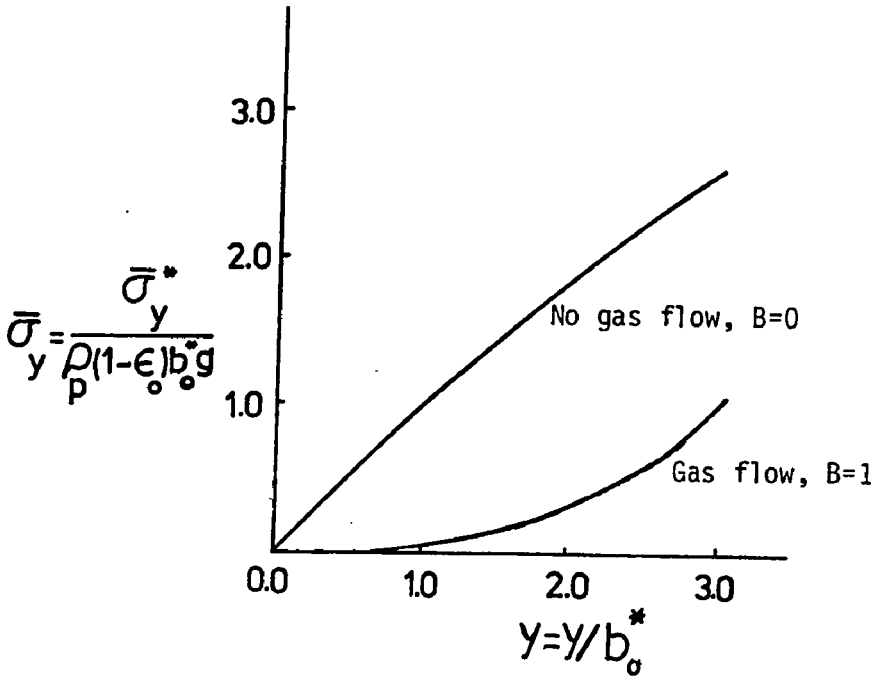

For	Multiply by
$(\tau_{xy})_w$	0.08009
$(\sigma_y)_w$	0.9650
$(\tau_{xy})_s$	-0.0151
$(\sigma_y)_s$	1.0110
σ_x	0.2203

Figure 33a Stress distributions obtained using the method differential slices (MOS) in the active case ($\delta=40^o$, $\delta_w=20^o$, $\delta_s=4^o$ and H=3)

nular region of a cylindrical spouted bed. In their analysis they have chosen $D_s=D_w=1$, an assumption which is shown later (section 5.3.6) that is valid only for a short distance (about half of the annulus width) from the top of the annulus. However, the results of their analysis also indicate that the stresses do not approach asymptotically to a constant if the gas flow is considered. To further investigate the deep bed assumption for spouted beds the average normal stress $\bar{\sigma}_y$ has been plotted for deeper beds. Figure 33b shows $\bar{\sigma}_y$ for three different depth H. It is clear that the deep bed assumption is not a valid approximation for spouted beds. Results shown in Figures 33a and 33b also indicate to the fact that moving down from the free surface stresses increase but not as rapidly as in the annular bin in which the flow is absent. In the case of spouted bed at maximum spoutable height (B=1) the stresses are relaxed near the free stress surface. In this case, the drag of upward flowing gas supports most of the weight of the annular material, the particles are fluidized at the top of the bed and this may account for the leveling off the stresses, and, also, reducing the numerical value of stresses. Results of the analysis for different wall indicate that as the wall roughness increases $\bar{\sigma}_y$ decreases slightly since the wall can support more shear stress, as shown in Figure 34.

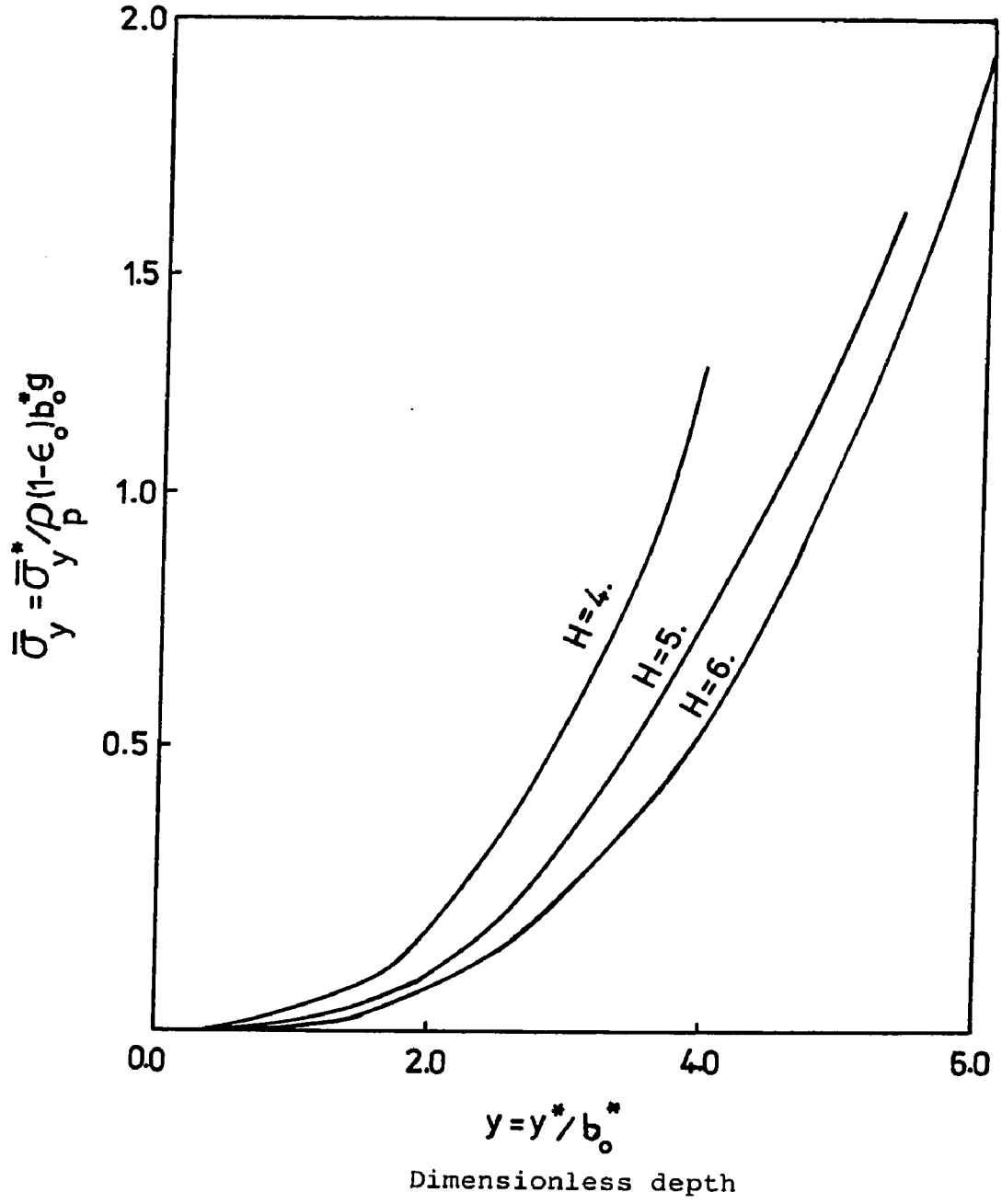

Figure 33b Distribution of the average normal stress ($\bar{\sigma}_y$) obtained for three different bed depth using the method of slices considering the gas flow (B=1) ($\delta=40^o$, $\delta_w=20^o$ and $\delta_s=4^o$)

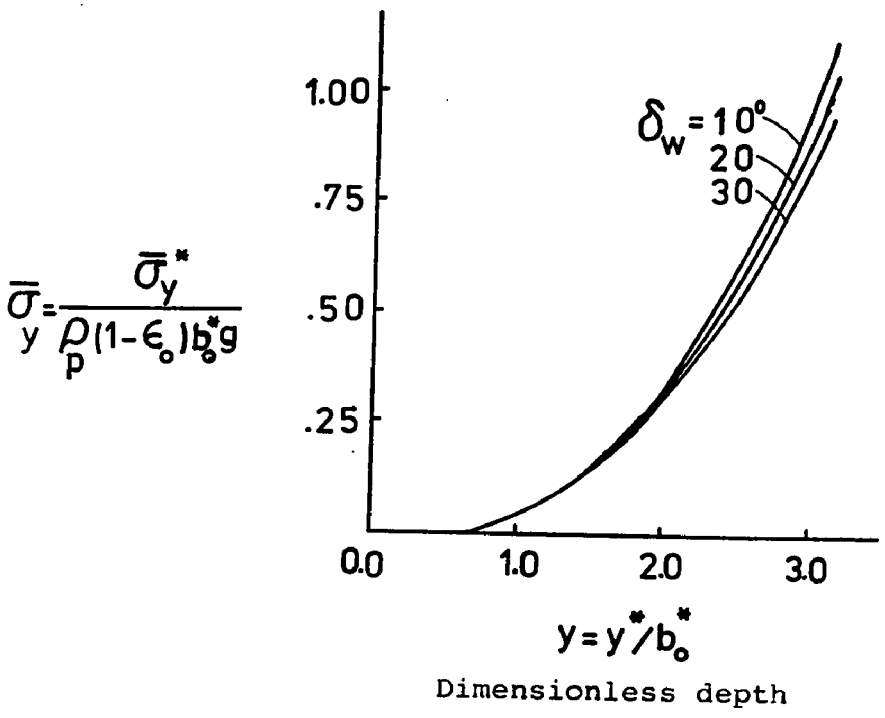

Figure 34 Distribution of the average normal stress for various δ_w ($\delta=30^o$, $\delta_s=3^o$, H=3)

The MOS was not used to determine the stress distribution in the conical section of the annulus basically because of the uncertainity about the distribution factors. Walters (1973a) has made a theoretical analysis of stresses in axially symmetric hoppers and bunkers where he has used the distribution factors. He has employed the deep bed assumption to evaluate D, but as a result of this assumption a limit must be imposed on the angle of inclination of the hopper wall. Recently Nedderman (1982) in a review paper has argued that since it is only possible to evaluate D at great depth in a vertical part, it is far from clear that the value of D evaluated for a converging part corresponds to an appropriate value.

In conclusion the MOS is the simplest up to date method capable of determining the approximate stresses in bins and spouted beds. However, because of the discussed approximations this method was not used to calculate the velocity field. It provides, however, an insight into the stresses distribution in the vertical region of the spouted bed and of the effect of the gas flow on those stresses.

5.2 Stress Field by Method of Integrals (MOI)

The stresses developed in the annulus part of a spouted bed may be analyzed by the method of integral relations. This method was originally proposed by Dorodnitsyn (1962) as a technique to solve the non-linear equations containing partial derivatives arising on aerodynamics problems. The method of Karman-Pohlhausen integral applied to the boundary layer type of problems can be considered a special case of the general technique of the method of integral relations. This method was used later by Belotserkovskii and Chuskin (1965) as a numerical tool to solve problems in gas dynamics. They found that the method gives greater accuracy than the method of finite differences. The method of integral relations has also the advantage of using the very well-developed numerical methods for solving ordinary differential equations. Savage and Yong (1970) have also used this method to analyze the stresses developed by a cohesionless material in bins. Savage's analysis which is somewhat analogous to the Karman-Pohlhausen integral method (Schlichting, 1978) commonly used in fluid mechanics for the analysis of boundary layers, is adopted here to determine the approximate stress field for the material contained in the annulus.

The integral relations method basically reduces, by integration, the system of non-linear partial differential equations to the numerical solution of some approximating system of ordinary differential equations. In this procedure the governing partial differential equations are not satisfied at every point within the region of interest, but they are satisfied in some average way across the width of the pertinent region. In this method a curvilinear strips conforming to the shape of the region of integration is made. The integration is then performed across these strips using the most general form of interpolation expressions (approximating polynomials) for the integrand functions. A systematic numerical approximation to the stress field can be obtained by the method of characteristics which is discussed in 5.3. This method which provides numerical solutions can be used to assess the accuracy of other approximate methods. Unfortunately, the method is complicated when there are regions of stress discontinuities within the region of interest. Two regions where stress discontinuitties occur in a bin or in the annulus part of a spouted bed are the upper corners of the bed (formed by the free surface and the walls), and the junction of the upper vertical part with the conical part (Jenike and Johanson 1968, Walker, 1966). The presence of the discontinuities are detected by the coalescence of the

characteristics if the exact method is used. On the other hand, the method of integrals has the advantage that it can average through stress discontinuities, thus circumventing the difficulties arising in the exact method of characteristics. An analysis of the discontinuity, the consequent shock front together with the techniques to solve the associated numerical difficulties is given in 5.3.4. The method of integral relations developed here for the computation of stresses in the annulus part of a spouted bed can be looked upon as an extension of the simple analysis of "Method of Differential Slices" discussed in section 5.1.

5.2.1 The governing equations

The governing equations are those described in section 3.3.1. Taking the integral of each term in the equations (3.3.1-9) and (3.3.1-10) between the spout wall x=0 and the wall bordering the annulus region x=b(y), Figure 14, it can be written

$$\sigma_{xw}^* - \sigma_{xs}^* + \int_S^W \frac{\partial \tau^*}{\partial y^*} dx^* = 0 \qquad (5.2.1\text{-}1)$$

$$\int_S^W \frac{\partial \sigma_y^*}{\partial y^*} dx^* + \tau_w^* - \tau_s^* = \rho_e b^* \qquad (5.2.1\text{-}2)$$

where τ_w^* and τ_s^* are τ_{xy}^* at the bed and the spout wall, respectively.

The distribution of σ_y^* and τ^* across the width of the annulus may be assumed as

$$\sigma_y^* = \sigma_{ys}^* + a^*(y^*)(x^*/b^*)^2 \qquad (5.2.1\text{-}3)$$

$$\tau^* = \tau_s^* + (\tau_w^* - \tau_s^*)(x^*/b^*) \qquad (5.2.1\text{-}4)$$

These types of distribution have been used by Savage and Yong (1970) to obtain stress distribution for the solids flowing in a bunker, on the basis of physical intuition and with the benefit of the knowledge gained from the method of characteristics solutions. Because of the similarity between the solid motion in an annular region of a spouted bed and a bin (Bridgwater and Mathur, 1972) they are adopted in the present analysis. This type of distributions is called by Savage "one-strip scheme". Chan (1967, see Savage and Yong, 1970) has extended the one-strip scheme by using a more general "two-strip scheme". In this scheme Chan has increased the order of the approximating polynomials corresponding to equations (5.2.1-3) and (5.2.1-4) by a fourth and third order increasing the accuracy of the computations. Additional approximating polynomial coefficients are then obtained by multiplying the governing equations by a weighting function $f(x)=x$ and integrating across the width of the domain. However, Savage and Yong (1970) indicate that the results obtained are not very different from those by the

simpler "one-strip" scheme.

Substituting equations (5.2.1-3) and (5.2.1-4) into the equations (5.2.1-1) and (5.2.1-2), making them dimensionless and integrating yields

$$\sigma_{xw} - \sigma_{xs} + \frac{b}{2b_o}\frac{d\tau_s}{dy} + \frac{b}{2b_o}\frac{d\tau_w}{dy} - \frac{1}{2b_o}(\tau_w-\tau_s)\frac{db}{dy} = 0 \qquad (5.2.1\text{-}5)$$

$$\frac{b}{b_o}\frac{d\sigma_{ys}}{dy} + \frac{b}{3}\frac{da}{dy} - \frac{2}{3}a\frac{db}{dy} + (\tau_w-\tau_s) = \frac{\rho_e}{\rho_b}\frac{b}{b_o} \qquad (5.2.1\text{-}6)$$

At the spout and the bed wall the principal stress angles ϕ_s and ϕ_w are given by the equations (3.3.3-12) and (3.3.3-8), also from the relations (3.3.1-4,5,6), or the corresponding Mohr diagram Figure 17 (a and b), the following relations can be established

$$\sigma_{xs} = S_s\sigma_{ys} \quad , \quad \sigma_{xw} = S_w\sigma_{yw}$$
$$\tau_s = T_s\sigma_{ys} \quad , \quad \tau_w = T_w\sigma_{yw} \qquad (5.2.1\text{-}7)$$

in which the constants are:

$$S_s = \frac{1-\sin\delta\cos 2\phi_s}{1+\sin\delta\cos 2\phi_s} \quad , \quad S_w = \frac{1-\sin\delta\cos 2\phi_w}{1+\sin\delta\cos 2\phi_w}$$

$$T_s = \frac{\sin\delta\sin 2\phi_s}{1+\sin\delta\cos 2\phi_s} \quad , \quad T_w = \frac{\sin\delta\sin 2\phi_w}{1+\sin\delta\cos 2\phi_w}$$

Notice that T's are identical to the B's used in the MOS, section 5.1. These relations correspond to the both cases of active and passive state of stress depending on the values of ϕ's ($\phi<45^o$ implies to active and $\phi>45^o$ to passive state). Substituting relations (5.2.1-7) into the equations (5.2.1-5) and (5.2.1-6), considering the distribution of σ_y and after some rearrangement the following system of two ordinary differential equations for the unknown functions σ_{yw} and a(y) is obtained:

$$\frac{b}{2}(T_s+T_w)\frac{d\sigma_{yw}}{dy} - \frac{b}{2}T_s\frac{da}{dy} + [(S_w-S_s) \frac{1}{2}(T_s-T_w)\frac{db}{dy}]\sigma_{yw} + (S_s - \frac{1}{2}T_s\frac{db}{dy})a = 0 \qquad (5.2.1\text{-}8)$$

$$b\frac{d\sigma_{yw}}{dy} - \frac{2}{3}b\frac{da}{dy} + (T_w-T_s)\sigma_{yw} + (T_s - \frac{2}{3}\frac{db}{dy})a = \frac{\rho_e}{\rho_b}b \qquad (5.2.1\text{-}9)$$

where $b_o=1$. Equation (5.2.1-8) and (5.2.1-9) can be integrated numerically subject to the boundary conditions $\sigma_{yw}(0)=0$ and $a(0)=0$. It is also possible to combine these two equations to obtain a single second order differential

equation for σ_{yw} which may be solved analytically. Doing so we obtain:

$$A\, b^2 \frac{d^2\sigma_{yw}}{dy^2} + B\, b \frac{d\sigma_{yw}}{dy} + c\, \sigma_{yw} = D\left(\frac{\rho_e}{\rho_b}\right) b - \frac{3T_s}{2}\, b^2\, \frac{d}{dy}\left(\frac{\rho_e}{\rho_b}\right)$$

in which (5.2.1-10)

$$A = T_w - T_s/2$$

$$B = (2S_w+S_s) + \left(\frac{db}{dy} - 3T_s\right)T_w \qquad (5.2.1\text{-}11)$$

$$C = (T_s-T_w)\left[b\frac{d^2b}{dy^2} + \left(\frac{db}{dy}\right)^2\right] + 3(T_wS_s-T_sS_w) + 2(S_w-S_s)\frac{db}{dy}$$

$$D = 3\left(S_s - T_s\frac{db}{dy}\right)$$

The parameter a(y) is given by

$$a = \frac{1}{3T_s^2-S_s}\left\{\frac{b}{2}(T_w-T_s/2)\frac{d\sigma_{yw}}{dy} + \left[(S_w-S_s) + \frac{db}{2dy}(T_s-T_w) - (3T_s/4)(T_w-T_s)\right]\sigma_{yw} + (3T_s/4)b(\rho_e/\rho_b)\right\}$$

(5.2.1-12)

Equation (5.2.1-10) with the coefficients given by (5.2.1-11) represents the general form of the differential equation for the determination of the stresses for the

granular material contained in the annular region of the spouted bed.

Analyzing the stresses developed in the vertical and conical parts separately, using equation (5.2.1-10), the results are then combined to obtain the complete stress distribution in the annulus.

5.2.2 The vertical part

In the vertical part b is constant and equal to b_o. Using equation (3.2-5) for ρ_e/ρ_b the differential equation (5.2.1-10) can then be written

$$A_1\frac{d^2\sigma_{yw}}{dy^2} + B_1\frac{d\sigma_{yw}}{dy} + C_1\sigma_{yw} = D_1[1 - \cos(\pi y/2H)] - (3\pi T_s/4H)\sin(\pi y/2H) \qquad (5.2.2\text{-}1)$$

in which the coefficients A_1, B_1, C_1 and D_1 are those given by (5.2.1-11) with $b=b_o=1$ and $db/dy=d^2b/dy^2=0$. The boundary conditions of equation (5.2.2-1) are

$$\text{at } y = 0 \qquad \sigma_{yw} = 0 \qquad (5.2.2\text{-}2)$$

$$\frac{d\sigma_{yw}}{dy} = 0 \qquad (5.2.2\text{-}3)$$

The first boundary condition corresponds to the no surcharge at the free surface, which implies also $a(0)=0$. The

second boundary condition can be obtained from the differential equations of equilibrium (5.2.1-8) and (5.2.1-9). They give, assuming that there is no surcharge (σ_{yw}=a(0)=0) and the bed is at its maximum spouting height (ρ_e/ρ_b=0)

$$\frac{b}{2}(T_s+T_w)\frac{d\sigma_{yw}}{dy} - \frac{b}{2}T_s\frac{da}{dy} = 0$$

$$b\frac{d\sigma_{yw}}{dy} - \frac{2}{3}b\frac{da}{dy} = 0$$

which implies $d\sigma_{yw}/dy = 0$. The solution to (5.2.2-1) subject to the boundary conditions (5.2.2-2) and (5.2.2-3) is given by

$$\sigma_{yw} = K_1 e^{r_1 y} + K_2 e^{r_2 y} + D_1/C_1 - \frac{1}{(Z_1^2+Z_2^2)}\{Z_1[D_1\cos(Z_0 y) + (\frac{3T_s}{2})Z_0\sin(Z_0 y)] + Z_2[D_1\sin(Z_0 y) - (\frac{3T_s}{2})Z_0\cos(Z_0 y)]\} \qquad (5.2.2\text{-}4)$$

where r_1 and r_2 are the roots of the characteristics equation, given by

$$r_{1,2} = -(B_1/2A_1)[1-(1-4A_1C_1/B_1^2)^{1/2}] \qquad (5.2.2\text{-}5)$$

which are real for all cases of practical interest. The integration constants K_1 and K_2 are given by

$$K_1 = -\frac{r_2 D_1/C_1}{r_2-r_1} - \frac{1}{(r_2-r_1)(Z_1^2+Z_2^2)}[Z_1(3T_s Z_0^2/2 - r_2 D_1) + B_1 Z_0^2(D_1+3T_s r_2/2)] \quad (5.2.2\text{-}6)$$

$$K_2 = -\frac{r_1 D_1/C_1}{r_2-r_1} - \frac{1}{(r_2-r_1)(Z_1^2+Z_2^2)}[Z_1(3T_s Z_0^2/2 - r_1 D_1) + B_1 Z_0^2(D_1+3T_s r_1/2)] \quad (5.2.2\text{-}7)$$

and the constants are

$$Z_0 = \omega/2H$$
$$Z_1 = C_1 - A_1 Z_0^2$$
$$Z_2 = B_1 Z_0$$

The parameter a(y) is given by (5.2.1-12) having determined σ_{yw}, $d\sigma_{yw}/dy$ as well as $b=b_0$.

The complete stress field for the vertical part of the annulus can thus be obtained using equations (5.2.2-4) together with the relations (5.2.1-3,4) and (5.2.1-7).

5.2.3 The conical part

It is more convenient to switch the coordinates from x-y to x-y_c as shown in Figure 35. The boundary of the dead zone can be expressed by

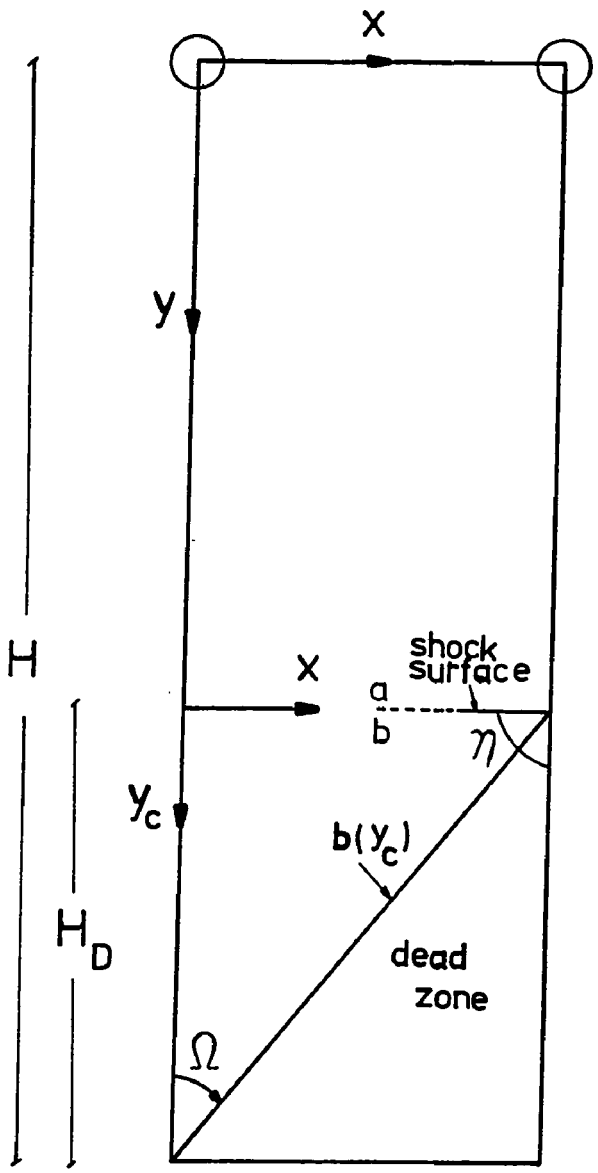

Figure 35 Half spouted bed and position of x-y and $x-y_c$ coordinates

$$b(y_c) = 1 - y_c/H_D \qquad (5.2.3\text{-}1)$$

The angle ϕ_b is given by the equation (3.3.3-10).

The differential equation determining the stress distribution for this part can be written as

$$A_2(1-\frac{y_c}{H_D})^2\frac{d^2\sigma_{yw}}{dy_c^2} + B_2(1-\frac{y_c}{H_D})\frac{d\sigma_{yw}}{dy_c} + C_2\sigma_{yw} =$$

$$D_2\{1-\cos[Z_0(y_c+H-H_D)]\}(1-\frac{y_c}{H_D})$$

$$-(3T_s/2)(1-\frac{y_c}{H_D})^2\sin[Z_0(y_c+H-H_D)] \qquad (5.2.3\text{-}2)$$

in which the coefficients A_2, B_2, C_2 and D_2 are those given by (5.2.1-11) with $db/dy_c=-1/H_D$ and $d^2b/dy_c^2=0$. Notice that if the dead zone boundary were not a straight line, that is if $d^2b/dy_c^2\neq 0$, the coefficients would not be constant. This could lead to a second order differential equation (5.2.1-10) without a solution that can be expressed in terms of elementary functions. It will become clear in section 5.4 that existance of the analytical solution to the stress field, by the method of integral relations, greatly simplifies the velocity field computations.

The boundary conditions of equation (5.2.3-2) can be

written in general as

$$\text{at } y_c=0 \qquad \sigma_{yw} = BC_1 \qquad (5.2.3\text{-}3)$$

$$\frac{d\sigma_{yw}}{dy_c} = BC_2 \qquad (5.2.3\text{-}4)$$

These boundary conditions are calculated using the solution to the vertical part together with the discontinuity relations. The values of the boundary conditions along with a brief discussion of the discontinuity relations are given in 5.2.4. Applying the method of variation of parameters (Rainville and Bendient, 1974), the general solution of (5.2.3-2) is given by

$$\begin{aligned}\sigma_{yw} = {} & K_1(1-\frac{y_c}{H_D})^{r_1} + K_2(1-\frac{y_c}{H_D})^{r_2} \\ & + \frac{H_D}{A_2(r_2-r_1)}(1-\frac{y_c}{H_D})^{r_1}\{D_2\int_0^{y_c}F_1(y_c)dy_c \\ & - (3\pi T_s/4H)\int_0^{y_c}F_2(y_c)dy_c\} \\ & - \frac{H_D}{A_2(r_2-r_1)}(1-\frac{y_c}{H_D})^{r_2}\{D_2\int_0^{y_c}F_3(y_c)dy_c \\ & - (3\pi T_s/4H)\int_0^{y_c}F_4(y_c)dy_c\} \qquad (5.2.3\text{-}5)\end{aligned}$$

in which r_1 and r_2 are the roots of the characteristic equation given by

$$r_{1,2}=-\frac{1}{2}\left[(1+B_2H_D/A_2) \pm \sqrt{(1+B_2H_D/A_2)^2-4C_2H_D^2/A_2}\right] \qquad (5.2.3\text{-}6)$$

The parameters K_1 and K_2 are given by

$$K_1 = (r_2BC_1+H_DBC_2)/(r_2-r_1) \qquad (5.2.3\text{-}7)$$

$$K_2 = -(r_1BC_1+H_DBC_2)/(r_2-r_1) \qquad (5.2.3\text{-}8)$$

and the functions F_1, F_2, F_3 and F_4 are given by

$$F_1(y_c) = \frac{1-\cos[\pi(y_c+H-H_D)/2H]}{(1 - y_c/H_D)^{r_1}}$$

$$F_2(y_c) = \frac{\sin[\pi(y_c+H-H_D)/2H]}{(1 - y_c/H_D)^{r_1-1}} \qquad (5.2.3\text{-}9)$$

$$F_3(y_c) = \frac{1-\cos[\pi(y_c+H-H_D)/2H]}{(1 - y_c/H_D)^{r_2}}$$

$$F_4(y_c) = \frac{\sin[\pi(y_c+H-H_D)/2H]}{(1 - y_c/H_D)^{r_2-1}}$$

The complete stress field for the conical part of the annulus can thus be obtained using (5.2.3-5) together with the relations (5.2.1-3,4) and (5.2.1-7).

5.2.4 Stress discontinuity and the boundary conditions

Stress discontinuities exist at the two top corners of the annulus as well as the junction of the vertical and conical parts. The discontinuities originate at the inter-

sections where the angle ϕ is double valued. It was mentioned earlier in this section that the method of integrals fits a smooth stress distribution through the regions of discontinuities. These types of discontinuities are called relatively weak by Savage and Yong (1970) since the jumps in the stress components and ϕ are small, there is no switch from active to passive condition where ϕ undergoes a drastic change. Example of such discontinuities are the two top corners of the annulus shown by a circle in Figure 35. The stress discontinuities occuring at the top corners are due to the different boundary conditions at the free surface and the walls. Normally the angle ϕ at the top free surface does not match with those at the corners and the jump in the stress distributions are usually small. The method of integral relations is capable of performing a meaningful averaging (smoothing) of the jumps without cusing too much error in the local values of stresses (this averaging is done with the help of the integrand interpolating polynomials). At the junction of the vertical and conical parts there is a switch of state of stress from active to passive and angle ϕ undergoes a drastic change. The jumps in the stress distributions are usually large and the method of integrals can not provide a meaningful average of the discontinuities. The results of this method in this case can

not closely approximate the local values of stresses. The discontinuities of these type where a switch of state of stress occurs and the nature of the stress solution undergoes a drastic change from the active condition to the passive condition must be dealt explicitly using the discontinuity relations.

To analyze a more general situation where the method of integrals is incapable of providing a meaningful average of the discontinuous stresses, the discontinuity relations are used to determine the stresses at the top of the conical part, thus providing necessary boundary conditions for this region. These relations are discussed in detail in Appendix 2. Recalling that the angle of the discontinuity surface (or the shock front) η, shown in Figure 35, can be expressed by

$$2\eta = \phi_b + \phi_a - \cos^{-1}[\sin\delta\cos(\phi_b-\phi_a)] \qquad (A.2\text{-}5)$$

Using (A.2-5), (A.2-6) and relation (3.3.3-4) the first boundary condition (5.2.3-3) can be written

$$BC_1=(\sigma_{yb})_{y_c=0}=\frac{\sin2(\phi_w-\eta)(1+\sin\delta\cos2\phi_b)}{\sin2(\phi_b-\eta)(1+\sin\delta\cos2\phi_w)}(\sigma_{yw})_{y=H-H_D} \qquad (5.2.4\text{-}1)$$

The value of σ_{yw} at the $y=H-H_D$ is obtained from the solution to the vertical part. Notice that if ϕ_w was equal to

ϕ_b there would be no jumps in the stresses, The second boundary condition is obtained using the parameter a(y) as follows: the value of σ_{ys} at $y=H-H_D$ is obtained using (5.2.1-3). The angle of the front η at the spout wall is calculated using (A.2-5). An identical expression to (5.2.4-1) is used for the spout wall to compute the σ_{ys} on the other side of the front. This value along with the σ_{yb} at $y_c=0$ from (5.2.4-1) is then applied to compute the value of a(y) in the conical region (b side of Figure 35). Thus, the second boundary condition can be written as

$$BC_2 = \left(\frac{d\sigma_{yw}}{dy}\right)_{y_c=0} = \frac{1}{1/2\ T_w - 1/4\ T_s}\{$$
$$(3/4\ T_s^2 - S_s)(a_b)_{y_c=0} - [(S_w - S_s)$$
$$+1/2\ (T_s - T_w)\frac{db}{dy} - 3/4\ T_s(T_w - T_s)(\sigma_{yb})_{y_c=0}$$
$$- 3/4\ T_s[1-\cos(\frac{\pi}{2H}(H-H_D))]\} \qquad (5.2.4\text{-}2)$$

in which the term $(a_b)_{y_c=0}$ is the value of a(y) at the conical region side of $y=H-H_D$ (b side at Figure 35).

5.2.5 Results and discussion

The complete distribution of the stress components for the vertical part are graphically shown in Figures 36, 37 and 49, 50, 51. These Figures correspond to the case of $\delta=40^o$, $\delta_w=20^o$, $\delta_s=4^o$ and the maximum spoutable bed

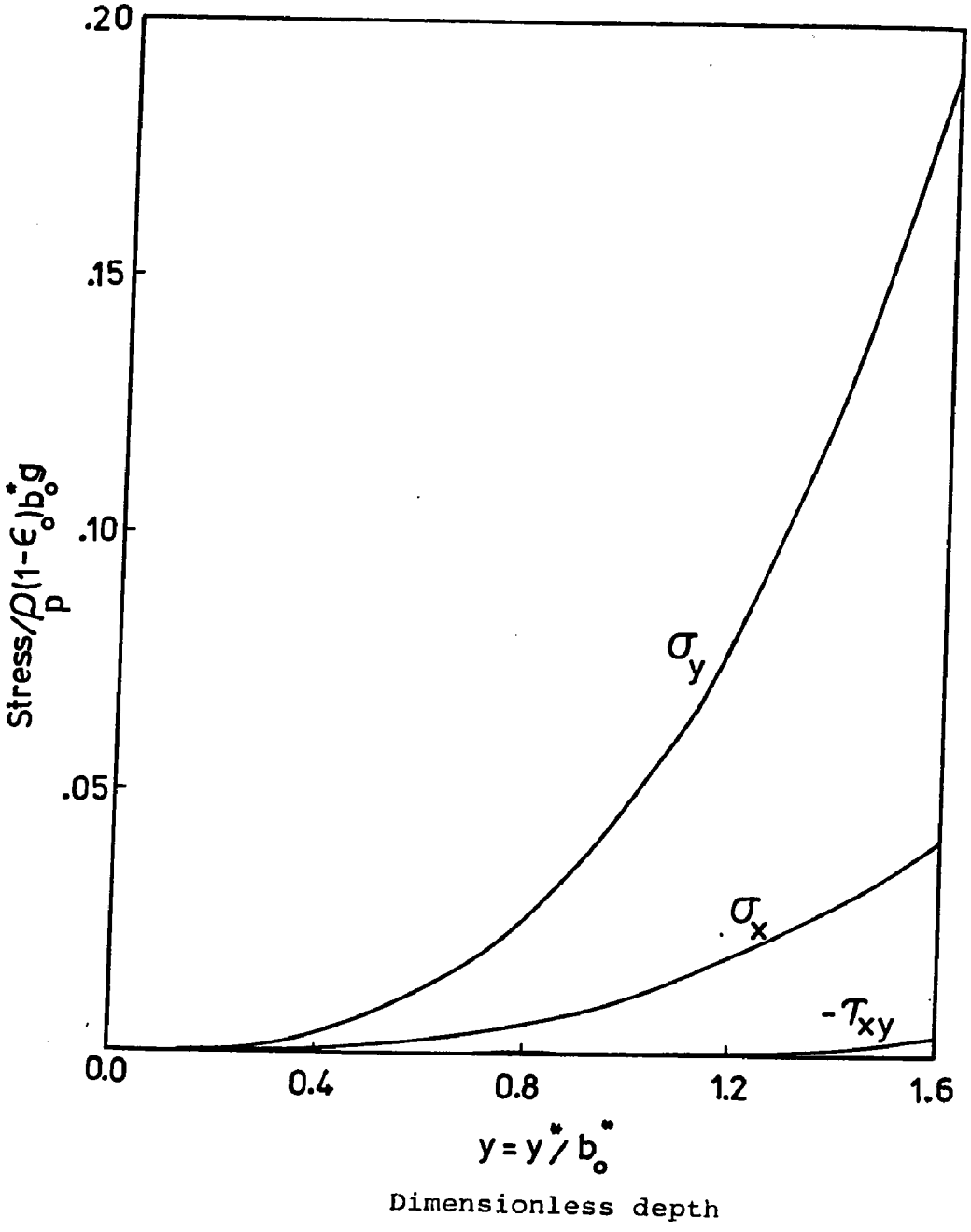

Figure 36 Dimensionless stresses at the spout wall obtained for the vertical part of the annulus using the method of integral relations ($\delta=40^o$, $\delta_w=20^o$, $\delta_s=4^o$)

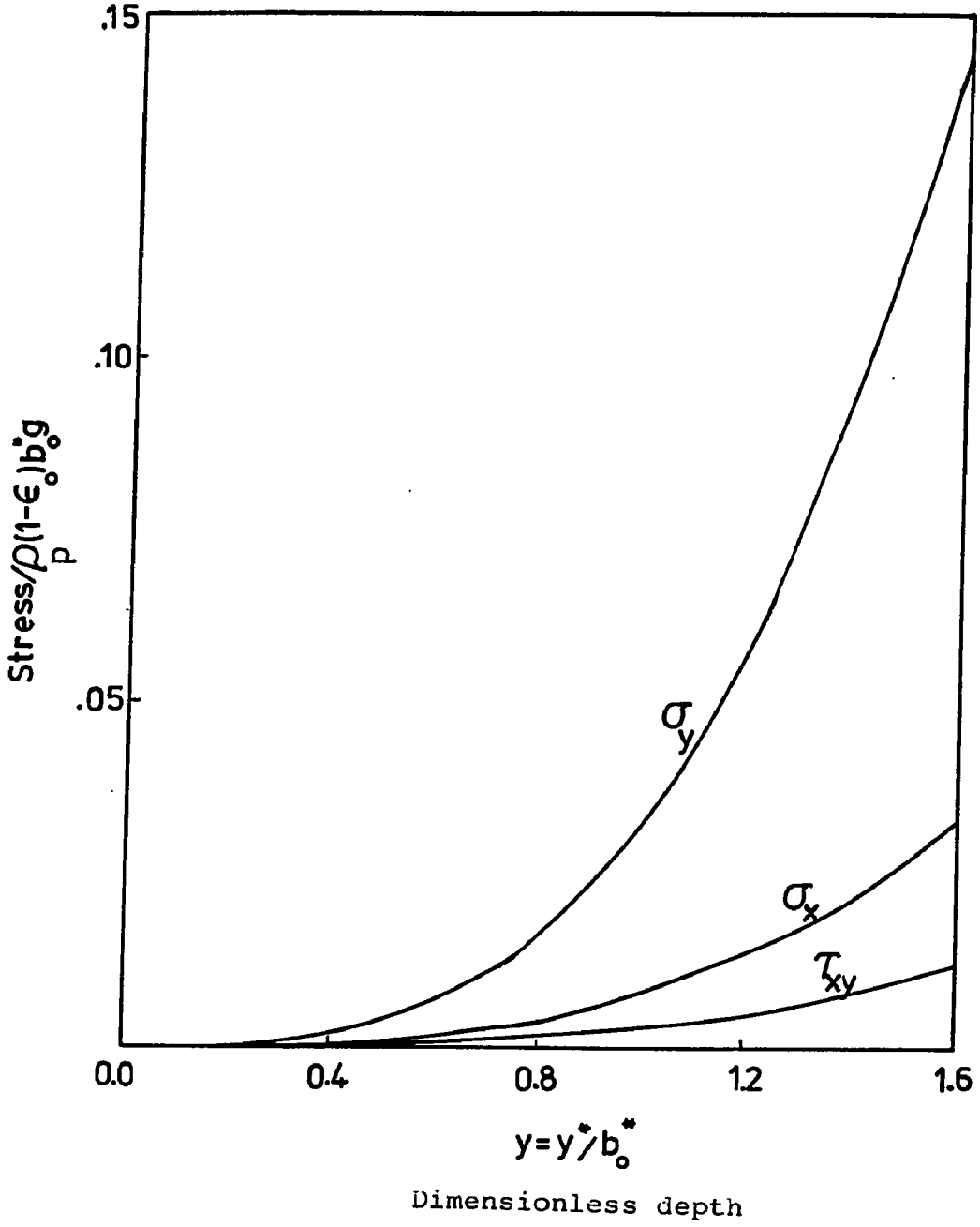

Figure 37 Dimensionless stresses at the bed wall obtained for the vertical part of the annulus using the method of integral relations ($\delta=40^o$, $\delta_w=20^o$, $\delta_s=4^o$)

height H=3 with the gas flow in the annulus (B=1). The stresses increas with depth from the top boundary in the vertical part of the annulus. They do not show any sign of the deep bed approximation.

It was attempted to find the stress distribution for the conical region with the angle of friction at the boundary of dead zone given by $\delta_b=\delta=40^o$ (fully rough wall). It was however found that stresses go to infinity at the spout entrance which seems to be an unrealistic result. It was attempted to find out that if a limiting solution exists for the conical region at all. For the case of the flow of bulk solids in hoppers the ranges of half angle hopper Ω where a limiting or non-limiting equilibrium solution exists has been found by Sokolovski (1965) and is discussed below. The angle of the boundary of dead zone Ω (Figure 35) was then compared with these ranges and it was found that Ω lies in the range of where a limiting solution does not exist. For the case of the hopper this would indicate to a dead region of material where there is no plastic equilibrium. For the case of spouted beds, however, this indicates that an analysis based on the limit equilibrium may not be appropriate in the conical region. It may be more appropriate to consider the full momentum equations containing the inertial

terms for the conical region since the inertial terms become important in this region. The following analysis is based on the findings for the case of flow of bulk solids in hoppers.

Sokolovski (1965) has determined the ranges of the half angle hopper where a limiting solution exists. These ranges for the case of passive state of stress are given by

Continuous:

$$\Omega=0 \quad , \quad \delta_w=0$$

Discontinuous:

$$0 \leq \Omega \leq [\pi/2 - \delta_b + \cos^{-1}(\sin\delta_b/\sin\delta)]/2$$

Non-limiting:

$$\Omega > [\pi/2 - \delta_b + \cos^{-1}(\sin(\delta_b/\sin\delta)]/2$$

and for the case of active state of stress

Continuous:

$$0 \leq \Omega \leq [\pi/2 - \delta_b - \cos^{-1}(\sin\delta_b/\sin\delta)]/2$$

Discontinuous:

$$[\pi/2-\delta_b-\cos^{-1}(\sin\delta_b/\sin\beta)]/2 \leq \Omega \leq [\pi/2-\delta_b + \cos^{-1}(\sin\delta_b/\sin\delta)]/2$$

Non-limiting:

$$[\pi/2 - \delta_b + \cos^{-1}(\sin\delta_b/\sin\delta)]/2 < \Omega$$

Horne and Nedderman (1978b) have used these range to analyze the stress distribution in hoppers by the method of characteristics and compared the results of their

analysis with different approximate methods of Walker (1966), Walters (1973a), and Jenike's radial stress field (1961). If the method of characteristics were used, the divergence or convergence of the characteristics from the top corner of the conical part determines whether a continuous (fan of characteristics) or discontinuous (shock front) solution results. As concluded by Horne and Nedderman (1978b) under normal conditions a continuous solution arises in the active case and a discontinuous one in the passive case. The angle of the shock front η is a function of Ω. If $\Omega<\eta$ then a limiting solution exists. For larger Ω than this η, the calculated discontinuity position is outside the annulus region and a limiting solution can not be found. For the given values of $\delta=40^{o}$, $\delta_w=20^{o}$ and $\delta_b=40^{o}$ and using (3.3.3-10) it was found that for $|\Omega|>18.93^{o}$ there is no limiting solution. For the $\Omega=-18.93^{o}$ we have $\phi_w=\phi_b$ and $\eta=-18.93^{o}$, the front then coincide with the boundary of dead zone and there is no discontinuity and a limiting continuous solution exists. Since for our case $|\Omega|=35.54^{o}>18.93^{o}$ the front is located outside the conical region ($\eta=-28.22^{o}$) and a limiting solution can not be predicted. An attempt was made to find an upper limit for δ_b for which a limiting stress solution exist using Sokolovski's range of half hopper angle. Employing the given non-limiting range relation with $\Omega=-35.54^{o}$, a

trial and error calculation gives $\delta_b < 37.58^o$. Thus, for a boundary of dead zone with the angle of friction greater than 37.58^o there seems to be no limiting stress solution.

In an attempt to find a limiting stress distribution in the conical region the boundary of dead zone was replaced by a wall having angle of friction of 20^o ($\delta_b = \delta_w = 20^o$). A horizontal stress discontinuity was assumed at the junction of the vertical/conical part. Stress distributions for the two walls are shown in Figures 38 and 39. There is a large jump in the horizontal normal stress of the spout wall at the vertical/conical junction due to the switch of stress state from active (in the vertical) to passive (in the conical) where ϕ_s undergoes a drastic change. Notice that the horizontal normal stress σ_x is greater at the spout wall and smaller at the conical region wall than the vertical normal stress σ_y, indicating to a transition from passive (at the spout wall) to active (at the conical region wall) in the conical region. The transition of course could be realized before a complete solution and just from the variation of angle ϕ knowing the values of this angle at the boundaries. Notice that $\phi < 45^o$ implies to an active and $\phi > 45^o$ to a passive state of stress. The passive to active transition in the conical region invalidates the assumption of

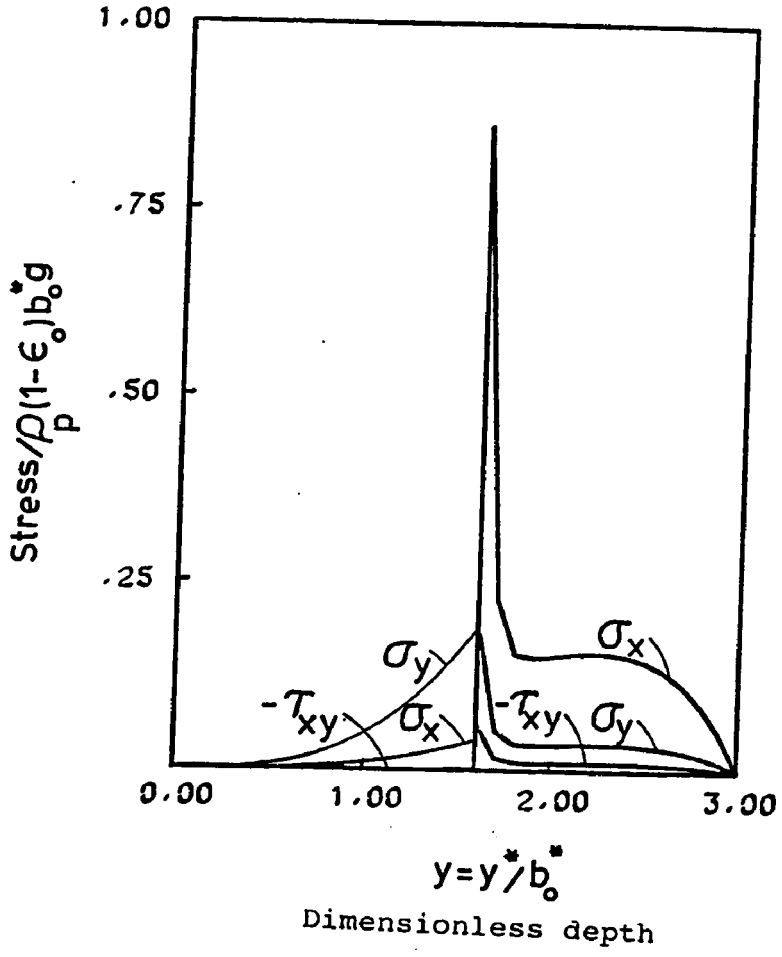

Figure 38 Dimensionless stresses at the spout wall obtained using the method of integral relations (MOI) (δ=40°, δ_w=20°, δ_s=4°)

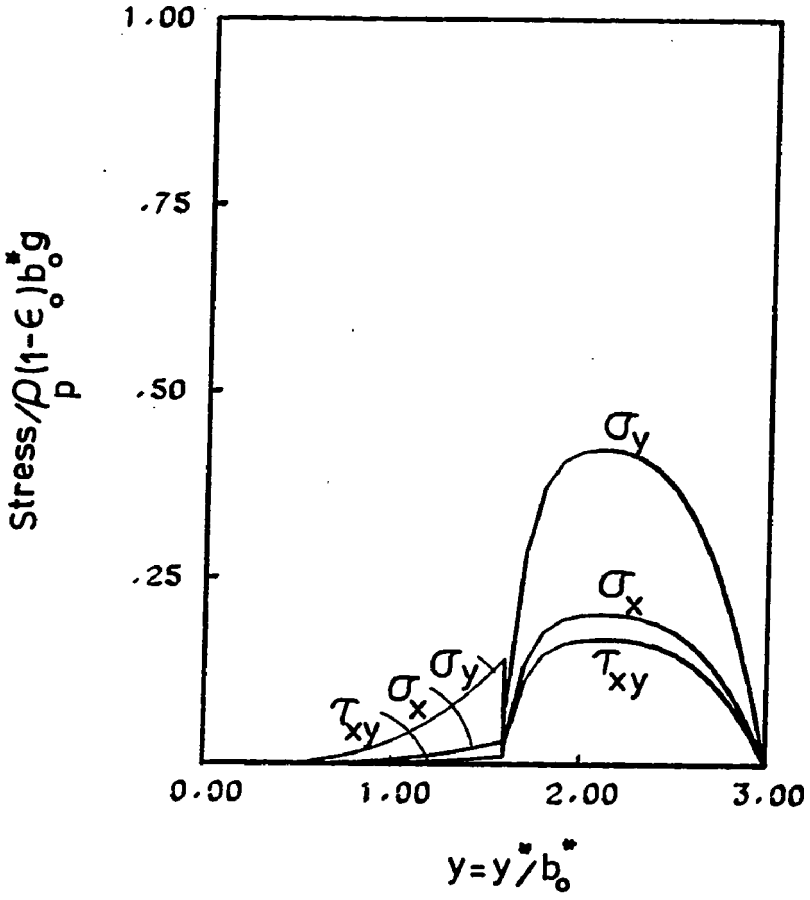

Figure 39 Dimensionless stresses at the spout wall obtained using the method of integral relations (MOI)
($\delta=40^o$, $\delta_w=20^o$, $\delta_s=4^o$)

linear variation of shear stress (shear stress is maximum at $\phi=45^{o}$), and on the other hand if a velocity field solution is attempted this transition greatly complicates the computations of the velocity characteristics, as mentioned in 5.4.2.

In Figures 38 and 39 stresses increase from zero at the top surface and pass through the jumps (discontinuities) at the vertical/conical junction. While, there is a sharp decrease after the discontinuity at the spout wall (Figure 38) after which the stresses are somewhat relaxed and go to zero at the spout entrance, the stresses at the conical wall increase after the discontinuity and reach a maximum value, after which decrease rapidly to zero at the spout entrance. The maximum horizontal compression at the spout wall after the discontinuity jump is about one annulus width (b_o^*) from the bottom of the bed. The maximum vertical compression at the conical wall is also about one annulus width (b_o^*) from the bottom of the bed. Profiles of Figures 38 and 39 show that the material pass from one fluidization state (zero effective stress) at the top of the bed to another at the bottom of the bed.

Stress distributions at different horizontal level of

the vertical part of the annulus are shown in Figures 49, 50 and 51. These distributions are compared with those by the method of characteristics and the method of differential slices in these Figures. The details of the comparison are given in 5.3.6.

5.3 Stress Field by the Method of Characteristics (MOC)

The method of characteristics (MOC) applied to the numerical integration of partial differential equations of the hyperbolic type was first proposed by Massau in 1899 (see Belotserkovskii and Chushkin, 1965). This method has been widely used for the solution of a variety of problems in physics and mechanics. The method can only be applied to the solution of equations of hyperbolic type. The solution by the method of characteristics is computed with the aid of a grid of characteristic lines, which generally is constructed during the course of the computations.

The method has been used in gas dynamics primarily for the calculation of steady two-dimensional and unsteady one-dimensional gas flows (Courant and Friedrichs, 1948, Ferri, 1959, Kochin, 1963). One of its advantages is that the point of origination of secondary shock wave within the field of flow, a result of the intersection of characteristics of one family can be determined accurately. It has also being used in solid mechanics to construct a technique for the numerical calculation of slipline fields (Hill, 1950, Prager and Hodge, 1951, Sokolovski, 1960) in the solution of the plasticity problems and to study the flow of bulk solids (Jenike and Johanson, 1962, Horne and

Nedderman, 1976, Savage and Yong, 1969). These workers used the method of characteristics to assess the accuracy of various approximate analysis since this method does provide "exact" numerical solutions. More recently computers made it possible to develop the numerical method of characteristics in its most general form. For example, Lister (1960) has developed a code for numerical computation of the general form of a two simultaneous quasi-linear partial differential equations for the case of two dependent and two independent variables. The approach of Lister has been used by Savage and Yong (1970) to compute the stress field within the bulk solid contained in a bin.

5.3.1 The characteristics equations

A form of a quasi-linear system of equations for the case of two independent variables x,y and two dependent variables p,q which is a general form of our governing equations is considered here. For this type of system there are two directions, called characteristic directions, each of which appears when seeking linear combinations of the differential equations containing derivatives of the two unknown functions in one direction only. Courant and Friedrichs (1948) have shown that, in the case of n quasi-linear partial differential equations in two

independent variables, there are n characteristic directions through each point, some of which may coincide. In this case (when n>2) the characteristic curves become characteristic surfaces and the size of the computations are greatly increased and not many problems have been solved for the case of n>2. The basic techniques outlined by Courant and Friedrichs (1948) can be related to the case of two equations in two unknowns.

The general form of a quasi-linear system of two simultaneous first order equations with two dependent variables of p(x,y) and q(x,y) can be written

$$\begin{aligned} a_{11}\frac{\partial p}{\partial x} + a_{12}\frac{\partial p}{\partial y} + b_{11}\frac{\partial q}{\partial x} + b_{12}\frac{\partial q}{\partial y} &= e_1 \\ a_{21}\frac{\partial p}{\partial x} + a_{22}\frac{\partial p}{\partial y} + b_{21}\frac{\partial q}{\partial x} + b_{22}\frac{\partial q}{\partial y} &= e_2 \end{aligned} \qquad (5.3.1\text{-}1)$$

where a_{11}, b_{11}, ..., b_{22}, e_1, e_2 are functions of x, y, p, q. Both p and q are prescribed along an initial arc Γ in the xy plane, Figure 40. It can be shown that the slopes χ of the two families of characteristic curves are the roots of the equation (Greenberg, 1978, Hildebrand, 1968, Panov, 1963)

$$A\,\chi^2 - B\,\chi + C = 0 \qquad (5.3.1\text{-}2)$$

where

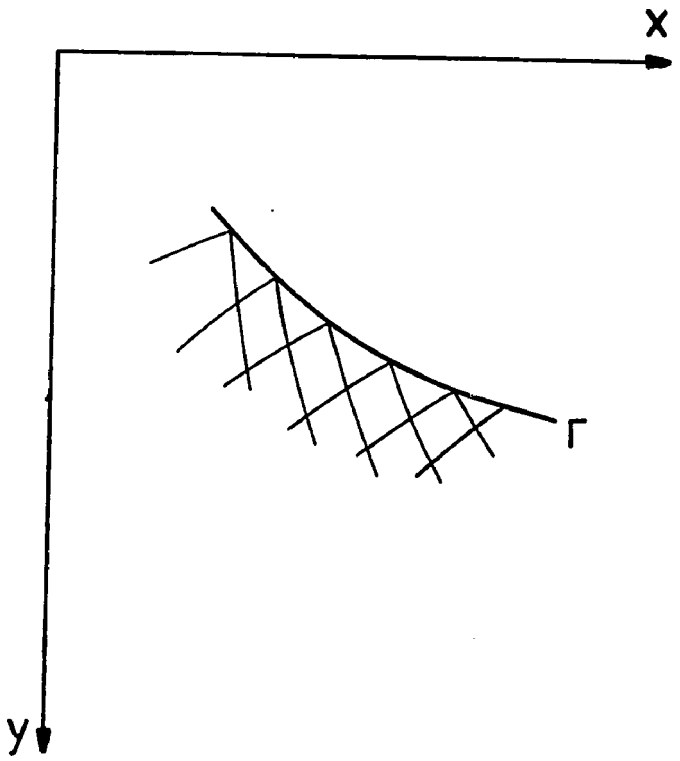

Figure 40 Initial arc Γ and the associated characteristics mesh

$$\chi = \frac{dy}{dx} \quad ; \qquad A = \begin{vmatrix} a_{11} & b_{11} \\ a_{21} & b_{21} \end{vmatrix}$$

$$B = \begin{vmatrix} a_{11} & b_{12} \\ a_{21} & b_{22} \end{vmatrix} + \begin{vmatrix} a_{12} & b_{11} \\ a_{22} & b_{21} \end{vmatrix} \quad ; \qquad C = \begin{vmatrix} a_{12} & b_{12} \\ a_{22} & b_{22} \end{vmatrix}$$

(5.3.1-3)

Note that whenever $B^2 > 4AC$ the system is hyperbolic and there are two distinct real roots that provide two differential equations

$$\chi_1 = \frac{dy}{dx} \quad \text{and} \quad \chi_2 = \frac{dy}{dx} \qquad (5.3.1\text{-}4)$$

for the two families of characteristic curves. The solution of the hyperbolic system (5.3.1-1) is then reduced to the integration of the characteristic equations along the characteristic curves. These equations have the form of

$$E\,dp + (A\,\chi - F)\,dq = H\,dx - G\,dy \qquad (5.3.1\text{-}5)$$

where the coefficients are defined as:

$$E = \begin{vmatrix} a_{11} & a_{12} \\ a_{21} & a_{22} \end{vmatrix} \qquad F = \begin{vmatrix} a_{12} & b_{11} \\ a_{22} & b_{21} \end{vmatrix}$$

$$H = \begin{vmatrix} e_1 & a_{12} \\ e_2 & a_{22} \end{vmatrix} \qquad G = \begin{vmatrix} e_1 & a_{11} \\ e_2 & a_{21} \end{vmatrix}$$

The characteristic directions and the characteristic equations belonging to the first and second family can then be

written:

$$dy = \lambda_1 dx \quad ; \quad E\,dp + (A\lambda_1 - F)dq = H\,dx - G\,dy$$
$$dy = \lambda_2 dx \quad ; \quad E\,dp + (A\lambda_2 - F)dq = H\,dx - G\,dy$$

(5.3.1-7)

The solution to the system (5.3.1-7) is equivalent to the solution of the original system (5.3.1-1). Different problems are distinguished for the system (5.3.1-1) by postulating different supplementary conditionss. The system (5.3.1-7) may be solved by plotting the characteristics network (mesh) and computing the values of p and q on the lattice (grid) points from the differential relations. The approximate determination of the coordinates of the characteristic grid points and of the values of p and q at those points is possible by writing the system (5.3.1-7) in finite difference form, and solving the subsequent resulting algebraic equations simultaneously. This can be done for each grid point.

5.3.2 Characteristic equations of the stress field

Starting with the equilibrium equations (3.3.1-11) and (3.3.1-12) and following the procedure described in section (5.3.1), the characteristic directions and the stress characteristic equations which hold along the two directions are (see Appendix 3):

$$\frac{dy}{dx} = \cot(\phi+\mu) \; ; \; d\sigma + 2\sigma\tan\delta d\phi = (dy - \tan\delta dx)(\rho_e/\rho_b)$$

$$\frac{dy}{dx} = \cot(\phi-\mu) \; ; \; d\sigma - 2\sigma\tan\delta d\phi = (dy + \tan\delta dx)(\rho_e/\rho_b)$$

(5.3.2-1)

where $\mu = \pi/4 - \delta/2$ and ρ_e/ρ_b is given by (3.2-6):

$$\frac{\rho_e}{\rho_b} = 1 - B\cos\frac{\pi}{2H}\, y \qquad (3.2\text{-}6)$$

Hence, the angle between the two characteristic directions is equal to 2μ.

Suppose now at points 1 and 2 of Figure 41 in the xy plane all the necessary magnitudes are known, i.e. x_1, y_1, σ_1, ϕ_1 and $x_2, y_2, \sigma_2, \phi_2$. The position of a typical grid point M is approximately determined as the intersection of a straight lines running through points 1 and 2 with the same inclinations as the pertinent characteristics. The coordinates x_M and y_M are found consequently from the equations

$$\begin{aligned} y_M - y_1 &= \chi_1[x_1, y_1](x_M - x_1) \\ y_M - y_2 &= \chi_2[x_2, y_2](x_M - x_2) \end{aligned} \qquad (5.3.2\text{-}2)$$

which have replaced the equations (5.3.1-4). χ_1 and χ_2 are given by

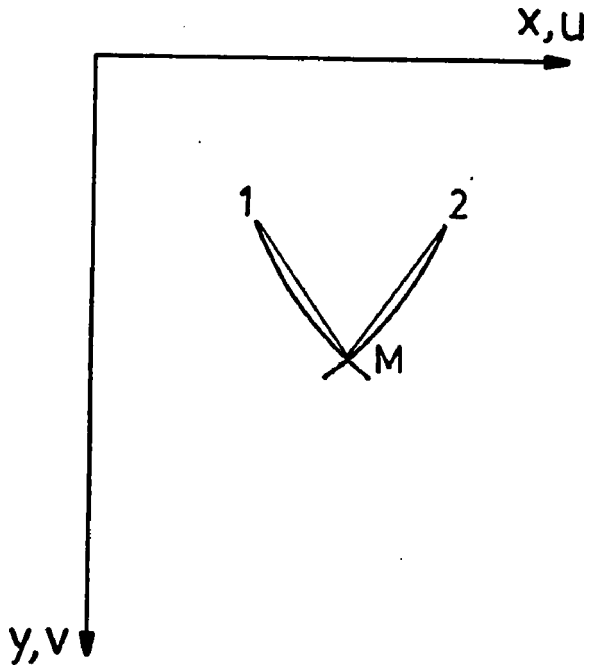

Figure 41 Characteristic curves approximated by straight lines

$$\chi_1[x_1,y_1] = \cot(\phi_1+\mu)$$
$$\chi_2[x_2,y_2] = \cot(\phi_2-\mu) \qquad (5.3.2\text{-}3)$$

The magnitudes of stress parameters σ and ϕ at the point M are found by replacing the differentials with differences in the characteristic equations (5.3.2-1):

$$(\sigma_M-\sigma_1) + 2\sigma_1\tan\delta(\phi_M-\phi_1) = [(y_M-y_1) - \tan\delta(x_M-x_1)](\rho_e/\rho_b) \qquad (5.3.2\text{-}4)$$

$$(\sigma_M-\sigma_2) - 2\sigma_2\tan\delta(\phi_M-\phi_2) = [(y_M-y_2) + \tan\delta(x_M-x_2)](\rho_e/\rho_b)$$

The general procedure may then be established to first compute the value of x_M from (5.3.2-2) as:

$$x_M = \frac{\chi_2 x_2 - \chi_1 x_1 - y_2 + y_1}{\chi_2 - \chi_1} \qquad (5.3.2\text{-}5)$$

this value is then used in the computation of y_M from

$$\text{or} \quad \begin{aligned} y_M &= y_1 + \chi_1(x_M - x_1) \\ y_M &= y_2 + \chi_2(x_M - x_2) \end{aligned} \qquad (5.3.2\text{-}6)$$

and finally, knowing the values of x_M and y_M, the system (5.3.2-4) is solved simultaneously to obtain σ_M and ϕ_M.

5.3.3 Improvement of the accuracy of the computations

The accuracy of the computations at point M can be improved using corrected values for the variables not ap-

pearing in a difference form. These corrected values are the average of the variables between the two points:

$$x_1'=(x_1+x_M)/2 \quad , \quad x_2'=(x_2+x_M)/2$$

$$y_1'=(y_1+y_M)/2 \quad , \quad y_2'=(y_2+y_M)/2$$

$$\sigma_1'=(\sigma_1+\sigma_M)/2 \quad , \quad \sigma_2'=(\sigma_2+\sigma_M)/2 \qquad (5.3.3\text{-}1)$$

$$\phi_1'=(\phi_1+\phi_M)/2 \quad , \quad \phi_2'=(\phi_2+\phi_M)/2$$

The equations for the computations at point M with the corrected values can then be written as

$$x_M = \frac{\chi_2' x_2 - \chi_1' x_1 - y_2 + y_1}{\chi_2' - \chi_1'} \qquad (5.3.3\text{-}2)$$

where

$$\chi_1'=\cot(\phi_1'+\mu)$$
$$\chi_2'=\cot(\phi_2'-\mu) \qquad (5.3.3\text{-}3)$$

or

$$y_M=y_1+\chi_1'(x_M-x_1)$$
$$y_M=y_2+\chi_2'(x_M-x_2) \qquad (5.3.3\text{-}4)$$

$$(\sigma_M-\sigma_1) + 2\sigma_1'\tan\delta(\phi_M-\phi_1) = [(y_M-y_1) - \tan\delta(x_M-x_1)](\rho_e/\rho_b)'$$

$$(\sigma_M-\sigma_2) - 2\sigma_2'\tan\delta(\phi_M-\phi_2) = [(y_M-y_2) + \tan\delta(x_M-x_2)](\rho_e/\rho_b)' \qquad (5.3.3\text{-}5)$$

in which $(\rho_e/\rho_b)'$ indicates to the value of (ρ_e/ρ_b) evaluated at point (x',y'). A sequential procedure must

then be used for the computations at point M. This procedure may be started by first guessing ϕ_M (a good guess is the average of ϕ's between points 1 and 2) and calculating x_M and y_M from (5.3.3-2) and (5.3.3-3), respectively. The system (5.3.3-5) can then be solved to find σ_M and ϕ_M. Applying equations (5.3.3-2) and (5.3.3-4) once again, x_M and y_M can be obtained for the calculated ϕ_M. The position of M (x_M, y_M) based on the calculated ϕ_M is now compared with the previous position of M (x_M, y_M) based on the guessed ϕ_M. If the two successive computed x_M and y_M coincide within the limits of accuracy, then the computation of x_M, y_M, σ_M and ϕ_M is to be considered as final. Otherwise, the process of computations is repeated.

5.3.4 Treatment of discontinuities

The discontinuities in the stress field are caused by the occurrence of discontinuous boundary conditions, such as the corners formed by the free surface and the bed or spout walls where ϕ_t is unlikely to match with ϕ_w or ϕ_s. It has been shown (Savage et al., 1970, Sokolovski, 1960) that a discontinuity is required to satisfy the quasi-static equilibrium equations along with the proper boundary conditions within the context of limit equilibrium analysis.

There are actually three regions in the annulus where the discontinuities may be emanated: two top corners and the junction of the vertical and conical parts. Two possibilities exist for the stress field solution depending on whether the characteristics of the same family diverge or converge and intersect. In the case of divergence a fan of characteristics radiates from the origin of the discontinuity and a continuous solution exists, whereas the convergence of the like characteristics produce an overlap region where the stress parameters within the region would be multivalued. The continuous fan solution normally occurs in the active state of stress and discontinuous solution in the passive state of stress (Horne and Nedderman, 1976).

The discontinuous solutions in plasticity were first introduced by Prager (1948,1951). The method was then used by other investigators like Sokolovski, Savage, and Nedderman to develop techniques to treat the discontinuities in the field of flow of bulk solid in bins and hoppers. While the stress tensor is discontinuous across the discontinuity the shear and normal stress must be the same in the plane of the discontinuity. These conditions along with the shock surface computations with the associated characteristics are given in Appendix 2. Sokolovski

(1960) has indicated that these interior discontinuity lines are not physically realized. Savage et al. (1969) have indirectly shown the existence of the discontinuity line experimentally by comparing the observed failure lines with those obtained by the analysis based on the discontinuity line.

In the case of passive state of stress in the vertical region, the discontinuities generated at the corners formed by the free surface with the bed and spout walls intersect each other somewhere between the two walls (since the spout and the bed walls friction angles are different the inclination of the shocks formed at the corners are not equal, the point of the intersection will not be at the center of the annulus) and are then reflected from the walls. There are subsequent intersections and reflections which occur throughout the depth of the vertical part. In the case of an active state of stress in the vertical part two fan of characteristics radiate from the two corners with an active Rankine zone between them. The fans will overlap right after the Rankine zone deeper in the vertical region. Another shock front or a fan, emanating from corner point of the bed wall and the dead zone boundary is formed at the vertical/conical junction due to the changes in ϕ's.

This front or fan will then interact with those emanated from the top corners throughout the depth of the conical part. The determination of the front involves a point-by-point computation to first locate and then pass through the shock. In actual practice the numerical computation of stress field in which several discontinuities exist is complicated and time consuming problem when using the MOC. Horne and Nedderman (1978a) have analyzed the problem of switch stresses for a bunker at the junction of bin (vertical part) and hopper (conical part). They have considered an active state for the bin and a passive state for the hopper, and concluded that for a steep hopper ($\phi_{hopper} > \phi_{bin}$) a fan of characteristics must emanate from the corner point of the bin/hopper junction, which consequently generates a shock front at the center line. This front then extends through the hopper with subsequent reflections between the hopper wall and the centerline. For a shallow hopper ($\phi_{hopper} < \phi_{bin}$) a shock front must emanate from the corner point and extend into the bin hence destroying part of the domain of the dependence of the solution of the bin which is an impossible situation. Based on this result Horne and Nedderman (1978a) have concluded that no fully plastic solution exists near the transition of a bunker with shallow hopper.

The source of the discontinuities, as discussed before, is the mismatch of ϕ at two boundaries meeting at the corner points. With this in mind, it is seen that if the friction at the wall were zero, the ϕ's would match at the top corners and no fan or shock would emanate from these corners. In order to circumvent the difficulties associated with the computation of discontinuities and obtain some stress distribution for frictional walls (no discontinuity would exist if the walls were frictionless), it can be assumed that δ_w (or δ_s) gradually increases from zero at the free surface (y=0) to the actual wall friction value at some y station, after which it can be taken to have a constant value. Although such a variation is unlikely, this technique prevents the initial generation of stress discontinuities. Applying this method may give only approximate stresses near the top of the annulus, but it is expected that the proper values will be approached in the lower portion of the vertical and conical regions. This procedure employed earlier by Savage and Yong (1970) to calculate the stress distribution in a bunker is adopted in the present analysis.

5.3.5 Corner points and computations near the walls

The computations of the characteristics at the corner points and near the walls are somewhat different from

those of a regular grid point. A detailed description of these types of computations is given in this section.

Assume that the computations are being started by using the data at points 1 and 2 of Figure 42 to obtain of those at point 3 applying equations (5.3.3-2), (5.3.3-4) and (5.3.3-5). Recalling that $\sigma_1=\sigma_2=0$ (no surcharge) and $\phi_1=\phi_2=0$, it is seen that ϕ_M can not be computed from the system (5.3.3-5) for the given data. This is because of the no surcharge condition. The system, however, may be solved for σ. Using the half angle relation, the solution is

$$\sigma = \frac{(\rho_e/\rho_b)\, y}{1 + \sin\delta} \qquad (5.3.5\text{-}1)$$

Notice that (5.3.5-1) is an analytical solution of the basic equation (3.3.1-11) and (3.3.1-12) corresponding to an active Rankine zone where $\phi=0$. If there were surcharge Q on the top boundary, equation (5.3.2-4) with the condition $\phi_1=\phi_2=0$ would yield

$$\phi_3 = 0 \qquad (5.3.5\text{-}2)$$

since point 3 belongs to the active Rankine zone. Thus the stress parameters at point 3 are given by (5.3.5-1) and (5.3.5-2) and the triangle 123 belongs to the region of an active Rankine state. The stress parameters for the

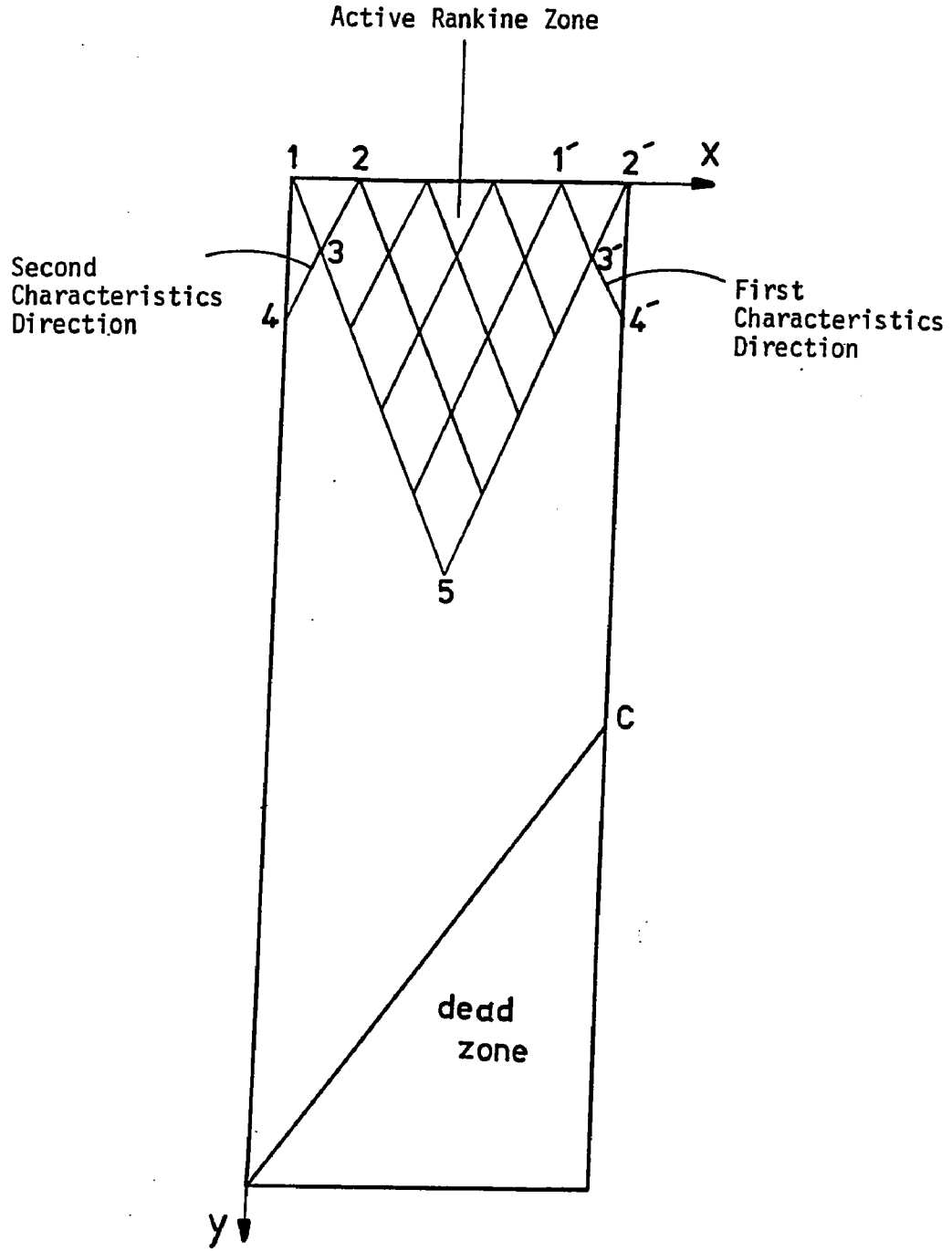

Figure 42 Characteristics of the Active Rankine Zone and computations at the corner points and near the walls

points of the first row of the grid characteristics such as 3 or 3' are given by (5.3.5-1) and (5.3.5-2). Having determined the stress parameters for these points, the points of the second row can be considered as regular grid points and the computations can be performed, applying (5.3.3-2), (5.3.3-4) and (5.3.3-5), to determine the coordinates and the stress parameters of these points. Following this procedure it is found that triangle 12'5 of Figure 42 belongs to an active Rankine zone. In this zone the shear stress is zero and the characteristics of each family are parallel straight lines.

There is a discontinuity of stress at the corner points (points 2' and 1 of Figure 42) where the angle ϕ is double valued. The discontinuity may be treated explicity so that depending on the state of stress at this region a fan of characteristics or a shock front could emanate from the corners. In the case of a spouted bed a fan of characteristics normally arises since we have assumed that active state of stress exists and presents a continuous stress solution. The detail of the computation of the continuous fan solution is given by Sokolovski (1960) and Hancock and Nedderman (1974) (the procedure of computation of the discontinuous solution is given by Horne and Nedderman, 1976). While the presence of discon-

tinuity is independent of the existance of a surcharge, Hancock and Nedderman (1974) have indicated that for the case of zero surcharge the characteristics of the radial zone (a zone adjucent to the active Rankine zone) become "ill-behaved" and cross the Rankine zone. They overcame this difficulty by the application of a local solution in the region of difficulty. This solution termed Radial Stress Field (RSF) is described in detail in Chapter 5 of Sokolovski's book (1960) and has been used extensively by Jenike (1961, 1964) to analyze the stresses in silos. We will not use it here.

As said before, in the present analysis it is assumed that the walls friction angles (δ_w and δ_s) change in a continuous manner such that ϕ's of the walls at the top corners match that at the top boundary. Notice that in the case of passive state of stress the discontinuity computation involves point-by-point computations to first locate the shock and then pass through it. This type of computation is very complex and time consuming. The functions chosen to present the variation of the two wall friction angles that prevent generation of fans of characteristics (active case) are given in section 5.3.6.

To expand the Rankine zone characteristics the con-

ditions at the walls must be used. If these conditions were not known the solution would be restricted to the triangle 12'5 that is the domain of dependence of the solution to the boundary condition at the top surface. The characteristics converge to form this triangle. Fortunately the conditions at the walls are known and the characteristics can be expanded such that the grid mesh may fill the entire annulus region. The MOC requires the knowledge of only two of the four variables x, y, σ and ϕ or relationships among them at the boundaries. Both the position and ϕ are known at the bed wall ($x=1, \phi=\phi_w$), spout wall ($x=0, \phi=\phi_s$), and the boundary of the dead zone [$x=b(y), \phi=\phi_b$] (see Figure 18). Thus, the unknown variables at a typical point on the spout wall, such as 4 of Figure 42, can be determined by inserting the known variables at 4 into the second characteristic relations emanated from 3. Same procedure can be followed for a typical point at the bed wall such as 4' using the first characteristic relations emanated from 3'. Notice that point 4 (or 4') can now be treated as a regular grid point in expanding the mesh. The mathematical formulas used to compute the boundary points are given in Appendix 4. There is a stress discontinuity at the junction of the vertical and conical region. A discontinuity line or a fan of characteristics radiates from the corner point C of

Figure 42 depending on the convergence or divergence of the characteristics from this corner. Because of the complexities involved, as mentioned before, the MOC was only used to determine the stress distribution in the vertical region. The discontinuity relation and the procedure of computing the shock front along with the associated characteristics are given in Appendix 3 as a reference.

5.3.6 Results and discussion

Computations were carried out for the case of $\delta=40^{o}$, $\delta_{w}=20^{o}$, $\delta_{s}=4^{o}$ and H=3 as an example for the calculations by the MOC. The determination of the characteristics was started from the top of the annulus by dividing its width into five equidistant intervals. The solution was then carried forward by choosing any two initial points of the top boundary and applying the characteristics equations to them in obtaining a new grid point of the mesh along with its corresponding stress parameters σ and ϕ. Repeating this procedure, the first row of the grid points were obtained. Equation (5.3.5-1) was used to calculate σ for this row. To expand the mesh, the two wall boundary conditions were used. As discussed in section 5.3.4 variable wall friction angles were applied to prevent initiation of a fan of characteristics. Different functions were tried to express the wall friction angles satisfying the con-

ditions discussed in section 5.3.4. The wall friction angle was chosen to vary in the following manner:

$$\delta_{w(s)} = \delta_{max,w(s)}[1 - (1-y)^2] \qquad y \leq 1$$
$$\delta_{w(s)} = \delta_{max,w(s)} \qquad y > 1 \qquad (5.3.6\text{-}1)$$

where δ_{max} correspond to the correct value of the wall friction angles. Figure 43 shows the stress characteristic mesh for the vertical portion of the annulus considering the gas flow in the annulus, B=1 (case of a spouted bed). Computations were also carried out for the case of no gas flow in the annulus with B=0 (case of a bin). The stress characteristics appeared to be not very differnt from those of Figure 43.

Figures 44, 45 and 46 show the distribution of the stress components at the spout and bed walls for the case of no gas flow in the annulus (B=0). The normal stresses varying almost linearly with depth. From these figures it is seen that stresses have not yet approached to a constant value. The plots of the normal stresses, Figures 44 and 45, show that $(\sigma_y)_w$ is identical to $(\sigma_y)_s$ and $(\sigma_x)_w$ is identical to $(\sigma_x)_s$ only for a depth of half annulus width, suggesting that the method of differential slices (MOS) estimates the correct values of stress only for a short depth from the top surface. Figure 46 shows the

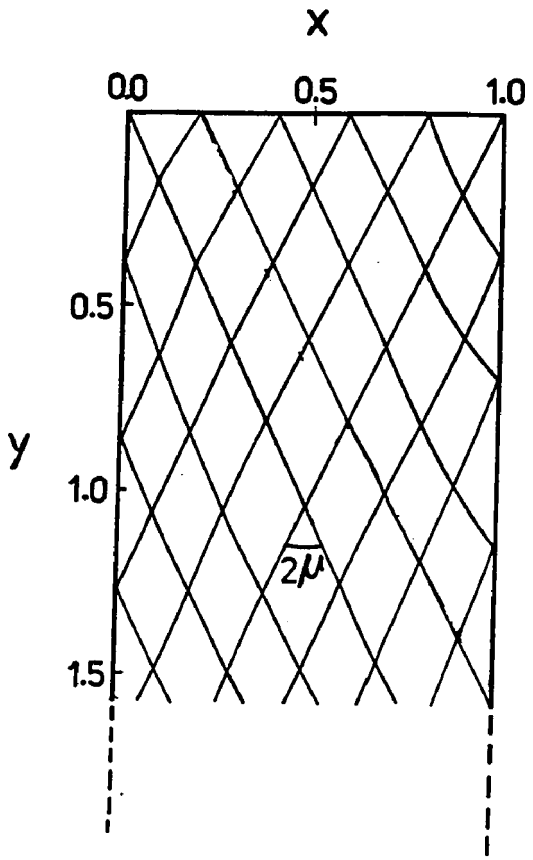

Figure 43 Stress characteristics for the case of spouted bed (gas flow, B=1) and variable wall friction angles ($\delta=40^{o}$, $\delta_{w_{Max}}=20^{o}$, $\delta_{s_{Max}}=4^{o}$)

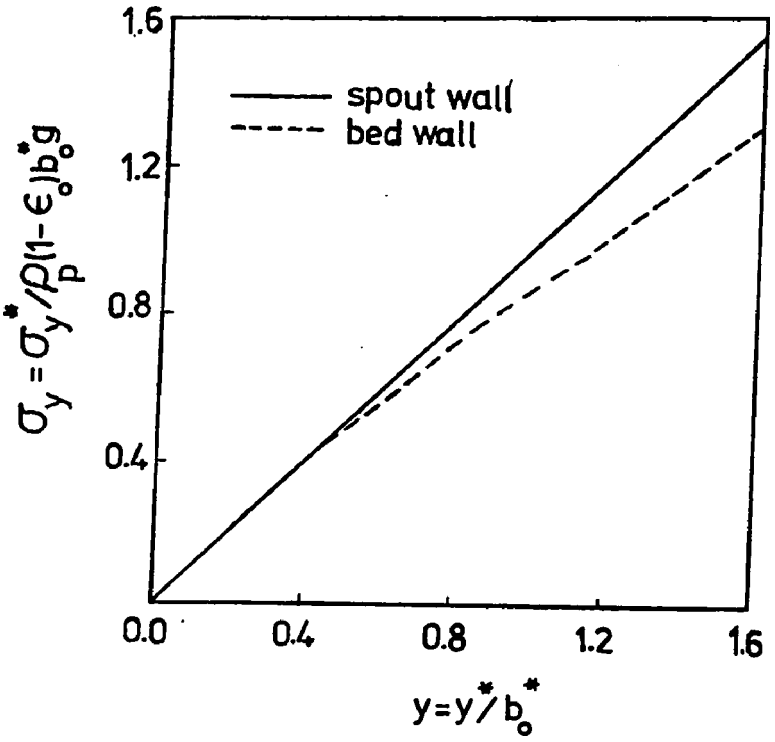

Figure 44 Distribution of the vertical normal stress at the spout and bed walls obtained using the method of characteristics for the case of no gas flow in the annulus (B=0)
($\delta=40^o$, $\delta_{w_{Max}}=20^o$, $\delta_{s_{Max}}=4^o$)

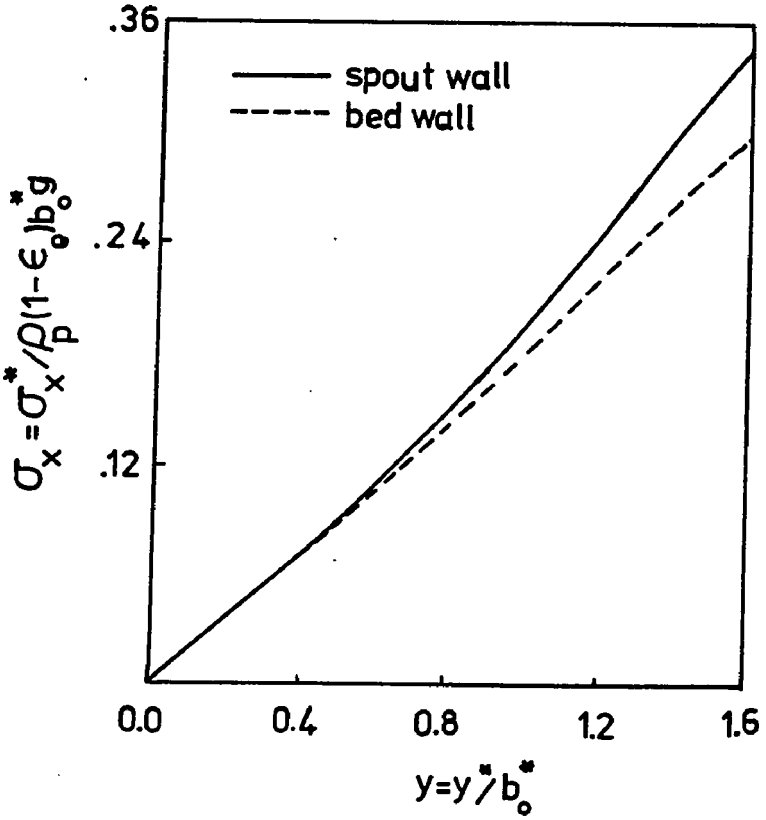

Figure 45 Distribution of the horizontal normal stress at the spout and bed walls obtained using the method of characteristics for the case of no gas flow in the annulus (B=0)
($\delta=40^o$, $\delta_{w_{Max}}=20^o$, $\delta_{s_{Max}}=4^o$)

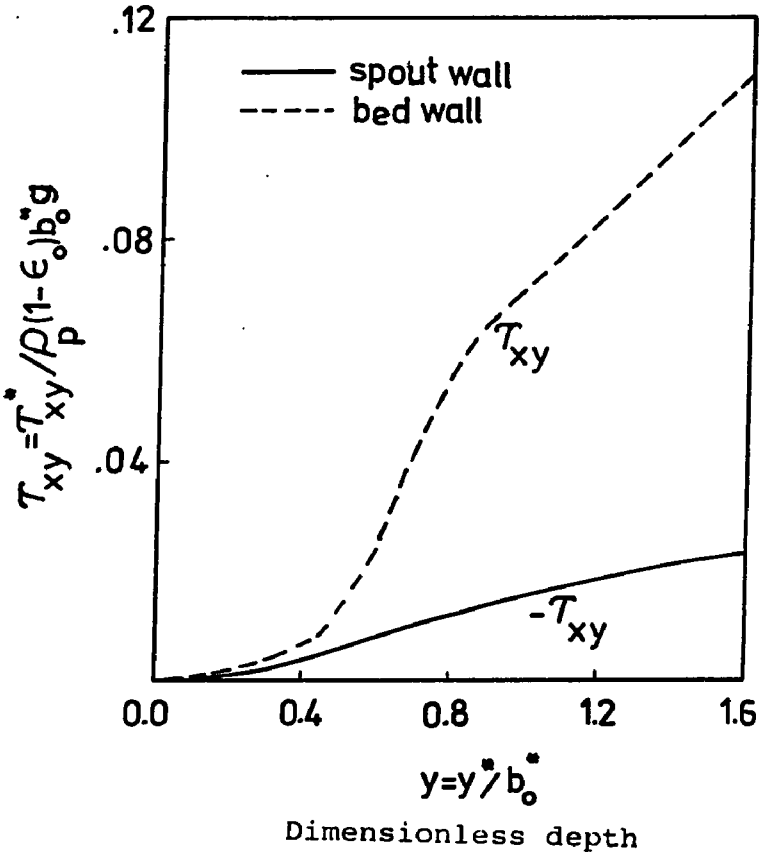

Figure 46 Distribution of the shear stress at the spout and bed walls obtained using the method of characteristics for the case of no gas flow in the annulus (B=0)
(δ=40°, $\delta_{w_{Max}}$=20°, $\delta_{s_{Max}}$=4°)

shear stresses at the spout and bed walls. The shape of the bed wall shear stress for y<1 is because of the varying δ_w.

Figures 47 and 48 show the stress distributions at the bed and spout walls for a spouted bed case (B=1). For this case where the gas flow in the annulus is considered the density of material changes according to (3.2-5) and at the top of the bed the weight of the material is balanced by the gas flow pressure, the particles are almost fluidized, and the effective stress is zero. The components of stress thus start quite flatly at the free surface and increase with depth, but not linearly as was the case for the annular bin. The profiles suggest that the MOS estimates the correct values of stress only for a short depth from the top surface. It is interesting to note that the equality of the vertical normal stress at the two walls implies that the distribution factors D_s and D_w (ratio of the normal stress at the wall to the average normal stress) used in MOS are almost one. McNab and Bridgwater (1979) have done a similar analysis to MOS presented in this work for an annular region of a cylindrical spouted bed. They have indicated that at the top of the bed where the value of the average normal stress is close to zero $D_s=D_w=1$, and have chosen this

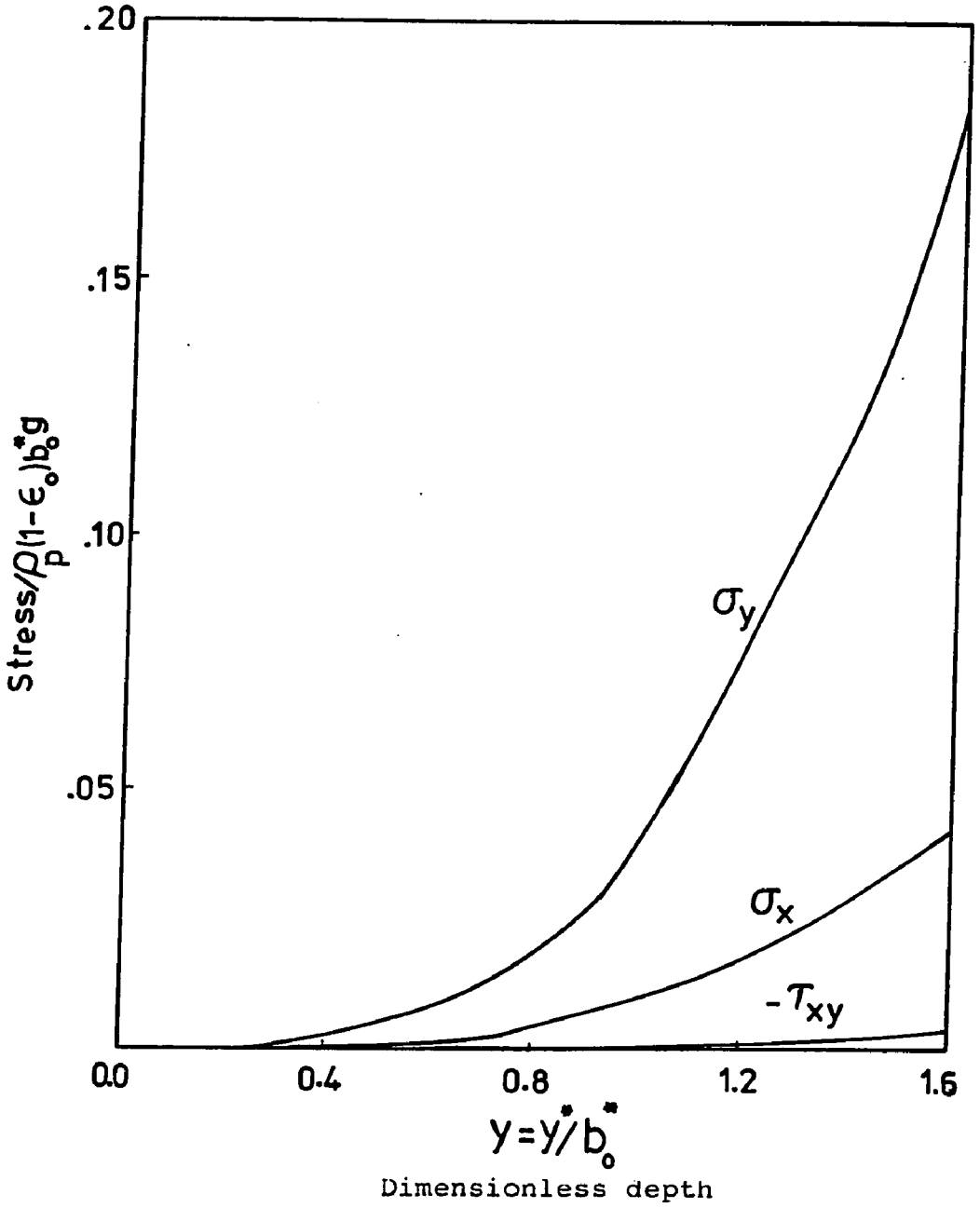

Figure 47 Dimensionless stresses at the spout wall obtained for the vertical part of the annulus using the method of characteristics for the spouted bed (gas flow, B=1)
($\delta=40^o$, $\delta_{w_{Max}}=20^o$, $\delta_{s_{Max}}=4^o$)

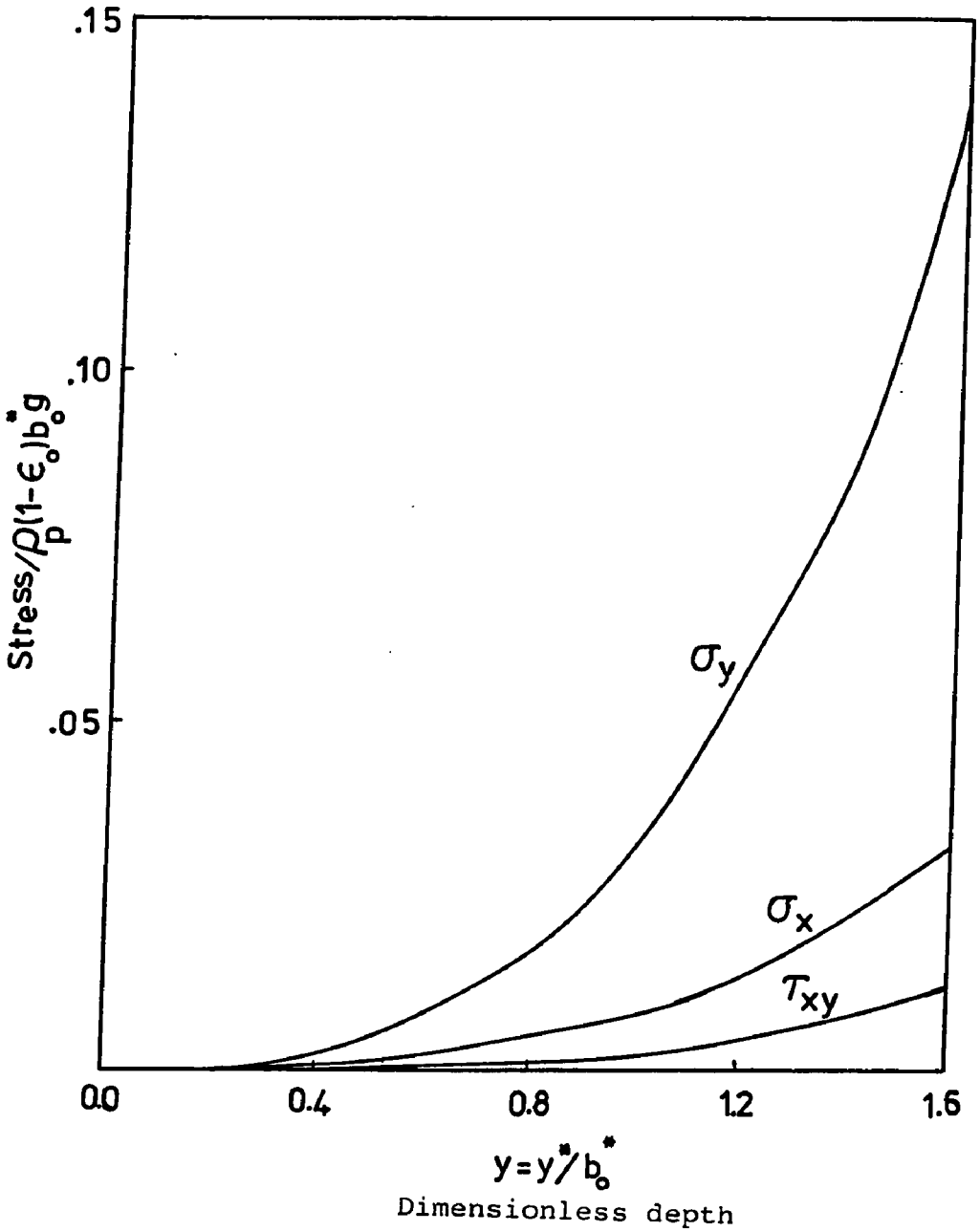

Figure 48 Dimensionless stresses at the bed wall obtained for the vertical part of the annulus using the method of characteristics for the spouted bed (gas flow, B=1)
($\delta=40^o$, $\delta_{w_{Max}}=20^o$, $\delta_{s_{Max}}=4^o$)

value for the entire annulus depth. The results of the present analysis on the other hand show that this is not a very good approximation for the entire annulus region of a spouted bed. The profiles of Figures 47 and 48 also show once again that the deep bed approximation is inappropriate for spouted beds. The slope of the stress profiles increase with depth.

The stress distributions by the MOS and MOI are compared with those by the MOC in Figures 49, 50 and 51 for the vertical part of the annulus. These Figures indicate that the results of the two methods are in general agreement with the exact method, MOC. The agreement between the MOS and MOI is excellent close to the free surface but not as good deeper in the bed. Both methods (MOS and MOI) assume that the shear stress changes linearly across the width of the annulus. In addition to this assumption the MOS takes a constant normal horizontal stress σ_x across the width of the annulus. Thus the difference between these two methods is the variation of σ_x. It is then evident why the results of the two methods agree so well in a region close to the top surface, if one refers to the distribution of σ_x across the annulus width by the MOI, Figure 50, or the wall stress distributions by MOI, Figures 35 and 36. These Figures show that the MOI

predicts almost a constant horizontal normal stress σ_x across the width of the annulus for depths close to the top surface (for the given conditions this depth is about half of the annulus width, $b_o^*/2$). Figures 49, 50 and 51 show that the results by the MOI are in good agreement with those by the MOC. Deviation between the predictions by MOIand MOS with those of MOC (especially for the shear stress, Figure 51) for depth close to the free surface may be due to the variable wall friction angle used in the method of characteristics. As mentioned before although the variable wall friction angles used in MOC circumvents the difficulties associated with the discontinuities, it gives approximated results near the top of the annulus. But, it is expected that the stress components approach to proper values in the deeper portion of the annulus. Figures 49, 50 and 51 show that the agreement between both MOS and MOI with MOC improves considerably deeper in the bed. The stress distributions predicted by the MOI are in better agreement with MOC than MOS, and for this reason the method of integrals with an analytical solution was employed to compute the velocity field. Notice that MOS can provide approximate ϕ distribution using the analytical solution (equation 5.1-15 and Figure 33a) along with the equations (A.1-2) and (A.1-6).

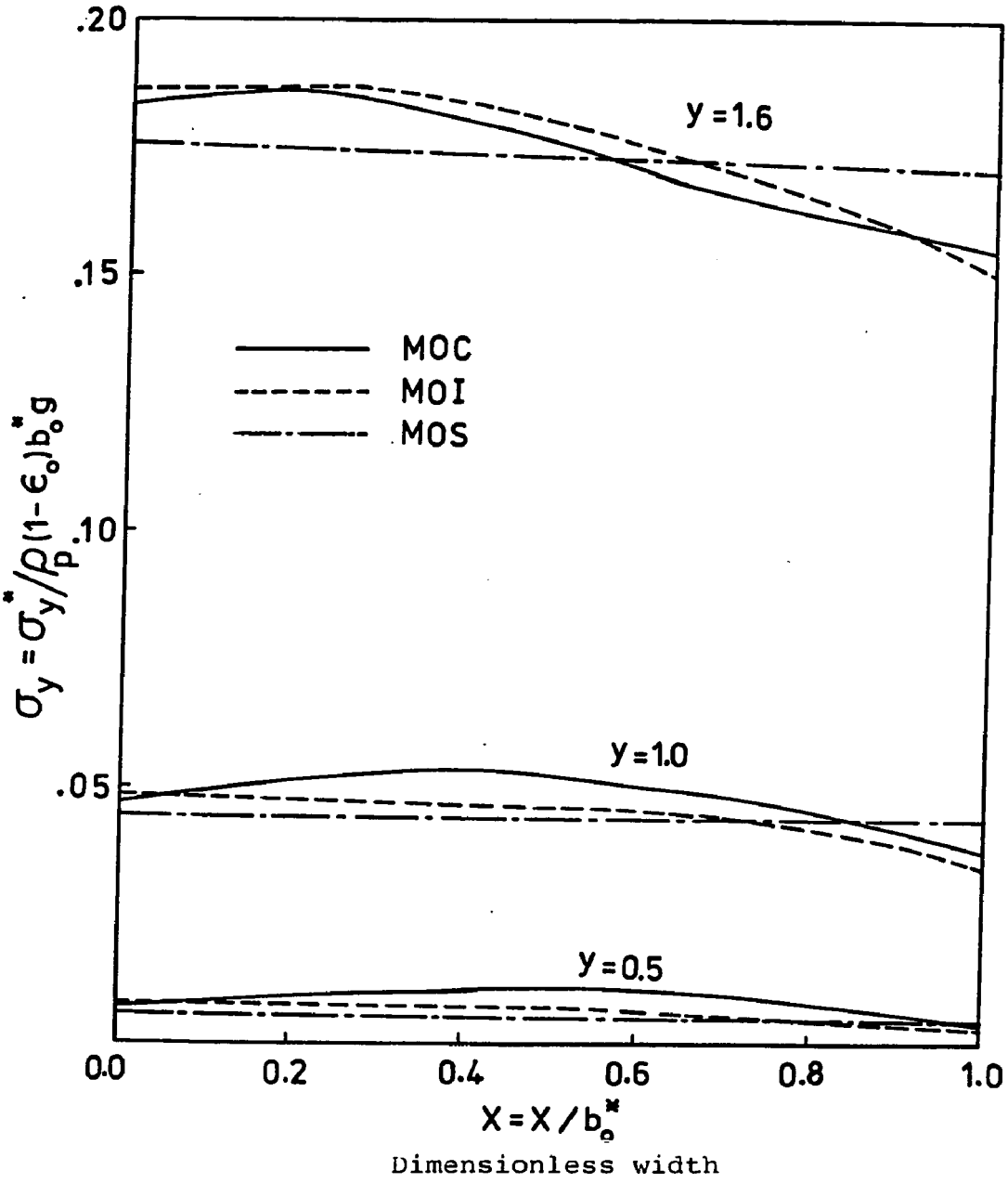

Figure 49 Horizontal variation of the vertical stress component by the method of characteristics, method of integrals and method of slices at different depth of the vertical part of the spouted bed annulus
($\delta=40^o$, $\delta_{w_{Max}}=20^o$, $\delta_{s_{Max}}=4^o$)

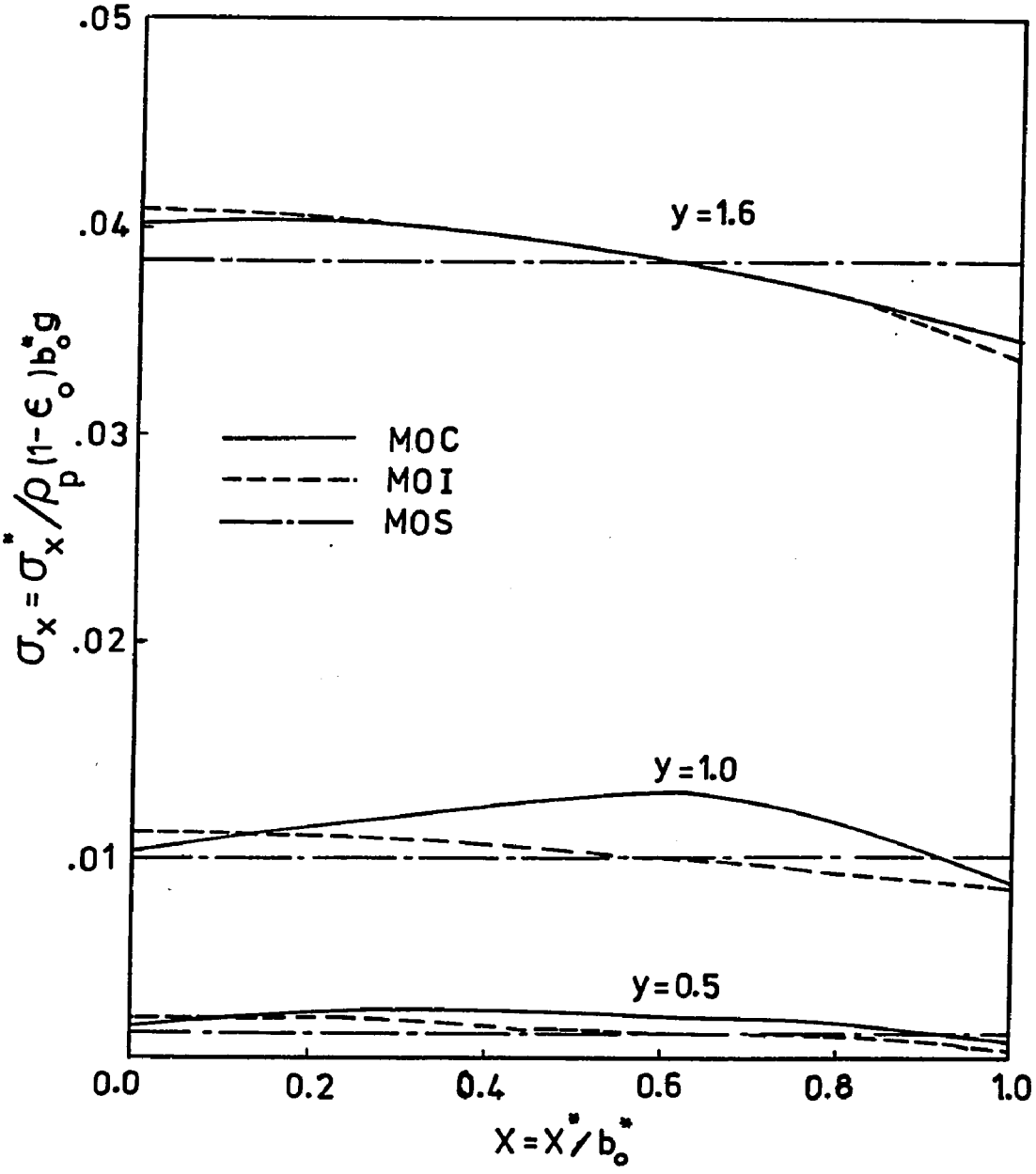

Figure 50 Horizontal variation of the horizontal stress component by the method of characteristics, method of integrals and method of slices at different depth of the vertical part of the spouted bed annulus
($\delta=40^o$, $\delta_{w_{Max}}=20^o$, $\delta_{s_{Max}}=4^o$)

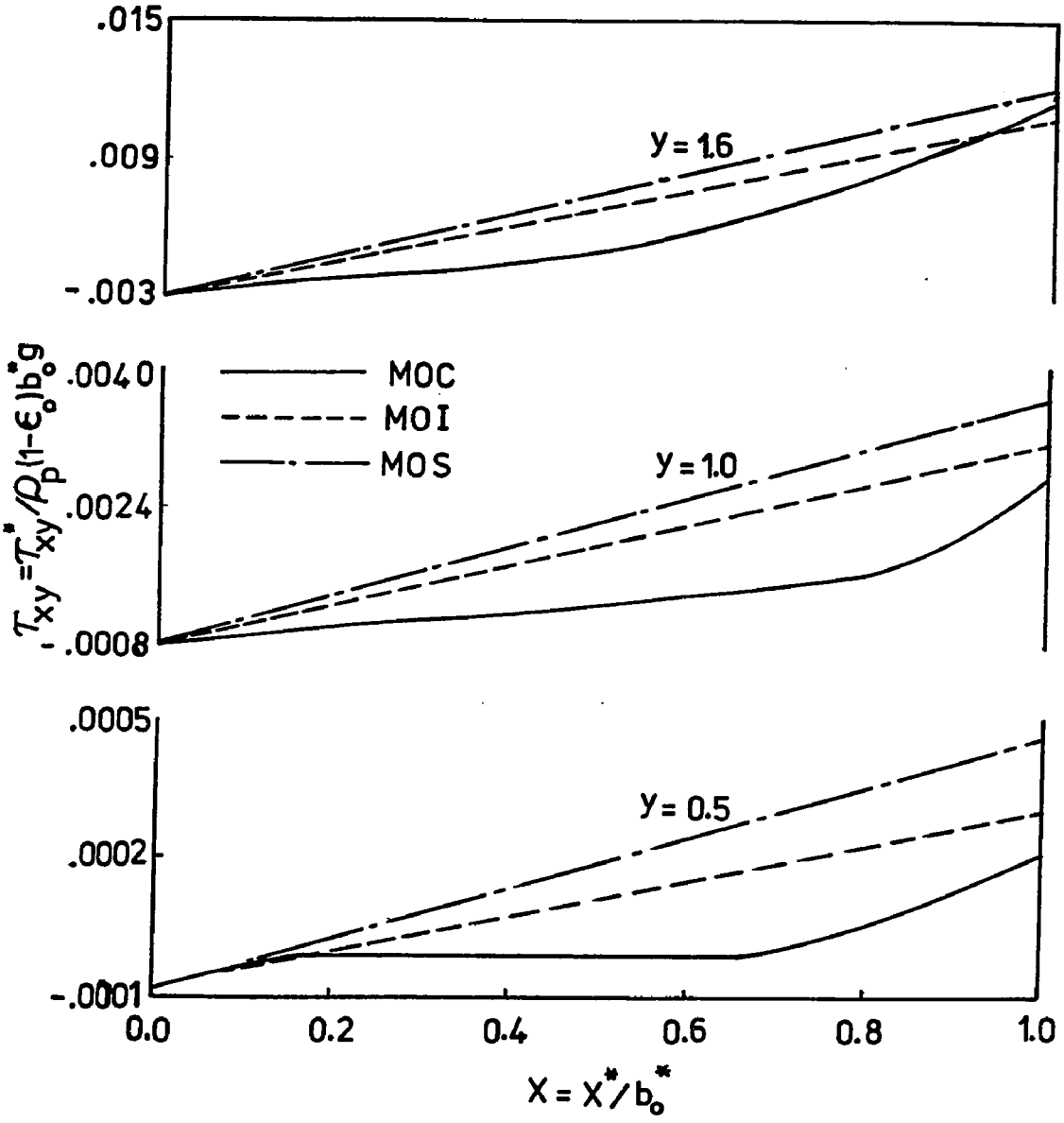

Figure 51 Horizontal variation of the shear stress component by the method of characteristics, method of integrals and method of slices at different level of the vertical part of the spouted bed annulus
(δ=40°, $\delta_{w_{Max}}$=20°, $\delta_{s_{Max}}$=4°)

The method of characteristics was not employed to determine the stress distributions in the conical region because of the lack of a limiting solution (see 5.2.5) as well as the complexity of the computations caused by the discontinuities at the vertical/conical junction of the spout and bed walls. It is interesting to note that the direction of the second characteristic given by (5.3.2-3) coincides with the boundary of the dead zone with $\delta_b=\delta$ (fully rough wall), that is this boundary is a slip line (see 5.3.7). However, this coincidence does not prevent the expansion of the characteristics mesh in the conical region (if there were a solution). If a wall with less friction is replaced for the boundary of dead zone with the same inclination (called conical wall, with $\delta_b<\delta$), a fan of characteristics or a shock front would emanate from the corner point of the vertical/conical junction depending on the divergence or convergence of the characteristics from this corner. This fan or front will then interact with another shock front originated at the spout wall. As mentioned before these discontinuity computations are complex and time consuming and applicable approximate methods such as MOI is strongly suggested.

It was attempted to employ the Radial Stress Field (RSF) in the conical region primarily to compute a Radial

Velocity Field (RVF) for this region. The RSF assumes that the mean normal stress σ is directly proportional to the radial distance from the origin and that the angle ϕ is a function of the angular position only. With these assumptions there is a similarity solution to the equilibrium equations, (3.3.1-9 and 10), written in terms of polar coordinates. The determination of stress field then reduces to the solution of a pair of ordinary differential equations. The RSF has been extensively applied to the problem of flow of bulk solids in hoppers by Jenike (1961, 1964) and Johanson (1964). Unfortunately, when applying this method to the conical region of a spouted bed preliminary calculations showed that there exists no similarity solution to the basic equations. This is due to the change of the effective density of particles with height.

5.3.7 Slip lines

If one compares the stress characteristic directions, equation (5.3.2-3), with those of slip lines, given in section 3.3.1, it is readily seen that these directions coincide. This means the characteristics shown in Figure 43 are slip lines. This is a coincidence, bearing in mind that the two concepts being quite distinct. The slip lines are representative of the slip planes in the physical

plane x-y. The slip planes are the planes on which the yield stresses develop. Thus, slip lines can be interpreted as the locus of the yield stresses. The characteristics on the other hand are lines of mathematical convenience, being the lines along which the partial differential equations reduce to ordinary differential equations. Notice, however, for the cohesive material the angles ϕ (angle of internal friction) and δ (effective angle of internal friction) are not equal, and the characteristics directions will not then lie along the slip surfaces. For a cohesive material the slip lines have the slopes of either of the two angles $\theta \pm (\pi/4 - \phi/2)$.

The slip lines make angle 2ψ with each other as do the stress characteristics (Figure 43). Since the direction of the major principal stress bisects the angle between the two slip lines (see Figure 16), this direction can simply be identified as the bisector of the angles between any two characteristics. In the active Rankine zone where the material flow without shear stress this direction is vertical. At greater depth the lines of major principal stress are not vertical indicating to the development of shearing stress within the material.

It is of greatest importance to realize although the

yield stresses develop on the slip planes, the shear strains do not, in general. The lines of maximum shearing stress are inclined at 45^{o} to the lines of major principal stress, as discussed in section 5.4.3. With the assumption of coaxiality these lines coincide with the lines of maximum shearing strain rate or shear lines. It is shown in section 5.4.1 that shear lines coincide with the velocity characteristics. On the other hand, it is seen that the lines of maximum shearing stress (or shear lines) can be identified just from the geometrical construction of the stress characteristics, without solving for the velocity field.

5.4 Velocity Field

The velocity field for steady flow is obtained using continuity equation for an incompressible solid together with the condition of coaxiality of principal stress and strain rate. These conditions were discussed in section 3.3.2.

Determination of the velocity field in plasticity has been considered by many investigators (for example see Hill, 1950, Prager, 1951, Sobotka, 1961). Prager in his book paid special attention to the computation of the velocity and construction of the shear lines or the lines of maximum shear strain rate (see 5.4.3). The complete solution of the problem of plasticity includes the statical solution defining the stress field with slip lines or slip surfaces and the kinematical solution determining the velocity field with shear lines (termed flow lines in Prager's book) or shear surfaces, respectively. In a statically determinate problem one may be able to solve the equations of equilibrium, given suitable boundary conditions, and thus determine the stress distribution in problems of plane plastic flow without further reference to the stress-strain relation and taking the associated velocity field into account. This is possible when the boundary conditions for the stress field contain only

statical variables (stress parameters), and not the kinematical variables (velocity components). However, the complete solution of both fields is needed in some cases (Sobotka, 1961). Determination of velocity field for flowing granular material in a bin applying plasticity theory has also been considered by some investigators (Davis, 1968 and Pariseau, 1969). Pariseau (1969) has shown experimentally that the conventional plasticity theory requiring coincidence of stress and velocity characteristics can not predict the streamlines of the flow of an ideally plastic material properly, rather it is the assumption of incompressibility that yields proper streamlines for this type of flow. The solution to the velocity field has been restricted to a few cases. The only major attempt to predict the velocity field in a hopper using plasticity arguments seems to be that of Jenike et al. (1961,1962) and only recently by Tuzun et al. (1982) and Jackson (1983). Jenike et al. established the general form of the differential equations based on the assumption of coaxiality, but only solved these for the particular case of "radial velocity field". The radial velocity field is the compatible velocity field to the radial stress field. This stress field which is in effect a particular integral to the general stress equations, applies to a region near the apex of a bin. Nedderman (1982)

and Tuzun et al. (1982) have recently pointed out that the radial stress field solution may not be a good approximation over considerable distance. The radial velocity field may be approached near the orifice, but the validity of this solution is in serious doubt further away from the apex. The employment of radial velocity field for a spouted bed is inappropriate since there is no radial stress field solution for spouted beds, as mentioned in 5.3.6.

Calculation of stress field without the corresponding velocity fields are often much simpler. The flow problems are complicated by the theories governing the flow rules, plastic potential, association of the flow rule and normality. In addition to the complexity of these theories, the uncertainity and/or inadequacy of proper boundary conditions leading to a non-unique velocity field have considerably affected the advancement of the velocity field determination in the plasticity. A unique velocity field may be obtained for a field with adequate boundary conditions. Nedderman et al. (1982) have recently enumerated these difficulties and concluded that there seems to be no general agreement on the basic principles governing the velocity distribution in granular media, although the majority of workers seem to favor the use of plasticity theory.

The velocity field obtained in this work is associated with the stress field obtained in section 5.2 or 5.3. Incompressibility and coaxiality were employed to determine the velocity field. The MOC was used to compute this field.

5.4.1 Characteristics equations of the velocity field

Starting with (3.3.2-1) and (3.3.2-2) and following the procedure described in section 5.3.1, the characteristic directions and the velocity characteristic equations which hold along the two directions can be calculated as

$$\frac{dy}{dx} = -\tan\left(\phi - \frac{\pi}{4}\right) \quad ; \quad \tan\left(\phi + \frac{\pi}{4}\right)du + dv = 0$$
$$\frac{dy}{dx} = -\tan\left(\phi + \frac{\pi}{4}\right) \quad ; \quad \tan\left(\phi - \frac{\pi}{4}\right)du + dv = 0 \qquad (5.4.1\text{-}1)$$

ϕ is determined by the stress field solution and this condition ties the velocity and stress fields together. The detail of derivation of system (5.4.1-1) is given in Appendix 3. This system indicates that the two velocity characteristics are orthogonal.

If the characteristic curves are approximated by straight lines (Figure 41) the data at a typical grid point M may be obtained using the data at points 1 and 2, and writing the velocity characteristic equations in the

finite difference form. The position of M is thus obtained from

$$x_M = \frac{\alpha_2 x_2 - \alpha_1 x_1 - y_2 + y_1}{\alpha_2 - \alpha_1} \qquad (5.4.1\text{-}2)$$

or

$$\begin{aligned} y_M &= y_1 + \alpha_1 (x_M - x_1) \\ y_M &= y_1 + \alpha_2 (x_M - x_2) \end{aligned} \qquad (5.4.1\text{-}3)$$

where

$$\begin{aligned} \alpha_1 &= -\tan(\phi_1 - \pi/4) \\ \alpha_2 &= -\tan(\phi_2 + \pi/4) \end{aligned} \qquad (5.4.1\text{-}4)$$

The magnitudes of u and v at point M are found by solving the system

$$\begin{aligned} \tan(\phi_1 + \pi/4)(u_M - u_1) + (v_M - v_1) &= 0 \\ \tan(\phi_2 - \pi/4)(u_M - u_2) + (v_M - v_2) &= 0 \end{aligned} \qquad (5.4.1\text{-}5)$$

The general procedure employed in determining the stress characteristics can be followed to calculate the velocity characteristics as well. The boundary conditions are those described in section 3.3.3.

Comparing the characteristic directions for the stress field, equation (5.3.2-3), with those of the velocity field, it can readily be seen that the characteristic directions for the two fields do not coincide.

This means that the coordinates of the stress characteristic grid points are different from those of the velocity. Thus, as far as the computations of the velocity characteristics are concerned an interpolation must be used to obtain the value of the angle ϕ at each velocity grid point, if the stress field by the MOC is employed to determine $\phi(x,y)$. This method requires the storage of all the calculated stress points as well as a great deal of computer time to search out the closest of these points to the point in question. It should be mentioned that the alternative techniques such as fitting a high order polynomial throughout the entire field by a least squares method, or, dividing the field into several small regions have been proven to be inaccurate (Jenike and Johanson, 1962). This major problem limits the possibility of velocity field calculation to the MOI, where an analytical solution exists for $\phi(x,y)$. However, since the results of the stress field computations by the two methods (MOC and MOI) were shown to be in good agreement, it is expected that the results of the velocity field computations corresponding to the two stress fields also agree reasonably well.

5.4.2 Results and discussion

The case of $\delta=40^{o}$, $\delta_{w}=20^{o}$, $\delta_{s}=4^{o}$ and H=3 was con-

sidered as an example of the velocity field computations. The calculation of the characteristics was started from the top of the annulus by dividing its width into five equidistance intervals. Typical grid points of the mesh were obtained applying the velocity characteristic equations. The general procedure followed was that of the stress characteristics, as described in section 5.3.6. At each point the MOI was used to obtain the value of ϕ at that point. To improve the accuracy of the computations the average of the variables not appearing in the difference form were used. This average was taken between a starting (1 or 2 of Figure 41) and the resulting grid point (point M). An iterative procedure was then required to calculate the coordinates of each grid point. This technique was programmed for a digital computer. To facilitate the computations, a subroutine of the MOI was provided to give the value of ϕ for any given x and y. The computed velocity characteristics mesh is shown in Figure 52. Notice that this mesh could be established in advance without solving the corresponding velocity equation (5.4.1-5) and knowing the values of u and v at the grid points. This is possible since the characteristic directions are functions of ϕ only which is given by the stress field solution and is independent of u and v.

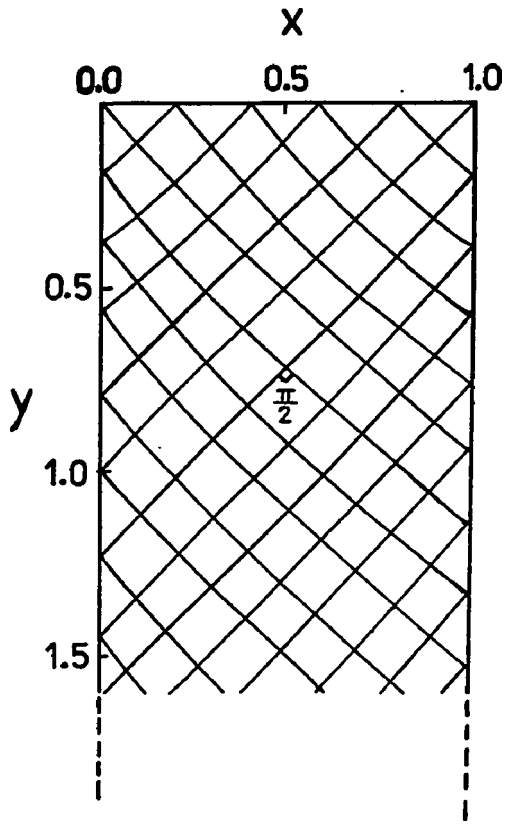

Figure 52 Velocity characteristic mesh
(δ=40°, $\delta_{w_{Max}}$=20°, $\delta_{s_{Max}}$=4°)

The velocity boundary conditions used were those discussed in section 3.3.3. The two velocity components u and v were specified at the top boundary. At the bed and spout walls only u was specified and at the dead zone boundary a relation between u and v was given (see Figure 18). At the top corner point of the bed wall, u of the top boundary and the wall are matched. At the other top corner point, u of the top boundary is not matched with that of the spout wall. Although this introduces a discontinuity, the computations can be continued without complications. It should be mentioned that the discontinuity relation in the velocity field, unlike the stress field, does not provide any additional information. The velocity characteristics are well behaved since they are independent of the velocity components. The presence of the discontinuity at the top corner of the spout wall is then reflected on the velocity distributions at this wall by a sharp change of the profiles at this point.

The major problem in computing a proper unique velocity field is the uncertainity of the boundary conditions at the top boundary and the spout wall. There are no empiritcal correlations of the velocities at these boundaries for a two-dimensional spouted bed, nor there are any experimental data for this type of bed. The only

available experimental data are those of Thorley et al. (see Mathur and Epstein, 1974) and Suciu and Patrascu (1978). Both group of investigators traced particle streamlines and obtained the data by observations and photographs against the flat wall of a half-cylindrical column with a conical bottom.

The velocity field could only be obtained for the vertical part of the annulus because of the difficulties encountered in the computation of the stress field in the conical region. These difficulties are discussed later in this section. The boundary condition at the spout wall was assumed to be a uniform horizontal velocity distribution. This assumption is based on the experimental evidence of the total solid circulation, which has been found by Mathur and Epstein (1974c) to change linearly with depth in the vertical portion of a cylindrical spouted bed. This boundary condition seems to be the best at hand. More experimental evidence is however required to assess the validity of this condition for a two dimensional spouted bed. Figures 53 and 54 show the velocity profiles at the bed and spout walls. The velocity profiles at the bed wall show that the conditions along the non-characteristic top boundary are extended along the vertical wall down to the point C of Figure 52, where the

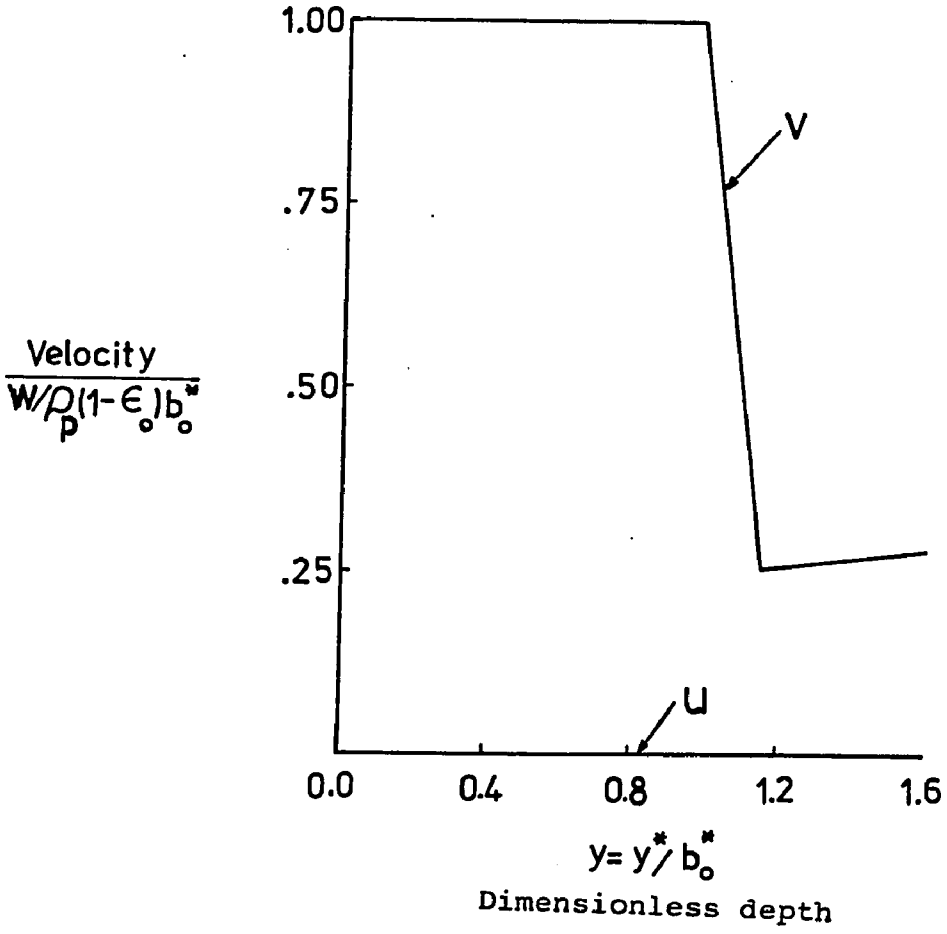

Figure 53 Dimensionless horizontal (u) and Vertical (v) velocity distributions at the bed wall for the vertical part of the annulus

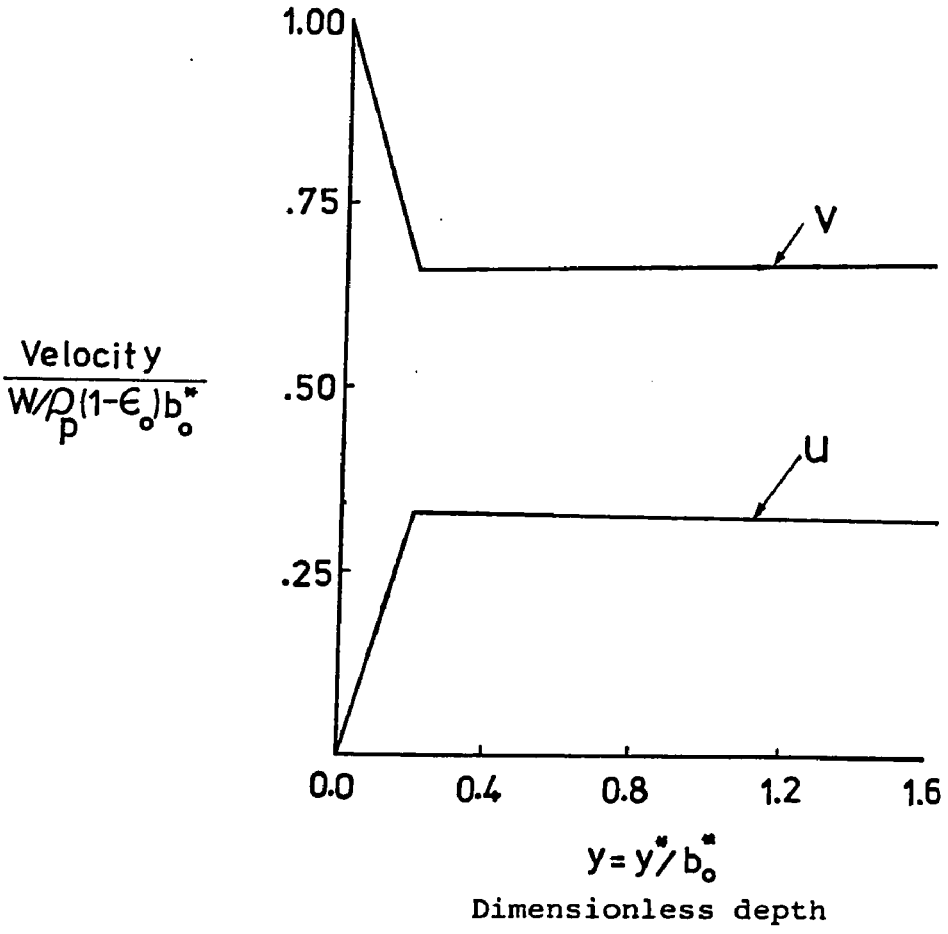

Figure 54 Dimensionless horizontal (u) and vertical (v) velocity distributions at the spout wall for the vertical part of the annulus

first characteristic emanated from the top corner of the spout wall meets the bed wall. The whole region ABC is then having velocities equal to those imposed across the noncharacteristic top boundary AB. This is due to the uniqueness of solution of hyperbolic type equations. The triangular region ABC is the domain of dependence of the solution on the boundary conditions defined in AB as discussed by Johanson (1964). The vertical component of velocity v at the bed wall is then constant down to point C of Figure 52, after which decreases sharply and then changes linearly. The horizontal component of velocity u remains zero at the bed wall which is the wall boundary condition. Figure 54 shows the velocity profiles along the spout wall. While, the horizontal velocity u was imposed to remain constant along the spout wall from the top surface, the computed vertical velocity v also remains almost constant along this wall. Thus, particle enter the spout more or less with the same direction for the vertical part. Figures 55 and 56 show u and v versus x at different depth. The velocity distributions in these Figures were obtained by interpolating the values of the velocity components between the grid points. There are sharp changes in the profiles of the vertical part due to the crossing of the characteristic AC and its reflection from the bed wall.

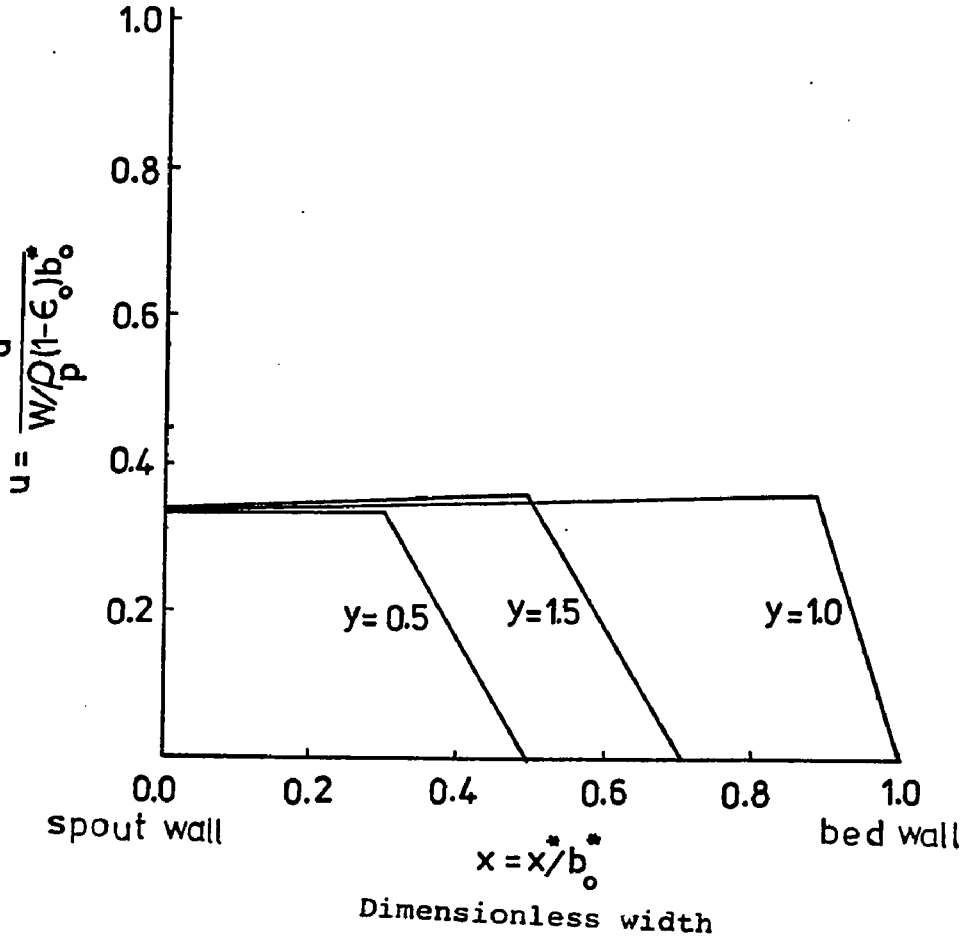

Figure 55 Horizontal variation of the horizontal velocity component at different depth of the vertical part of the annulus

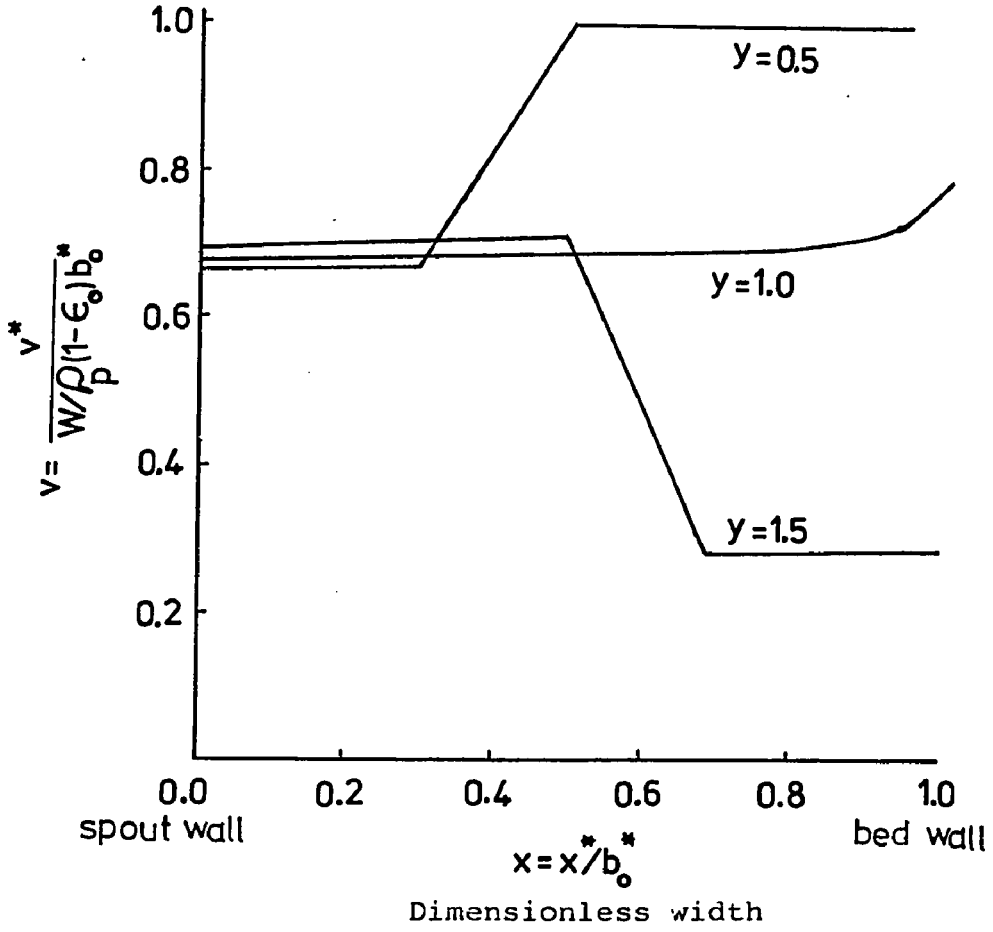

Figure 56 Horizontal variation of the vertical velocity component at different depth of the vertical part of the annulus

It was attempted to compute the velocity field by the MOC for the conical region. Unfortunately due to enormous computational difficulties this attempt was unsuccessful. The velocity field could not be computed for a fully rough wall (boundary of dead zone with $\delta_b=\delta$) because of the lack of a stress field solution for the conical region. It was mentioned before (see 5.2.5) that a plastic equilibrium analysis may not be appropriate in the conical region due to the importance of the inertial terms in this region. However, it is interesting to note that the boundary of dead zone coincides with one of the velocity characteristics, that is this boundary is a shear line (see 5.4.3). It was mentioned before that the boundary of dead zone is a slip line and a streamline. Thus at this boundary shear line, slip line and streamlines coincide. Attempts were also made to obtain a velocity field for the conical region (assuming that there is a plastic equilibrium in this region) with the boundary of dead zone replaced by a wall having an angle of internal friction of $\delta_b=\delta=20^{\circ}$. A solution to the stress field was already obtained for these conditions by the MOI. Results of the computation indicated that the velocity characteristic coalescences in the conical region. The coalescence of characteristics indicates to the existance of discontinuities in the field. These characteristic coalescences are likely caused by the

swift change of angle ϕ where passing from the vertical to the conical region due to the switch of the stress state from active to passive as well as transition of the stress state from passive at the spout wall ($\phi_s > 45^o$) to active at the conical region wall ($\phi_b < 45^o$). It then seems that to obtain a velocity field solution for the conical region, assuming plastic equilibrium, a detailed stress field containing the analysis of the discontinuities is required, and that the approximate method of integrals cannot provide these details in the conical region. There were also attempts to find an approximate velocity field for the conical region using the Radial Stress Field. The velocity field compatible to the RSF is called Radial Velocity Field. The RVF has been employed by Jenike (1961, 1964) and Jenike and Johanson (1962) to obtain a velocity field for bulk solids flowing in hoppers. After writing the continuity and coaxiality equations, (3.3.2-1) and (3.3.2-2), in terms of polar coordinates, the RVF assumes that the flow is purely radial. Solution to the velocity field is then reduced to a single integration of the resulted equation in polar coordinates employing only one boundary condition. Thus, the RVF can not satisfy both boundary conditions at the spout and at the boundary of dead zone at the same time. Regardless of this disadvantage the radial velocity field is not applicable to the

spouted beds since there is no similarity solution or radial stress field for spouted beds, as mentioned in section 5.3.6.

Figure 57 shows the approximate streamlines obtained by using the velocity vectors for the vertical portion of the annulus. As the streamlines show the particle move vertically downward in the triangular region of ABC of Figure 52. The particle change direction toward the spout after crossing the characteristic AC. The particle once again move almost vertially after crossing the reflected AC characteristic from the bed wall.

While there is no definite confirmation of the calculated velocity field quantitatively, unless compared with the experimental data, the computed results seem to agree qualitatively with the data in the literature and the observations. Data of Thorley et al. (see Mathur and Epstein 1974b) indicate to velocity oscillation at both horizontal and vertical sections throughout the annulus. The observations of the two-dimensional bed show that particles adjacent to the bed wall must move along the wall to a distance and then start departing from the wall in the region close to the dead zone. Photographs taken from the two dimensional bed (Figure 58) confirms the vertical

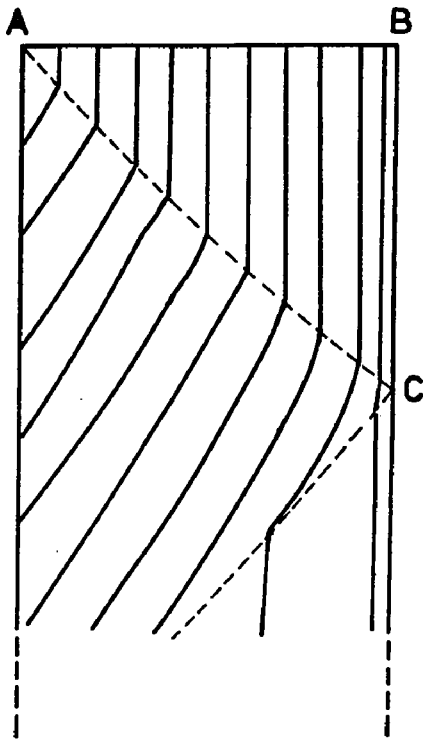

Figure 57 The computed solid particle streamlines in the vertical part of the annulus

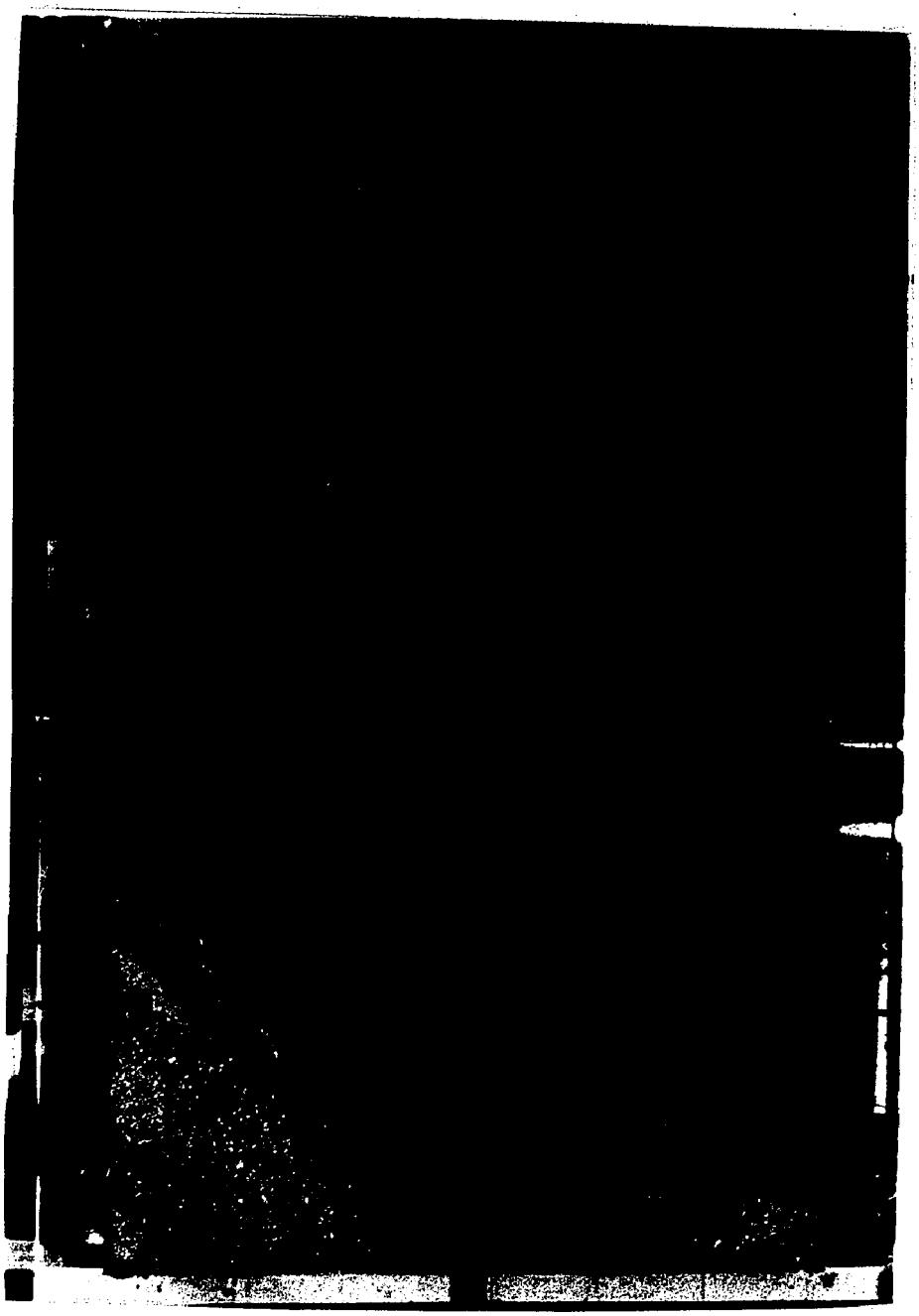

Figure 58 Photograph of a two-dimensional spouted bed

movement of the particles along the wall. Recent experimental results from a semi-cylindrical bed have shown that in a thin layer adjacent to the spout wall, particles move vertically downward along the spout wall. It should be noticed that the present analysis and the computed streamlines is concerned with the bulk motion of the solid particles using the coaxiality condition. A rigorous experimental analysis is required to confirm the results of the present work and to critically examine the validity of the application of the coaxiality condition to determine the velocity field for a spouted bed.

5.4.3 Shear lines

The lines of maximum shear strain rate (or simply shear lines) are inclined at angles $\pm\pi/4$ to the lines of the principal strain rate, and with the assumption of coaxiality, also to the lines of the principal stress. Therefore, the slope of these lines are $\phi \pm \pi/4$.

If one compares the velocity characteristic directions, equation (5.4.1-4), with the shear line directions it is readily seen that the two directions coincide. This means the characteristics shown in Figure 52 are the shear lines. This is a coincidence, bearing in mind the fundamental difference between the two concepts. The shear

lines are the representative of the planes upon which shear strain rates is a maximum when the material fails. The characteristics on the other hand are lines of mathematical convenience.

The two shear lines are perpendicular and the line of principal strain rate bisects their angles. Thus, the direction of principal stain rate can simply be identified as the bisector of the angle between the two velocity characteristics. The lines of maximum shear stress, on the other hand, perpendicular to each other, are the bisector of the lines of principal stresses. Therefore, with the coaxiality, the shear lines in a field of plane plastic flow indicate not only the directions of maximum rate of shear, also the directions of maximum shearing stress. The velocity characteristics are then lines of maximum shearing stress and maximum shearing strain rate. This depends only on the assumption of coaxiality not on the material rheology.

While the shear lines do not coincide with the slip lines, in general, it is interesting to analyze the case of an ideal material. For an ideal material where $\beta=\delta=0$, slip lines are perpendicular having slopes of $\phi \pm \pi/4$ and coincide with the shear lines. The physical meaning of

this coincidence is that the yield shear stress has reached the maximum value, and this is the Tresca condition: the yield occurs when the maximum shear stress reaches a critical value. Thus, for an ideal material the Coulomb law reduces to the Tresca yield criterion. On the other hand, referring to the Mohr diagram of Figure 16, $\phi=0$ implies the EYL to become parallel to the σ axis giving the maximum shear stress. In the principal stress space the Coulomb cone has then become the Tresca pyramid with closed base, Figure 10. The Tresca (or Von Mises) yield criterion does not explain the frictional behavior of granular material, and that is why the Coulomb criterion has been used for more than two hundred years for granular soils despite its controversial nature. The slip lines and the shear lines do not coincide when using the Coulomb criterion, as mentioned earlier. The difference between these two planes has occupied the attention of many workers in soil mechanics such as Rowe (1963). To avoid misunderstanding, Lambe & Whitman (1979) have distinguished between two types of failure plane by naming the slip line "theoretical failure plane" and the shear lines "observed failure plane". The lines of maximum shear strain rate are important because some of them may be observed through a transparent wall of a model.

CHAPTER SIX

6.0 CONCLUSION

In the first chapter the phenomena of spouting is discussed. Spouting was suggested by Mathur and Gishler (1955) as an alternative to fluidization for particles too uniform or too coarse for a stable fluidization.

In the second and third chapters the fundamentals of a rigorous model for the study of the motion of solid particles in the dense region of a spouted bed is presented. These concepts although used in this study for the case of a two-dimensional spouted bed, it can be applied, in principle, to any other type of (spouted) bed. The rules adopted here to characterize the fundamental mechanism of solid motion have been employed in the areas of soil mechanics and flow of bulk solids for many years. Extensive use of "Jenike's solid", or Coulomb's solids as well as yield surfaces proposed by Jenike and Sheild (1959) ties the present analysis with the two fields. The governing equations discussed in chapter three correspond to the case of plane strain, but they can simply be adapted for the other cases such as axial symmetry (case of cylindrical spouted beds). In the fourth chapter the experimental procedures are described. The experimental work was

limited to the observation of the basic qualitative features of a two-dimensional spouted bed, evaluation of the maximum spoutable height, observation of the particle motion in the dense region and verification of the boundary of dead zone predicted by the method of slices. Obviously, a rigorous experimental technique is required to confirm the effectiveness of the proposed models. While measuring stresses experimentally seems to be a very difficult task, particle velocities can be measured using different techniques such as high speed photography or Laser Doppler Anemometry. Also in this chapter a model to determine the dead zone boundary using the method of slices is presented and discussed. It is our belief that this method which has been extensively used in the slope stability problems of soil mechanics can effectively evaluate the boundary of dead zone for the flat bottomed beds.

The fifth chapter consists of the models developed to determine the stress and velocity fields for the material contained in the annulus. The solution to the stress field is presented by the method of differential slices (MOS), the method of integrals (MOI) and the method of characteristics (MOC). The method of slices is attractive for its simplicity, if the assumptions of the method can be justified. The MOI, on the other hand, provides an ap-

proximate analytical solution to the stress field for the entire annulus region when a solution exists. The advantage of this method in spite of the lengthy algebraic manipulations required, is its ability to provide a meaningful average solution through the regions of discontinuities in addition of supplying an analytical solution. The MOI can be used for both vertical and conical parts. The availability of the analytical solution is of greatest importance in the computation of velocity field, both from the stand point of the complexity of computation, and computer time consumption. While it was not possible to obtain the stress distribution for the conical region for a fully rough wall (boundary of dead zone, $\delta_b=\delta$), the result of this method for a wall with less friction ($\delta_b=\delta/2$) show that the material pass from one fluidization state at the top of the bed to another at the bottom of the bed (spout entrance).

The method of characteristics (MOC) converts the governing partial differential equations to ordinary differential equations without any approximation. The characteristic directions can then be integrated numerically thus, furnishing a systematic approximation to the solution. Unfortunately, the handling of the discontinuities that are generated at the boundaries or by intersection of

characteristics belonging to the same family makes the computation prohibitely cumbersome. It is suggested that this complexity be avoided by introducing a variable wall friction angle, when applicable and when a very accurate solution is not required. The use of variable wall friction angle clearly results in an approximate solution, but it seems that the deviations from the correct values are not significant and decay rapidly with the distance from the discontinuity region. At the junction of the vertical/conical part where the state of stress switches from active in the vertical to passive in the conical part strong discontinuities exist and a detailed point by point computations are required. Unfortunately, these computations are very complex and time consuming when using the MOC. The solution to the stress field by the MOC does provide the sliplines. The sliplines discussed in section 5.3.7 are not the lines representing the planes on which the shear strain is concentrated, rather they are the locus of the yield stresses.

The computation of velocity field is also discussed in chapter five. The use of stress solution by the MOC in determining the velocity field was found to be extremely tedious. The use of any approximate method such as the MOI providing stress parameters reasonably close to those by

the MOC is strongly suggested. The solution to the velocity field by the MOC provides the shear lines. These lines representing the plane upon which the shear strain rate is concentrated do not coincide with the slip lines for the frictional materials. The velocity profiles determined by the model are oscillatory. The literature experimental data (Mathur and Epstein, 1974, Suciu and Patrascu, 1978) also indicate to velocity fluctuations. Although a quantitative comparison between the outcome of the model and experiment is not given here, there are good qualitative agreements between the two. The model determinig the velocity field is felt to lack reliable experimental based boundary conditions. Such correlations used as the boundary conditions would undoubtably improve the accuracy of the proposed model. Because of the computational difficulties, as described in section 5.4.2, the velocity field could not be determined in the conical region using the MOC and the application of the radial stress field (leading to radial velocity field) also proved to be invalid for the spouted beds. It thus seems that a detailed computation of discontinuities at the vertical/conical junction is required to obtain the velocity field in the conical region if a limiting solution exists at all.

It is our contention that the fundamental mechanics of particle motion in the vertical portion of the dense region of a spouted bed, where the inertial terms are not important, can be described appropriately by the rules discussed in this work. Since the particles accelerate in the conical region and the inertial terms become important it seems that the employment of the limit equilibrium analysis may not yield to appropriate results. To obtain stress and velocity distributions in the conical region it seems more appropriate to consider the full momentum equations containing the inertial terms. These distributions may then be combined with those of the limit analysis for the vertical part to give a complete picture of the mechanics of particle motion in a dense region of a spouted bed. The models developed in this work can easily be extended to the case of cylindrical spouted beds. The emphasis of the study has been theoretical and is now required experimental supporting evidence. It might be also possible to apply the fundamental approach presented in this work to develop models for particle motion close to the nozzle of a fluidized bed, since a short internal spout forms at the nozzle entrance. Such an approach has been initiated by Rietema (1968) but no real progress has yet been reported.

Khoe (1980) has recently analyzed the problem of spouted beds from a different approach to the present analysis. By introducing a potential, Khoe has investigated the flow of fluid and solids in a spouted bed. He has also used the slope stability of packed beds percolated by a gas to find the stable (spout) and unstable (annulus) regions in a spouted bed thus approximating the position of the spout wall. Khoe's stability analysis and spout boundary approximation strongly depends on the experimental data (primarily on the limiting gas pressure) such that without these data the model is incapable of predicting the stable and unstable regions. It is our belief that the mechanics of spouted beds can be more appropriately described by the basic momentum equations along with the effective stresses. It migh be possible to combine the principles of the present analysis with those used by Khoe to provide an appropriate basis for a rigorous self supported mathematical model. Experimental results may be then used to assess the accuracy of such a model.

BIBLIOGRAPHY

Airy, W., "The Pressure of Grain", Minutes of Proceeding of the Institution of Civil Eng., V.81, No.3049, 1897

Becker, H.A., "An Investigation of Laws Governing the Spouting of Coarse Particles", Chem.Eng. Sci., V.13, P245, 1961

Belotserkovskii, O.M. and Chushkin, P.I., "The Numerical Solution of Problems in Gas Dynamics", Basic Development in Fluid Dynamics, Academic Press, New York, 1965

Bishop, A.W., "The Use of the Slip Circle in the Stability Analysis of Earth Slopes", Geotechnique, V.5, No.1, p7, 1955

Bridgewater, J. and Mathur, K.B., "Prediction of Spout Diameter in a Spouted Bed-A Theoretical Model", Powder Technology, 6, 183, 1972

Courant, R. and Friedrichs, K.O., "Supersonic Flow and Shock Waves", Wiley, New York, 1948

Cowan, C.B., Peterson, W.S. and Osberg, G.L., " Drying of Wood Chips in a Spouted Bed", Pulp and Paper Mag., Dec., 139, 1951

Crandall, S.H. and Dahl, N.C., "An Introduction to the Mechanics of Solids", McGraw-Hill, New York, 1959

Davidson, J.F. and Nedderman, R.M., "The Hour-Glass Theory of Hopper Flow", Trans.Inst.Chem.Engrs., V.51, 1973

Davis, E.H., "Soil Mechanics", Selected Topics, Edited by I.K., Butterworths, London, 1968

Dorodnitsyn, A.A., "General Method of Integral Relations and its Application to Boundary Layer Theory", Advances in Aeronatical Sciences, 3, millan, New York, 1962

Drucker, D.C. "A More Fundamental Approach to Plastic Stress-Strain Relations", Proc. 1st U.S. National Congress of Applied Mechanics, ASME, p487, 1951

Drucker, D.C., Gibson, R.E. and Henkel, D.J., "Soil Mechanics and Work-Hardening Theories of Plasticity", Trans. ASCE, 122, p338, 1957

Epstein, N. and Levine, S., "Non-Darcy Flow and Pressure Distribution in a Spouted Bed", Proc. Second Enging. Foundation Conference on Fluidization Cambridge Univ. Press, p98, 1978

Epstein, N., Lim, C.J. and Mathur, K.B., "Data and Models for Flow Distribution and Pressure Drop in Spouted Beds", Can. J. Chem.Eng., V.56, 1978

Ferri, A., "Advances in Aeronautical Science", Edited by T. Von Karman, V.2, Pergaman Press, New York, 1959

Fraiman, R.S. and Luzanova, T.I., "Propagation of the Fluidized Region in the Volume of a Bulk Medium with the Blowing of Jet of Gas", Translated from Teoreticheskie Osnovy Khimicheskoi Tekhnologii, V.5, p273, 1971

Ghosh, B. and Osberg, G.L., "Heat Transfer in Water Spouted Beds", Can. J. Chem.Eng., V.37, 1959

Grbavcic, Z.B., Vukovic, D.V., Zdanski, F.K. and Littman, H. "Fluid Flow Pattern, Minimum Spouting Velocity and Pressure Drop in Spouted Beds", Can. J. Chem.Eng., V.54, 1976

Greenberg, M.D., "Foundations of Applied Mathematics", Prentice-Hall, Inc., 1978

Hancock, A.W. and Nedderman, R.M., "Prediction of Stress on Vertical Bunker Walls", Trans.Inst.Chem.-Engrs., V.52, 1974

Hildebrand, F.B., "Finite-Difference Equations and Simutions", Prentice-Hall, Inc., 1968

Hill, R., "The Mathematical Theory of Plasticity", Oxford, 1950

Horne, R.M. and Nedderman, R.M., "An Analysis of Switch Stresses in Two-Dimentional Bunkers", Powder Technology, V.19, p235, 1978a

Horne, R.M. and Nedderman, R.M. "Analysis of the Stress Distribution in Two-Dimensional Bins by the Method of Characteristics", Powder Technology, V.14, p93, 1976

Horne, R.M. and Nedderman, R.M., "Stress Distribution in Hoppers", powder Technology, V.19, p243, 1978b

International Symposium on Spouted Beds, Can. J. Chem.Eng., V.52, 1974

(Second)International Symposium on Spouted Beds, Can. J. Chem.Eng., V.61, 1983

Janbu, N., "Earth Pressure and Bearing Capacity by Generalized Procedure of Slices", Proc.-European Conf.Int.Soil Mech., 2, p207, 1957

Jackson, R., "Some Mathematical and Physical Aspects of Continuum Models for the Motion of Granular Materials", Theory of Dispersed Multiphase Flow, Ed. by R.E. Meyer, Academic Press, 1983

Jenike, A.W., "Gravity Flow of Bulk Solids", Utah Eng. Experiment Station, University of Utah, Bulletin No.108, V.52, 29, 1961

Jenike, A.W., "Storage and Flow of Solids", Utah Eng. Experiment Station, University of Utah, Bulletin No.123, V.53, 26, 1964

Jenike, A.W., Elsey, P.J. and Wooley, R.H., "Flow Properties of Bulk Solids", Trans.American Society for Testing Materials (ASTM), V.60, 1960

Jenike, A.W. and Johanson, J.R., "Stress and Velocity Fields in Gravity Flow of Bulk Solids", Utah Eng. Experiment Station, University of Utah, Bulletin No.116, V.53, 21, 1962

Jenike, A.W. and Johanson, J.R., "Bins Loads", J. Struct. Div. ASCE, ST4, 94, p1011, 1968

Jenike, A.W. and Shield, R.T., "On the Plastic Flow of Coulomb Solids Beyond Original Failure", J. of Applied Mechanics, 81B, p599, 1959

Johanson, J.R., "Stress and Velocity Fields in the Gravity Flow of Bulk Solids", J. of Applied Mechancs, Tans. of ASME, p499, 1964

Khoe, G.K., "Mechanics of Spouted Beds", Dissertation Delft-University of Technology", 1980

King, D.F. and Harrison, D., "The Minimum Spouting Velocity of a Spouted Bed at Elevated Pressure", Powder Technology, 26, p103, 1980

Klassen, J. and Gishler, P.E., "Heat Transfer from Column Wall to Bed in Spouted, Fluidized and Packed Systems", Can. J. Chem.Eng., V.36, 1958

Kochin, N.E., Kibel, I.A. and Rose, N.V., "Theoretical Hydrodynamics", 4th ed., Macmillan, New York, 1963

Lambe, T.W. and Whitman, R.V., "Series in Soil Engineering", John Wiley & Sons, New York, 1979

Lefroy, G.A. and Davidson, J.F., "The Mechanics of Spouted Beds", Trans. Ins. Chem. Engrs., V.47, 1969

Leva, M., Weintraub, M., Grummer, M., Pallchik, M. and Storch, H.H., "Flow of Fluid Theory Packed and Fluidized Particles", U.S. Bureau of Mines, Bulletin 504, 1951

Lim, C.J. and Mathur, K.B., "A Flow Model for Gas Movement in Spouted Beds", AIChE J., V.22, No.4, 1976

Lim, C.J. and Mathur, K.B., "Modeling of Particle Movement in Spouted Beds", Fluidization, Cambridge University Press, 1978

Lim, C.J. and Mathur, K.B., "Vapour Phase Chemical Reaction in Spouted Beds: A Theoretical Model", Chem.Eng. Sci., V.29, No.3, 1974

Lister, M., "The Numerical Solution of Hyperbolic Equations by the Method of Characteristics(Mathematical Methods for Digital Computers), John Wiley, New York, 1960

Littman, H., Morgan, M.H. and Vukovic, D.V., Zdanski, F.K., Grbavcic, Z.B., "A Theory for Predicting the Maximum Spoutable Height in a Spouted Bed", Can. J. Chem.Eng., V.55, 1977

Littman, H., Morgan, M.H. and Vukovic, D.V., Zdanski, F.K., Grbavcic, Z.B., "Prediction of the Maximum Spoutable Height and the Average Spout to Inlet Tube Diameter Ratio in Spouted Beds of Spherical Particles", Can. J. Chem.Eng., V.57 1979

Littman, H., Narayanan, P.V., Kim, S.J., Morgan, M.H. and Lazarek, G.M., "Flow in the Annulus of a Spouted Bed of Coarse Particles Near Minimum Spouting Model and Experimental Verification" Technical Information Series, General Electric Company, No.81, CRD231, 1981

Malek, M.A. and Lu, B C.-Y., "Heat Transfer in Spouted Beds" Can. J. Chem.Eng., V.42, 1, 1964

Malek, M.A. and Lu, B C.-Y., "Pressure Drop and Spoutable Bed Height in Spouted Beds", I&EC Process Design and Development, V.4, No.1, 1965

Malek, M.A., Madonna, L.A. and Lu, B C.-Y., "Estimation of Spout Diameter in a Spouted Bed", I&EC Process Design and Development, V.2, No.1, 1963

Mamuro, T. and Hattori, H., "Flow Pattern of Fluid in Spouted Beds", J. of Chem.Eng. of Japan, V.1, No.1, 1968

Mathur, K.B. and Epstein, N., "Developments in Spouted Bed Technology", International Symposium on Spouted Beds, Can. J. Chem.Eng., V.52, 1974(a)

Mathur, K.B. and Epstein, N., "Dynamics of Spouted Beds", Advances in Chem.Eng., V.9, Academic Press, 1974(b)

Mathur, K.B. and Epstein, N., "Spouted Beds", Academic Press 1974(c)

Mathur, K.B. and Gishler, P.E., "A Technique for Contacting Gases with Coarse Solid Particles", AIChE J., V.1, 1955(a)

Mathur, K.B. and Gishler, P.E., "Spouted Bed Technique to Wheat Drying", Presented to J. of Applied-Chemistry (London), V.5, p624, 1955(b)

McNab, G.S. and Bridgwater, J., "A Theory for Effective Solid Stresses in the Annulus of a Spouted Bed", Can. J. Chem.Eng., V.57, 1979

McNab, G.S. and Bridgwater, J., "Spouted Beds-Estimation of Spouting Pressure Drop and the Particle Size for Deepest Bed", Presented at Nuremburg Congress on Particle Technology, 1977

McNab, G.S. and Bridgwater, J., "The Application of Soil Mechanics to Spouted Bed Design", International Symposium on Spouted Beds, Can. J. Chem.Eng., V.52, 1974

Morgan, M.H. and Littman, H., "General Relationships for the Minimum Spouting Pressure Drop Ratio, $\Delta P_{ms}/\Delta P_{mf}$ and the Spout-Annulus Interfacial in a Spouted Bed", Fluidization, Plenum Press, New York, p287, 1980

Morgan, M.H. and Littman, H., "Predicting the Maximum Spoutable Height in Spouted Beds of Irregularly Shaped Particles", Ind.Eng.Chem. Fundam., V.21, p23, 1982

Morgenstern, N.R. and Price, V.E., "Analysis of the Stability of General Slip Surface", Geotechnique, 15:1, P79, 1965

Nedderman, R.M., "The Theoretical Prediction of Stress Distribution in Hoppers", Trans. Inst. Chem.Eng. V.60, p259, 1982

Nedderman, R.M., Tuzun, U., Savage, S.B., Houlsby, G.T.,"The Flow of Granular Material-I, Discharge Rate from Hoppers", Chem.Eng. Sci., V.37, p1597, 1982

Panov, D.J., "Formulas for the Numerical Solution of PDE's by the Method of Differences" Translated by Stern, Frederick Ungar Publishing Co., 1963

Pariseau, W.G., "Gravity Flows of Ideally Plastic Materials Through Slots", Trans. ASME(J. Engng. Ind.) V.91, No.2, 1969

Peterson, W.S., "Spouted Bed Drier", Can. J. Chem.Eng. P228, 1962

Piccinni, N. Grace, J.R. and Mathur, K.B., "Vapour Phase Chemical Reaction in Spouted Beds: Verification of Theory", Chem.Eng. Sci., V.34, No.10, 1979

Prager, W., "Discontinuous Solution in the Theory of Plasticity", Courant Anniversary Volume, 1948

Prager, W. and Hodge, P.G., "Theory of Perfectly Plastic Solids", Wiley, New York, 1951

Rainville, E.D. and Bedient, P.E., "Elementary Differential Equations", Fifth Edition, Macmillan Publishing Co., Inc., New York, 1974

Reddy, K.V.S., Fleming, R.J. and Smith, J.W.,"Maximum Spoutable Bed Depths of Mixed Particles-Size Beds" Can. J. Chem.Eng., V.46, 1968

Rietema, K., "Application of Mechanical Stress Theory to Fluidization", Proc. Int. Symp. Fluidization, 1967, Ed. by A.A.H. Drinkenburg, Amesterdam:

Netherlands University Press, p154, 1968
Rowe, P.W., "Stress-Dilatancy, Eart Pressure, and Sloped", the Soil Mechanics and Foundations Division, Proc. ASCE, V.89, No.SM3, p37, 1963
Savage, S.B., "Gravity Flow of a Cohesionless Bulk Solid in a Converging Conical Channel", Int. J. Mech. Sci., V.9, p651, 1967
Savage, S.B., "Gravity Flow of Cohesionless Granular Materials in Chutes and Channels", J. Fluid Mech., V.29, part 1, p53, 1979
Savage, S.B. and Yong, R.N., "Stresses Developed by Cohesionless Granular Materials in Bins", Int. J. Mech. Sci., V.12, p675, 1970
Savage, S.B., Yong, R.N. and McInnes, D.,"Stress Discontinuities in Cohesionless Particulate Materials", Int. J. Mech. Sci., V.11, p595, 1969
Schlichting, H., "Boundary Layer Theory", 7th Edition, McGraw-Hill, New York, 1978
Schofield, A. and Worth, P., "Critical State Soil Mechanics" McGraw-Hill, New York, 1968
Scott, R.F., "Principles of Soil Mechanics", Addison-Wesley, Reading, Mass., 1963
Shield, R.T., "Plastic Flow in a Converging Conical Channel" J. Mech. Phys. Solids, 3, p246, 1955(a)
Shield, R.T., "On Coulomb's Law of Failure in Soils", J. Mech. Phys. Solids, V.4, p10, 1955(b)
Singiser, R.E., Heiser, A.L. and Prilling, E.B., "Air-Suspension Tablet Coating", Chem.Eng. Prog., V.62, 1966
Sitting, M., "Fluidized Solids", Chem.Eng., P219, 1953
Smith, J.W. and Reddy, K.V.S., "Spouting of Mixed Particle-Size Beds", Can. J. Chem.Eng., V.42, 1964
Sobotka, Z., "Slip Lines and Slip Surfaces in the Theory of Plasticity and Soil Mechanics", Originally Published in the October 1961, issue of AMR
Sokolovski, V.V., "Statics of Soil Media", Translated by D.H. Jons and A.N. Schofield, Butterworths, 1960
Sokolovski, V.V., "Statics of Granular Media", Pergamon-Press, Oxford, 1965
Suciu, G.C. and Patrascu, M., "Particle Circulation in a Spouted Bed", Powder Tech., 19, p109, 1978
Thorley, B., Mathur, K.B., Klassen, J. and Gishler, P.E., "The Effect of Design Variables on Flow Characteristics in a Spouted Bed", Rep.Nat.-Res. Council of Canada, Ottawa, Canada, 1955
Thorley, B., Saunby, J.B., Mathur, K.B. and Osberg, G.L.,"An Analysis of Air and Solid Flow in a Spouted Wheat Bed", Can. J. Chem.Eng., V.37, 1959

Tuzun, U., Houlsby, G.T., Nedderman, R.M. and Savage, S.B., "The Flow of Granular Materials-II, Velocity Distribution in Slow Flow", Chem.Eng. Sci., V.37, p1691, 1982

Updike, D., Notes from the Course "Theory of Plasticity", Mech412, Dpet. of Mechanical Eng. and Mechanics, Lehigh University, Fall 1981

Volpicelli, G., Raso, G. and Massimilla, L., "Gas and Solid Flow in Bi-Dimensional Spouted Beds", Proc. Eindhoven Fluidizn, Symp, p123, Netherlands University Press, Amesterdam, 1967

Walker, D.M.,"An Approximate Theory for Pressure and Arching in Hoppers", Chem.Eng. Sci., V.21, p975, 1966

Walters, J.K., "A Theoretical Analysis of Stresses in Axially Symmetric Hoppers and Bunkers", Chem.Eng. Sci., V.28, p779, 1973(a)

Walters, J.K., "A Theoretical Analysis of Stresses in Silos with Vertical Walls", Chem.Eng. Sci., V.28, p13, 1973(b)

Walters, J.K. and Nedderman, R.M., "A Note on the Stress Distribution at Great Depth in a Silo", Chem.Eng. Sci., V.28, p1907, 1973

Whitman, R.V. and Bailey, W.A., "Use of Computers for Slope Stability Analysis", J. of the Soil Mechanics and Foundations Division, Proc. ASCE, SM4, P475, 1967

Zenz, F.A., "Size Cyclone Diplegs Better", Hydrocarbon Processing, p125, 1975

APPENDIX 1

Evaluation of D

The mean vertical stress over the cross section of the vertical part of the annulus region of a spouted bed is given by

$$\bar{\sigma}_y = \int_0^1 \sigma_y(x)dx \qquad (A.1\text{-}1)$$

where $\bar{\sigma}_y$ is the vertical stress at distance x from the wall. Following the Walker's assumption(1966) that the horizontal stress σ_x is constant over the cross section, the corresponding Mohr circle diagram of the stress at the bed wall, spout wall and a typical point within the material can be shown by Figure A-1. The vertical shear stress τ_{xy} is minimum at the spout wall and maximum at the bed wall. If the shear stress was zero at the spout wall then the circle S would be tangent to PQ at Q. Walker (1966) has shown rigorously that in silos and at great depth, where σ_y is independent of y, the shear stress is a linear function of x. Later, Walters (1973b) has assumed a linear relationship everywhere based on the two minimum and maximum values at the two ends. Following Walters' the shear stress is written

$$\tau_{xy} = (\tau_w - \tau_s)x + \tau_s \qquad (A.1\text{-}2)$$

where $\tau_w=(\tau_{xy})_w$ and $\tau_s=(\tau_{xy})_s$ for simplicity. Using

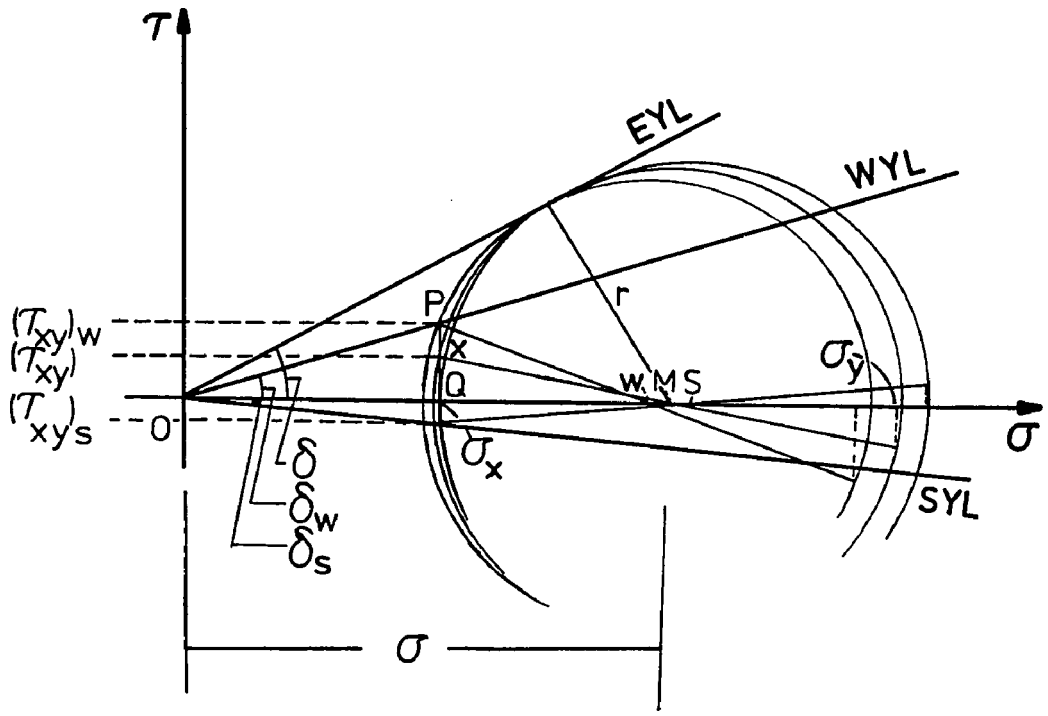

Figure A-1 Stresses and the corresponding Mohr circles (After Walters, 1973)

circle W represents stresses at the bed wall
circle M represents stresses at any point
circle S represents stresses at the spout wall

relationship (A.1-2) the shear stress then becomes:

$$\tau_{xy} = \sigma_x \tan\delta[(\psi_w-\psi_s)x+\psi_s] \qquad \text{(A.1-3)}$$

in which $\psi_w=\tan\delta_w/\tan\delta$ and $\psi_s=\tan\delta_s/\tan\delta$.

The radius of the Mohr circle r passing through the point X can be obtained from triangle MXQ, Figure A-1:

$$r^2 = \tau_{xy}^2 + \left(\frac{r}{\sin\delta} - \sigma_x\right)^2$$

This is a quadratic equation in r whose roots are

$$r = \frac{\tan\delta}{\cos\delta}\{\sigma_x \pm [(\sigma_x \sin\delta)^2-(\tau_{xy}\cos\delta)^2]^{1/2}\} \qquad \text{(A.1-4)}$$

Of the two circles through X which radius is given by equation (A.1-4) the one with larger radius is required for the active condition. From the geometry of the diagram we have:

$$\sigma_y = \frac{2\,r}{\sin\delta} - \sigma_x \qquad \text{(A.1-5)}$$

Substituting for r from (A.1-4) and for τ_{xy} from (A.1-3) into (A.1-5) yields:

$$\sigma_y = \left\{\frac{1+\sin^2\delta}{\cos^2\delta} + 2\frac{\tan\delta}{\cos\delta}\sqrt{1-[(\psi_w-\psi_s)x+\psi_s]^2}\right\}\sigma_x \qquad \text{(A.1-6)}$$

Equation (A.1-6) is in the form that can be used in

(A.1-1), doing so and taking the integral, the mean vertical stress is then:

$$\sigma_y = \left[\frac{a + b + c}{d}\right]\sigma_x \qquad (A.1\text{-}7)$$

where

$$a = \frac{1+\sin^2\delta}{\sin\delta}(\psi_w - \psi_s)$$

$$b = \psi_w\sqrt{1-\psi_w^2} - \psi_s\sqrt{1-\psi_s^2}$$

$$c = \sin^{-1}\psi_w - \sin^{-1}\psi_s$$

$$d = \frac{\cos^2\delta}{\sin\delta}(\psi_w - \psi_s)$$

But

$$D_w = \frac{\tan\delta_w}{B_w(\sigma_y/\sigma_x)} \qquad (A.1\text{-}8)$$

Using σ_y/σ_x obtained from (A.1-7) and substituting B_w from (5.1-6) then yields

$$D_w = \frac{(\cos\delta/\cos\delta_w)(\psi_w-\psi_s)(1+\sin^2\delta_w+\cos\delta_w\sqrt{\sin^2\delta-\sin^2\delta_w})}{\tan\delta[\cos\delta_w-\sqrt{\sin^2\delta-\sin^2\delta_w}][a+b+c]} \qquad (A.1\text{-}9)$$

Similarly,

$$D_s = \frac{\tan\delta_s}{B_s(\sigma_y/\sigma_x)} \qquad (A.1\text{-}10)$$

$$D_S = \frac{(\cos\delta/\cos\delta_s)(\psi_w-\psi_s)(1+\sin^2\delta_s+\cos\delta_s\sqrt{\sin^2\delta-\sin^2\delta_s}}{\tan\delta[\cos\delta_s-\sqrt{\sin^2\delta-\sin^2\delta_s}][a+b+c]}$$

(A.1-11)

APPENDIX 2

Determination of the Shock Front

Equilibrium of the element shown in Figure A.2-1 requires that

$$\sigma_{na} = \sigma_{nb} \qquad \text{(A.2-1)}$$

$$\tau_a = \tau_b \qquad \text{(A.2-2)}$$

but σ_{ta} may not be equal to σ_{tb}. Applying the well-known transformation formulas (Hill 1950, App. A), and using as variables the direction of the principal stress and the average normal stress equations (A.2-1) and (A.2-2) can be written, respectively

$$\sigma_a[1-\sin\delta\cos 2(\phi_a-\eta)] = \sigma_b[1-\sin\delta\cos 2(\phi_b-\eta)] \qquad \text{(A.2-3)}$$

$$\sigma_a \sin 2(\phi_a-\eta) = \sigma_b \sin 2(\phi_b-\eta) \qquad \text{(A.2-4)}$$

where η is the angle of the shock surface with the vertical axis. From equation (A.2-3) and (A.2-4) it can be found that

$$2\eta = (\phi_b+\phi_a) - \cos^{-1}[\sin\delta\cos(\phi_b-\phi_a)] \qquad \text{(A.2-5)}$$

$$\frac{\sigma_b}{\sigma_a} = \frac{\sin 2(\phi_a-\eta)}{\sin 2(\phi_b-\eta)} \qquad \text{(A.2-6)}$$

Equation (A.2-5) provides the shape of the shock surface at any point within the field, and equation (A.2-6) gives the value of σ on the opposite side of the surface.

Notice that (A.2-5) and (A.2-6) may also be obtained by using the Mohr circle of stress construction for the both sides of the shock surface as shown in Figure A.2-2 (see for example Nedderman, 1982). These equations along with those developed in section 5.3.3 can be used to calculate the shock surface (curve) and associated characteristic lines.

The numerical computation of the shock surface and the associated characteristic lines is described below. A detailed description of the numerical computation is given here for the region of the vertical/conical junction. The discontinuity of the stress parameters at point G of Figure A.2-3 necessitates the introduction of discontinuity emanating from G. Notice that the stress parameters are known throughout the region b.

The slope of the shock surface at point G, η_G, is obtained using (A.2-5) with $\phi_b=\phi_w$ and $\phi_a=\phi_{bound.}$. Equation (A.2-6) thus gives the σ at point G on the a side, knowing σ at this point on the b side. A discontinuity point, H, is located at a short distance from G along a line of slope η_G. The stress parameters at point H on the b side are obtained by first locating the grid quadrilateral containing H and then by interpolating for the

value of σ and ϕ at the grid points. The discontinuity relations, (A.2-5) and (A.2-6), are used to determine σ and ϕ on the a side of point H knowing σ on the b side and $\eta_H(=\eta_G)$. Point J is obtained by intersecting the (first) characteristic through H and the boundary of the dead zone. Since the characteristic grid expands it is necessary to generate extra points like P by interpolation between H and J. To specify the next point on the shock surface, K, there are five unknowns that must be determined: σ and ϕ on the b side of the discontinuity, x, y and η. The relationships provided to calculate the five unknowns are: two equations of the (second) characteristic applied to the interval PK, two discontinuity equations (A.2-5) and (A.2-6) and one equation of a straight line through H using the average of the discontinuity slopes at H and K as

$$y_K - y_H = (x_K - x_H)\cot\left(\frac{\eta_K + \eta_H}{2}\right) \qquad (A.2\text{-}7)$$

The five relations described here are not linear and an iterative procedure of solution must be used. Values of σ and ϕ on the b side of point K which are needed during the computations are found as described for the point H. Calculations can thus be continued to expand the shock surface and the characteristics mesh under the shock surface.

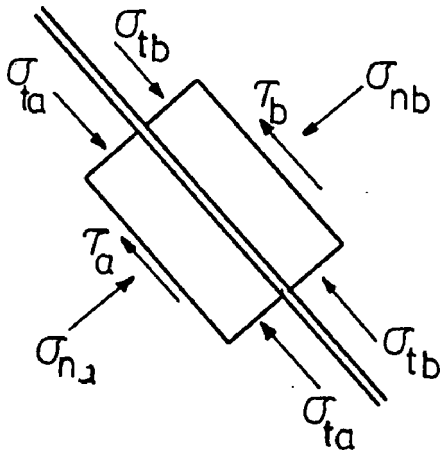

Figure A-2.1 Stresses on an elemnt at the discontinuity

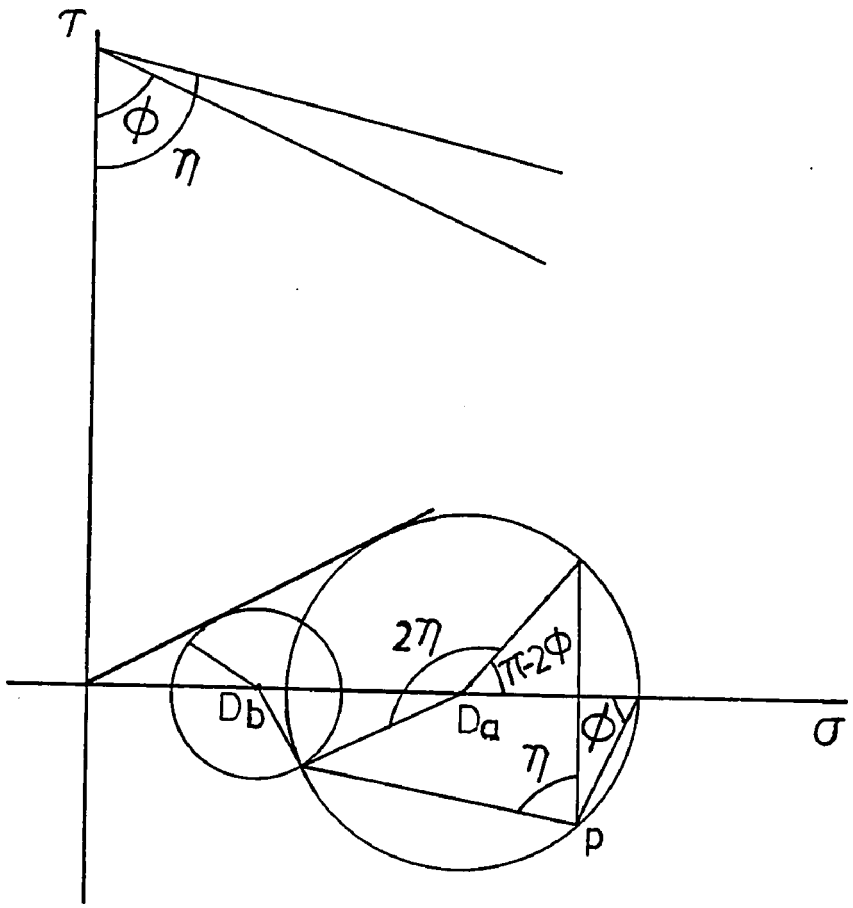

Figure A-2.2 Mohr circle and position of the shock surface

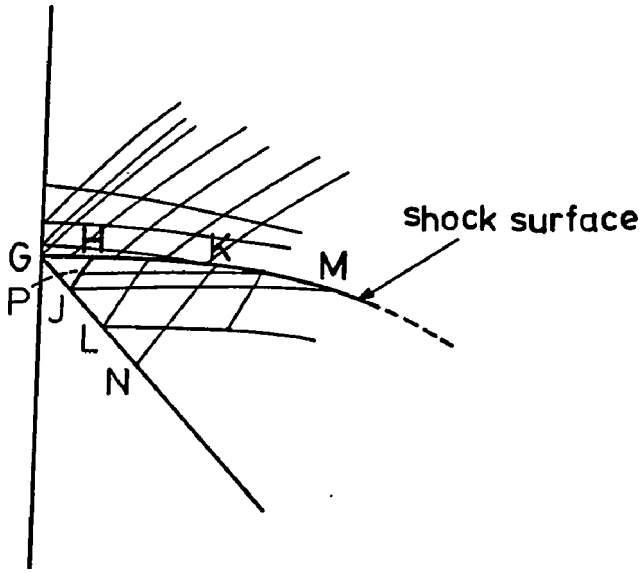

Figure A-2.3 Characteristics mesh and the shock surface

APPENDIX 3

A.3.1 Determination of the Characteristic Equations for the Stress Field

From equations (3.3.1-11) and (3.3.1-12) the coefficients of equation (5.3.1-1) for the stress field are:

$$\begin{aligned} a_{11}&=1-\sin\delta\cos 2\phi & a_{21}&=\sin\delta\sin 2\phi \\ a_{12}&=\sin\delta\sin 2\phi & a_{22}&=1+\sin\delta\cos 2\phi \\ b_{11}&=2\sigma\sin\delta\sin 2\phi & b_{21}&=2\sigma\sin\delta\sin 2\phi \\ b_{12}&=2\sigma\sin\delta\cos 2\phi & b_{22}&=-2\sigma\sin\delta\sin 2\phi \\ e_1&=0 & e_2&=1-\frac{dP_f}{dy}=\frac{\rho_e}{\rho_b} \end{aligned} \qquad \text{(A.3.1-1)}$$

The coefficients of the equation (5.3.1-2) are:

$$\begin{aligned} A&=2\sigma\sin\delta(\cos 2\phi-\sin\delta) \\ B&=-4\sigma\sin\delta\sin 2\phi \\ C&=-2\sigma\sin\delta(\cos 2\phi+\sin\delta) \end{aligned} \qquad \text{(A.3.1-2)}$$

The quadratic equation for the stress characteristic direction χ then is

$$(\cos 2\phi-\sin\delta)\chi^2+2\sin 2\phi\chi-(\cos 2\phi+\sin\delta)=0 \qquad \text{(A.3.1-3)}$$

where the solutions are

$$\chi_{1,2}=\frac{-\sin 2\phi\pm\cos\delta}{\cos 2\phi-\sin\delta} \qquad \text{(A.3.1-4)}$$

Introducing $2\mu=\pi/2-\delta$, the stress characteristic directions (A.3.1-4) can be written

$$\chi_{1,2}=\cot(\phi\pm\mu)$$

The coefficients of the compatibility relations holding

along the two characteristics

$$E=\cos^2\delta \qquad H=-\sin\delta\sin2\phi(\rho_e/\rho_b)$$
$$F=-2\sigma\sin\delta\sin2\phi \qquad G=-(1-\sin\delta\cos2\phi)(\rho_e/\rho_b) \quad \text{(A.3.1-5)}$$

Substituting these coefficients into equations (5.3.1-7) and using (A.3.1-4) yields

$$\cos^2\delta d\sigma+2\sigma\sin\delta\cos\delta d\phi = -[\sin\delta\sin2\phi dx + (1-\sin\delta\cos2\phi dy](\rho_e/\rho_b)$$
$$\cos^2\delta d\sigma-2\sigma\sin\delta\cos\delta d\phi = -[\sin\delta\sin2\phi dx + (1-\sin\delta\cos2\phi)dy](\rho_e/\rho_b)$$
$$\text{(A.3.1-6)}$$

After some algebraic manipulations the equations (5.3.2-1) are obtained. The fastest way to get from (A.3.1-6) to (5.3.2-1) is first to divide both sides of equations by $\cos^2\delta$, and second to add and subtract the term $(dy_{\mp}\tan\delta dx)$ from the right hand side of (A.3.1-6) inside the brackets. Notice that the (-) sign applies to the first and (+) sign to the second equation of (A.3.1-6). Then it is easy to show that the right hand sides vanish but the term $(dy-\tan\delta dx)$ inside the brackets.

Determination of the Characteristic Equations for the Velocity Field

From equations (3.3.2-1) and (3.3.2-2) the coefficients of equation (5.3.1-1) for the velocity field are

$$
\begin{array}{ll}
a_{11}=1 & a_{21}=\tan 2\phi \\
a_{12}=0 & a_{22}=1 \\
b_{11}=0 & b_{21}=1 \\
b_{12}=1 & b_{22}=-\tan 2\phi \\
e_1=0 & e_2=0
\end{array}
\qquad \text{(A.3.2-1)}
$$

The coefficients of the equation (5.3.1-2) are

$$
\begin{array}{l}
A=1 \\
B=2\tan 2\phi \\
C=-1
\end{array}
\qquad \text{(A.3.2-2)}
$$

The quadratic equation for the velocity characteristic direction χ then is

$$\chi^2 + 2\tan 2\phi\chi - 1 = 0 \qquad \text{(A.3.2-3)}$$

where the solutions are:

$$\chi_{1,2} = -\tan 2\phi \pm \frac{1}{\cos 2\phi} \qquad \text{(A.3.2-4)}$$

After some manipulations the velocity characteristic directions are

$$\chi_{1,2} = -\tan(\phi \mp \pi/4)$$

The coefficients of the compatibility relations holding along the two characteristics are

$$E=1 \quad , \quad F=H=G=0 \qquad \text{(A.3.2-5)}$$

Substituting these coefficients into equations (5.3.1-7) and using $\chi_{1,2}$ yields

$$
\begin{array}{l}
du - [\tan(\phi-\pi/4)]\, dv = 0 \\
du - [\tan(\phi+\pi/4)]\, dv = 0
\end{array}
\qquad \text{(A.3.2-6)}
$$

Using the trigonometry relations, the system (A.3.2-6) can be written as (5.4.1-1).

APPENDIX 4

Formulas Computing the Data at the Boundary Points

For the characteristics positions shown in Figure 40 the formulas are as follows:

For the bed wall:

$$\phi_4' = \phi_w$$

$$\phi = (\phi_3' + \phi_4')/2$$

$$\chi = \cot(\phi - \mu)$$

$$y_4' = y_3' + \chi(1 - x_3')$$

$$\sigma = (\sigma_3' + \sigma_4')/2$$

$$\sigma_4' = \sigma_3' + [(y_4' - y_3') + \tan\delta(1 - x_3')](\rho_e/\rho_b) + 2\sigma\tan\delta(\phi_4' - \phi_3')$$

For the spout wall

$$\phi_4 = \phi_s$$

$$\phi = (\phi_3 + \phi_4)/2$$

$$\chi = \cot(\phi + \mu)$$

$$y_4 = y_3 + \chi(1 - x_3)$$

$$\sigma = (\sigma_3 + \sigma_4)/2$$

$$\sigma_4 = \sigma_3 + [(y_4 - y_3) + x_3\tan\delta](\rho_e/\rho_b) - 2\sigma\tan\delta(\phi_4 - \phi_3)$$

Solutions to these equations require trial and error calculations like a regular grid point.

VITA

The author, Mohammad Seyed Amirshahidi, was born in Rasht, a northen city of Iran, on August 14, 1954.

He graduated from Kharazmi high school at Tehran with a major in mathematics in 1972. He entered to the Tehran Technical University in the same year and received a B.S. degree in Chemical Engineering there in 1977. He came to Lehigh University in January 1978 and received a M.S. degree in June 1980. He was appointed instructor, for the summer session 83, in the "Introduction to Transport Phenomena" at Lehigh.

He is a member of the "American Institute of Chemical Engineers".